(1)

L

2161

Department of Mechanical Engineering

University of Washington
Seattle, Washington 98195

AN EXPERIMENTAL INVESTIGATION OF THE TWO-DIMENSIONAL HYDRODYNAMIC CHARACTERISTICS OF BLUFF SYMMETRICAL FAIRING SECTIONS

D. E. CALKINS
Research Associate Professor

D. L. GRAY
Research Assistant

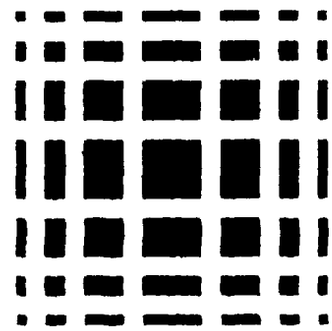

AN EXPERIMENTAL INVESTIGATION OF THE TWO-DIMENSIONAL HYDRODYNAMIC CHARACTERISTICS OF BLUFF SYMMETRICAL FAIRING SECTIONS

D. E. CALKINS
Research Associate Professor

D. L. GRAY
Research Assistant

UNCLASSIFIED

SECURITY CLASSIFICATION OF THIS PAGE

AD-A170 933

REPORT DOCUMENTATION PAGE

1a. REPORT SECURITY CLASSIFICATION: UNCLASSIFIED	1b. RESTRICTIVE MARKINGS: N/A
2a. SECURITY CLASSIFICATION AUTHORITY: N/A	3 DISTRIBUTION / AVAILABILITY OF REPORT: APPROVED FOR PUBLIC RELEASE; DISTRIBUTION UNLIMITED
2b. DECLASSIFICATION / DOWNGRADING SCHEDULE: N/A	
4. PERFORMING ORGANIZATION REPORT NUMBER(S): DEPARTMENT OF MECHANICAL ENGINEERING	5. MONITORING ORGANIZATION REPORT NUMBER(S)
6a. NAME OF PERFORMING ORGANIZATION: UNIVERSITY OF WASHINGTON; 6b. OFFICE SYMBOL (If applicable)	7a. NAME OF MONITORING ORGANIZATION: DAVID W. TAYLOR NAVAL SHIP RESEARCH AND DEVELOPMENT CENTER, Code 1504 (1505)
6c. ADDRESS (City, State, and ZIP Code): SEATTLE, WASHINGTON 98195	7b. ADDRESS (City, State, and ZIP Code): BETHESDA, MARYLAND 20084-5000
8a. NAME OF FUNDING / SPONSORING ORGANIZATION: Naval Sea Systems Command; 8b. OFFICE SYMBOL (If applicable): SEA 05R24	9. PROCUREMENT INSTRUMENT IDENTIFICATION NUMBER: Contract Number - N00014-82-K-0006
8c. ADDRESS (City, State, and ZIP Code): Washington, D. C. 20360	10 SOURCE OF FUNDING NUMBERS: PROGRAM ELEMENT NO 61153N; PROJECT NO SR 023 01; TASK NO 23454; WORK UNIT ACCESSION NO N/A

11 TITLE (Include Security Classification)
AN EXPERIMENTAL INVESTIGATION OF THE TWO-DIMENSIONAL HYDRODYNAMIC CHARACTERISTICS OF BLUFF SYMMETRICAL FAIRING SECTIONS

12 PERSONAL AUTHOR(S)
D. E. CALKINS AND D. L. GRAY

13a TYPE OF REPORT	13b TIME COVERED	14 DATE OF REPORT (Year, Month, Day)	15 PAGE COUNT
INTERIM	FROM _____ TO _____	March 1984	115

16 SUPPLEMENTARY NOTATION Sponsored under the Naval Sea Systems Command General Hydromechanics Research (GHR) Program administered by the David W. Taylor Naval Ship R&D Center, Code 1504(1505), Bethesda, Maryland 20084-5000

17 COSATI CODES		
FIELD	GROUP	SUB-GROUP
20	04	

18 SUBJECT TERMS (Continue on reverse if necessary and identify by block number)
(U) GHR Program (U) Bluff Symmetrical Sections
(U) 2D Hydrodynamic Characteristics of Bluff Bodies

19 ABSTRACT (Continue on reverse if necessary and identify by block number)

An experimental wind tunnel investigation has been conducted to determine the hydrodynamic characteristics of bluff symmetrical sections with high thickness/chord ratios. The sections are used as fairings for circular cylindrical members, such as towing cables and offshore drilling rig riser pipes, which are deeply immersed in the ocean environment so that they are cavitaion free. The fairings serve to reduce drag and lateral vibrations due to vortex shedding. The section tested had a 40 percent thickness/chord ratios. Measurements included the two-dimensional minimum drag coefficient, chordwise neutral stability point, yaw torque about the pivot center, and boundary layer transition and separation.

20 DISTRIBUTION / AVAILABILITY OF ABSTRACT	21 ABSTRACT SECURITY CLASSIFICATION
☒ UNCLASSIFIED/UNLIMITED ☐ SAME AS RPT ☐ DTIC USERS	UNCLASSIFIED
22a NAME OF RESPONSIBLE INDIVIDUAL: Mr. V. J. Monacella	22b TELEPHONE (Include Area Code): 202-227-1503; 22c OFFICE SYMBOL: Code 1504/1505

DD FORM 1473, 84 MAR 83 APR edition may be used until exhausted
All other editions are obsolete

SECURITY CLASSIFICATION OF THIS PAGE
UNCLASSIFIED

AN EXPERIMENTAL INVESTIGATION OF THE TWO-DIMENSIONAL HYDRODYNAMIC CHARACTERISTICS OF BLUFF SYMMETRICAL FAIRING SECTIONS

D. E. Calkins
Research Associate Professor

D. L. Gray
Research Assistant

March 1984

ONR Contract No. N0014-82-K-0006
General Hydromechanics Research Program
Naval Sea Systems Center
Admin: D. W. Taylor Naval Ship
Research and Development Center

University of Washington
Ocean Engineering Program
Dept. of Mechanical Engineering
Seattle, Washington

TABLE OF CONTENTS

ABSTRACT

An experimental wind tunnel investigation has been conducted to determine the hydrodynamic characteristics of bluff symmetrical sections with high thickness/chord ratios. The sections are used as fairings for circular cylindrical members, such as towing cables and offshore drilling rig riser pipes, which are deeply immersed in the ocean environment so that they are cavitation free. The fairings serve to reduce drag and lateral vibrations due to vortex shedding. The section tested had a 40 percent thickness/chord ratios. Measurements included the two-dimensional minimum drag coefficient, chordwise neutral stability point, yaw torque about the pivot center, and boundary layer transition and separation location.

This research was carried out under the Naval Sea Systems Command General Hydromechanics Research Program administered by the David W. Taylor Naval Ship Research and Development Center, under Office of Naval Research Contract No. N0014-82-K-0006.

1.0. INTRODUCTION

Marine applications of line structures (high length/diameter ratio) with circular cylindrical sections include moored and towed cable systems, risers for offshore drilling rigs, and the "cold water pipe" for the Ocean Thermal Energy Conversion (OTEC) system. All of these systems experience relative motion between the line structure and the surrounding water, due either to ship motion or current and wave motion. Because of this relative motion, the line structure experiences unsteady (time-dependent) hydrodynamic forces due to vortex shedding. When the frequency of the vortex shedding is close to the natural frequency of the line structure, a resonant structural

response condition will occur. This resonant condition will increase the drag force (force parallel to current field) which in turn will result in cyclic motions and stresses.

One solution to the shed vortex problem is to fair the circular cylinder with a streamlined shape. An obvious drawback is that the fairing, unless it is allowed to swivel freely and align itself with the flow field, will act as a wing and generate large transverse lift forces. However, this in turn dictates that the position of the hydrodynamic (aerodynamic) center must be aft of the mechanical center of rotation (central axis of the line structure) for weathervane stability.

It should be noted that the hydrodynamic center, or neutral stability point, is used in contrast to the center of pressure. The hydrodynamic center is defined as the position along the chord about which the moment coefficient is constant independent of lift coefficient, while the center of pressure position varies with lift coefficient. For symmetrical sections, this constant moment coefficient has a value of zero. The neutral point is defined as the point along the chord where the slope of pitching moment coefficient versus lift coefficient curve is zero. Therefore the terms hydrodynamic center and neutral point are synonymous for a symmetrical section and are used interchangeably.

2.0. PROBLEM DESCRIPTION

Rigid symmetrical fairings in short lengths are presently commercially available from Fathom Oceanology Ltd. for application to towing cables, Fig. 2.1. The fairings range in size from chord lengths of 5 to 15 cm for towing cable applications, to 2 m for a drill pipe riser fairing, [1]. Hydrodynamic problems with the towing cable fairings have been encountered, as discussed by Henderson [2]. A fairing section which had a thickness/chord ratio (t/c) of 25 percent was found to have a hydrodynamic center position at the 15.4 percent chord position, which was aft of the center of rotation by a distance of only 2.3 mm (2.9 percent chord). It was determined experimentally that boundary layer separation over the aft portion of the section caused this problem. The addition of a flat plate trailing edge extension, to fix the position of the aft stagnation point, increased the chord to 100 mm and resulted in the movement of the hydrodynamic center to the 25 percent chord position. The large diameters of line structures such as drill riser pipes (about 6.5 to 10 m) require that the fairing chord length be as small as possible for handling and installation considerations. This requirement results in fairing sections with very high thickness to chord radios (up to 50 percent). Boundary layer separation was apparently also observed in a series of wind tunnel tests, Grant [3], on high thickness/chord ratio (0.4 to 0.5 c) fairings designed for riser lines. It was observed that the fairing did not possess weathervane stability. In this particular application, the problem was solved by the addition of fins to the fairing trailing edge, which acted like a split flap and stabilized the fairing.

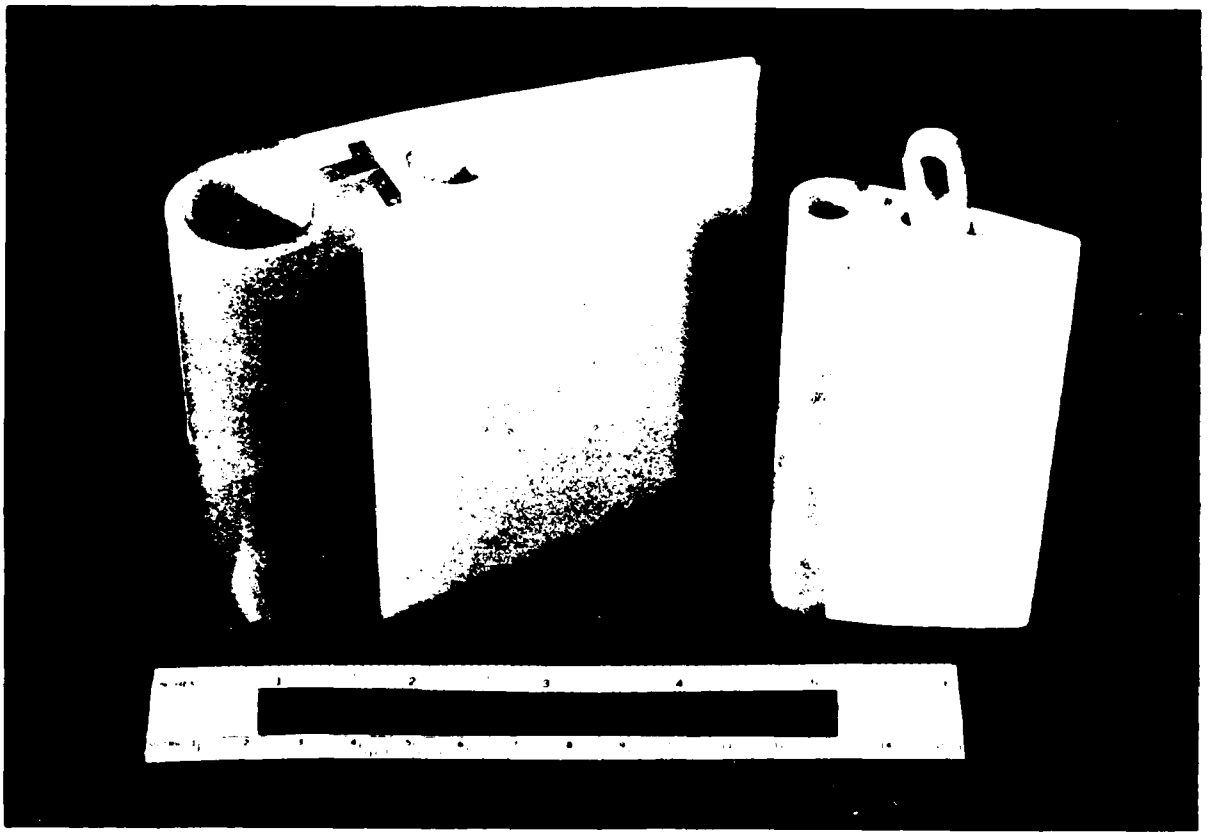

Fig. 2.1. Commercial cable fairings.

3.0. PROBLEM APPROACH

The selection of an optimum airfoil section shape for use as a fairing must include consideration of the following:

(1) streamlined symmetrical section for low drag

(2) position of maximum thickness/chord as close to the leading edge as possible in order for center of rotation to be forward of hydrodynamic center for weathervane stability

(3) high thickness/chord ratio (bluff) sections to reduce the chord size of the fairings

(4) separation free boundary layer.

The utilization of bluff sections as fairings will lead to problems with boundary layer separation, as already noted. Some means must therefore be used to prevent or control boundary layer separation and to provide rotational stability. Three techniques present themselves as appropriate solutions, either separately or synergistically. These include the use of separation resistant sections, vortex generators for boundary layer control and trailing edge wedges for stability.

Recent advances in the development of boundary layer separation resistant airfoil sections with specified pressure profiles have shown some interesting results. A section with a 53.6 percent t/c, designed by Liebeck, Smith [4], is the result of shaping the forward position of the section so that the pressure gradient is favorable to laminar flow, and then using the Stratford pressure recovery over the rear portion for separation control.

A passive technique for boundary layer control is the use of vortex generators. This technique relies on the increased mixing

between the external stream and the boundary layer as promoted by vortices trailing longitudinally over the surface from the generators. Vane type generators are the ones most often used. They consist of a row of small plates that project normal from the surface with each one set at an angle of incidence to the local flow to produce a single trailing vortex.

The use of "split-flap" wedges on the trailing edge of rudders has been investigated, Thieme [5], as a means to control the hydrodynamic moment. This suggests itself as a technique which might have application for the fairing configuration to achieve rotational stability.

4.0. SYMMETRICAL FAIRING SECTIONS

4.1. Section Geometry

A total of five symmetrical fairing sections were selected for this study. These included:

(1) Fathom fairing section

(2) NACA 0040

(3) Liebeck

(4) JfS 61-TR-40

(5) JfS 62-TR-40.

A thickness/chord ratio (t/c) of 40 percent was arbitrarily chosen as the maximum that might be successful in minimizing the chord length while hopefully operating with a separation free boundary layer. The one exception was the Fathom fairing, with a t/c of 25 percent. This section was selected to provide a baseline for data comparisons with past studies of this section, and to measure the degree of improvement, if any, provided by the thicker sections.

The section geometry may be described primarily by the following (Fig. 4.1).

(1) maximum thickness (t/c)

(2) chordwise position of maximum thickness (x_t/c)

(3) nose radius (r/c)

(4) trailing edge thickness (t_e/c).

In addition, the shape of the section aft of the maximum thickness location may be described as either concave or convex, Fig. 4.1. The individual fairing geometry is contained in Table 4.1, the sections are shown in Fig. 4.2, and the coordinates contained in Table 4.2.

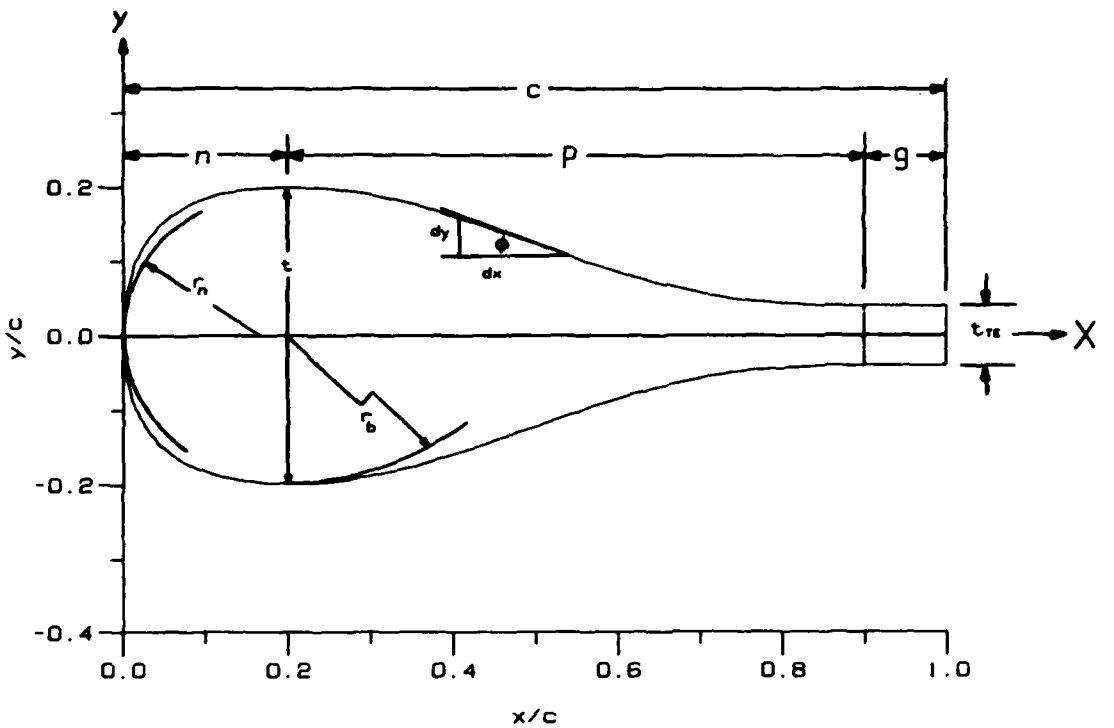

Fig. 4.1. Definition of geometric variables.

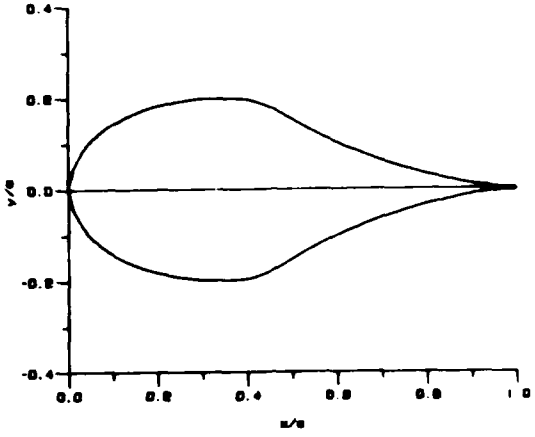

Liebeck 40% Section Profile

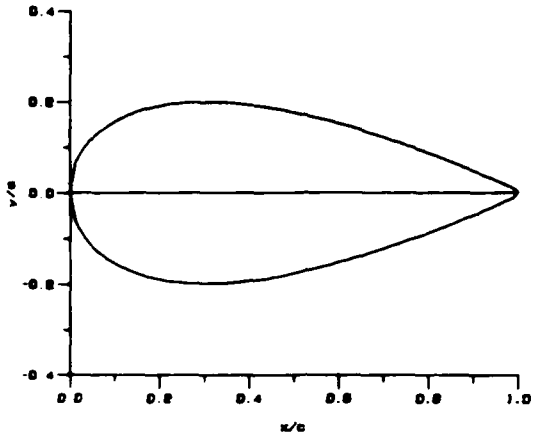

NACA 0040 Section Profile

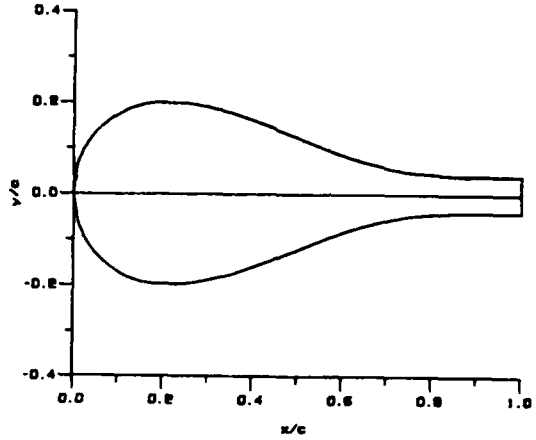

JfS 61M-TR-40 Section Profile

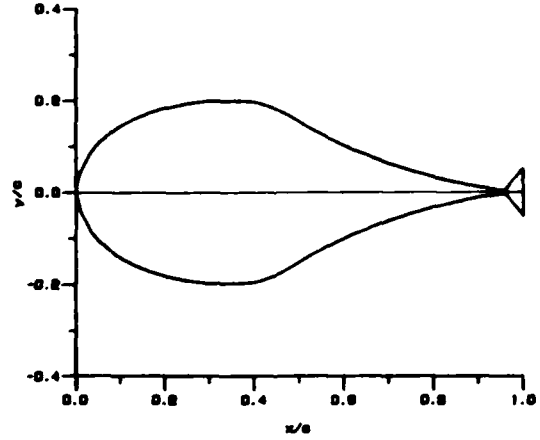

Liebeck 40% Section Profile with Trailing Edge Wedge

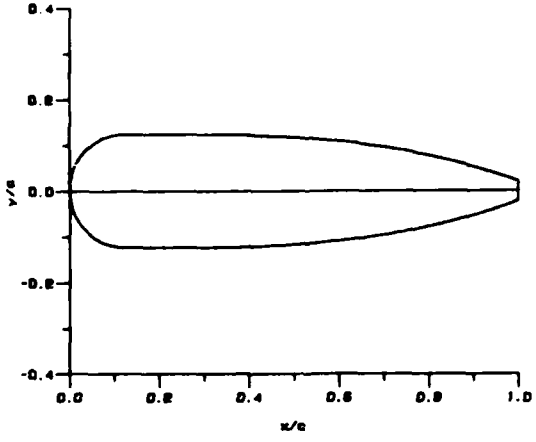

Pathom Flexnose 25% Section Profile

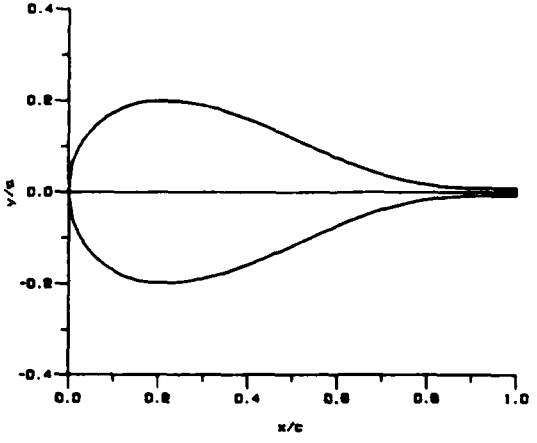

JfS 62M-TR-40 Section Profile

Fig. 4.2. Fairing sections.

Table 4.1 - Fairing Geometry

Section	t/c	x_t/c	r/c	After Section
Fathom	0.25	0.125	0.125	Convex
NACA 0040	0.40	0.30	0.125	Convex
Liebeck	0.40	0.35	0.1763	Concave
JfS 61-TR-40	0.40	0.20	0.25	Concave
JfS 62-TR-40	0.40	0.20	0.25	Concave

4.2. Section Description

4.2.1. Fathom Flexnose Fairing

The patented Fathom Flexnose fairing is one of the few commercially available cable fairings and is sold by Fathom Oceanology Ltd. of Port Credit, Ontario, Canada. The fairing is available in t/c's ranging from 0.13 to 0.27 and chord lengths of 6.35 cm to 42.44 cm. Fig. 2.1 shows fairings of chord lengths of 6.35 and 12.19 cm.

Henderson [2] has determined the hydrodynamic and mechanical characteristics of the Fathom Flexnose 25 percent fairing. Lift, drag, and pitching moment coefficients were measured at a Reynolds number of 2.2×10^5, which corresponds to towing a 5.08 cm fairing at 9.8 knots. Qualitative boundary layer flow visualization studies were also done at this Reynolds number. The aerodynamic center was determined from the lift and pitching moment data. A modification to the Fathom fairing trailing edge was made in an attempt to improve its hydrodynamic behavior. The two-dimensional hydrodynamic drag polars were also measured for this modified fairing.

Fathom Oceanology Ltd. produces several Flexnose fairings of slightly varying profiles. The profile chosen for this investigation

Liebeck 40%		NACA 0040		Fathom Flexnose	JfS 62M TR-40	JfS 61M-TR-40	
x/c	±y/c	x/c	±y/c	±y/c	±y/c	x/c	±y/c
0.00000	0.00000	0.000	0.00000	0.00000	0.00000	0.000	0.00000
0.01075	0.04319	0.004	0.03654	0.03137	0.03980	0.004	0.03980
0.03252	0.08273	0.010	0.05679	0.04899	0.06245	0.010	0.06245
0.06626	0.11841	0.020	0.07866	0.06782	0.08718	0.020	0.07866
0.10313	0.14402	0.040	0.10759	0.09165	0.12000	0.040	0.12000
0.15717	0.16874	0.060	0.12792	0.10677	0.14283	0.060	0.14283
0.22017	0.18653	0.080	0.14357	0.11662	0.16000	0.080	0.16000
0.27713	0.19561	0.120	0.16627	0.12490	0.18330	0.120	0.18330
0.33586	0.19874	0.125	0.16851	0.12500	0.18540	0.125	0.18540
0.40512	0.19310	0.160	0.18139	0.12500	0.19596	0.160	0.19596
0.44298	0.18154	0.200	0.19125	0.12494	0.20000	0.200	0.20000
0.49094	0.15644	0.250	0.19804	0.12470		0.270	0.19467
0.56479	0.11647	0.275	0.19958	0.12448	0.19381	0.340	0.17957
0.65158	0.07907	0.300	0.20006	0.12417		0.410	0.15709
0.74160	0.04832	0.350	0.19829	0.12323	0.17607	0.480	0.13040
0.82670	0.02564	0.425	0.19002	0.12080	0.14931	0.550	0.10299
0.89994	0.01099	0.500	0.17647	0.11680	0.11730	0.620	0.07824
0.96434	0.00233	0.575	0.15878	0.11083	0.08425	0.690	0.05891
1.00000	0.00056	0.650	0.13775	0.10250	0.05421	0.760	0.04648
		0.725	0.11388	0.09142	0.03064	0.830	0.04093
		0.800	0.08744	0.07718	0.01546	0.090	0.04000
		0.875	0.05848	0.05940	0.00864	1.000	0.04000
		0.950	0.02689	0.03769	0.00750		
		1.000	0.00420	0.02083	0.00750		

Table 4.2. Non-Dimensional Coordinates of the Tested Fairing Sections

was the same as the unmodified profile that was used in Henderson's study. This fairing was named Flexnose B by Wingham [6].

The experimental Reynolds number range was extended from 1.0×10^6 to 6.5×10^6 to complete the picture of the behavior of the Flexnose 25 percent fairing. The work of Henderson could thus be used as a basis for comparing with the results of this study.

4.2.2. NACA 0040 Section

The characteristics of the NACA 00XX series of symmetrical airfoils are well documented. Goett and Bullivant [7] tested the NACA 0009, 0012, and 0018 airfoils in 1938. In 1940, Bullivant [8] continued the study with the NACA 0025 and 0035 sections. Summaries of the results of the NACA 00XX tests are contained in Eastman, Jacobs and Abbott [9], Abbot and von Doenhoff [10], Hoerner [11], and Carmichael and Meggitt [12]. All of the airfoil characteristics for these sections were measured at high Reynolds numbers, ranging from 10^6 to 10^7. Althaus [13] tested the NACA 0033 section at Reynolds numbers of 8.0×10^4, 1.2×10^5, and 1.5×10^5. Although these Reynolds numbers are at the low end of the range of present interest, the reported drag coefficients indicated that an NACA 00XX section might be an acceptable choice for a cable fairing.

The NACA 0040 section was thus chosen for testing in part because this extensive set of data from earlier work could also act as a basis of comparison with the results the present investigation. In addition, it also serves as an example of a section with a convex after section.

4.2.3. Liebeck Section

The Liebeck fairing [4] was designed such that laminar flow would

be maintained along the forebody with no boundary layer separation occurring in the pressure recovery region at a Reynolds number of 10^7. The maximum t/c that theoretically met those requirements was 53.6 percent. The shape of tne aft section was designed using the theory of Stratford [14] for an imminent separation pressure recovery velocity distribution. Thus the afterbody was termed a "Stratford pressure recovery section." For this investigation the Liebeck fairing was reduced to a 40 percent t/c by a linear reduction of the coordinates. This shape was chosen for the study primarily because of the predicted low drag for its high t/c, and as an example of a section with a convex after section.

4.2.4. JfS Sections

JfS sections [5] are members of a family of balanced ship rudder profiles developed at the Shipbuilding Institute of the University of Hamburg. These profiles were developed by a systematic variation of form parameters which included: cross-sectional area, leading edge radius of curvature, length of forebody, length of pressure recovery section, length of trailing edge, thickness of trailing edge, surface slopes, and radius at maximum thickness. The profile coordinates are expressed as polynomials composed of so-called influence functions. One influence function was written for each of the form parameters. Thieme [5] gives a complete description of this technique. Two JfS sections of thickness/chord ratios of 25 percent were tested by Thieme, the JfS 61-TR-25, and the JfS 62-TR-25. Lift, drag, and pitching moment coefficients were measured at Reynolds numbers of 0.56×10^6, 0.70×10^6, and 0.79×10^6.

Two modifications were made to the JfS sections for this project. The thickness ratio was increased from 20 to 40 percent, and the

leading edge radius was modified to a forebody which was circular in section to the maximum thickness position. Because of these modifications, the JfS sections were renamed the JfS 61M-TR-40 and JfS 62M-TR-40.

4.3 Circular Cable Fairing Efficiency

An important geometrical consideration for a symmetrical section designed to fair a circular cylindrical cable is that the circular diameter be inscribed in the fairing as far forward as possible. Fig. 4.3 shows the nondimensional diameter, d/c, of these circles as a function of chord location. Each circle's center corresponds to the mechanical pivot location of the fairing. The largest diameter circle for the NACA 0040 is 40 percent of the chord located at x/c = 0.3, 39.6 percent located at x/c = 0.35 for the Liebeck section and 40.0 percent located x/c = 0.2 for the JfS sections. Thus the JfS sections are the most efficient in terms of the packaging of the circular cylinder.

4.4. Fairing Surface Slope

An important geometrical characteristic of the fairing shape is the local surface angle. Since the pressure gradient is a function of this angle, the surface slopes for each of the sections as a function of the chord are shown in Fig. 4.4. Also indicated are the trailing edge surface angle, θ_{t_e}. Note that both the NACA and Fathom fairings have convex pressure recovery sections, while the Liebeck and JfS sections have concave pressure recovery sections. For both JfS sections, the maximum slope in the pressure recovery section is less than the maximum slope for the Liebeck section.

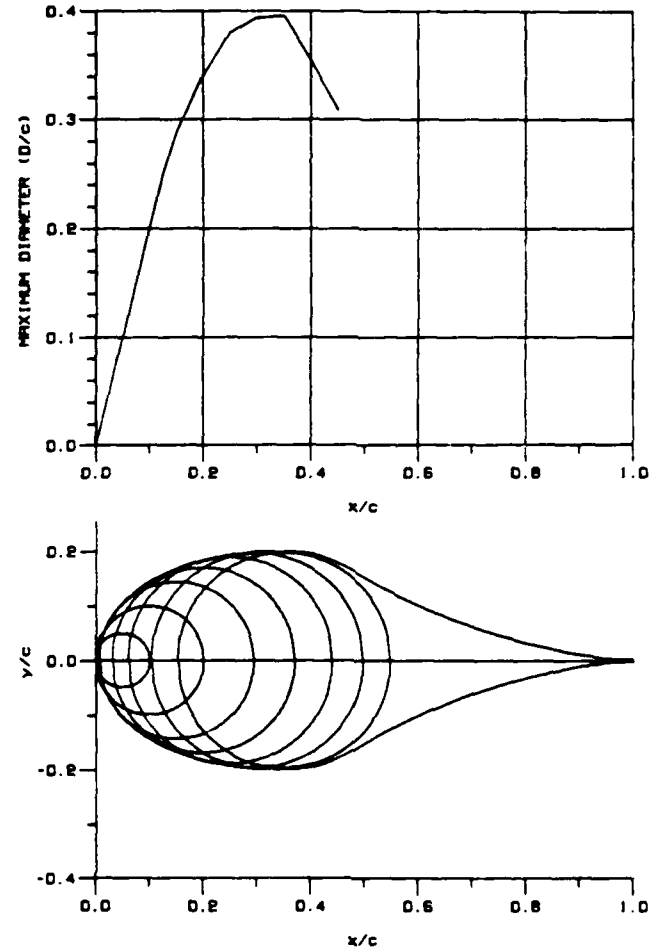

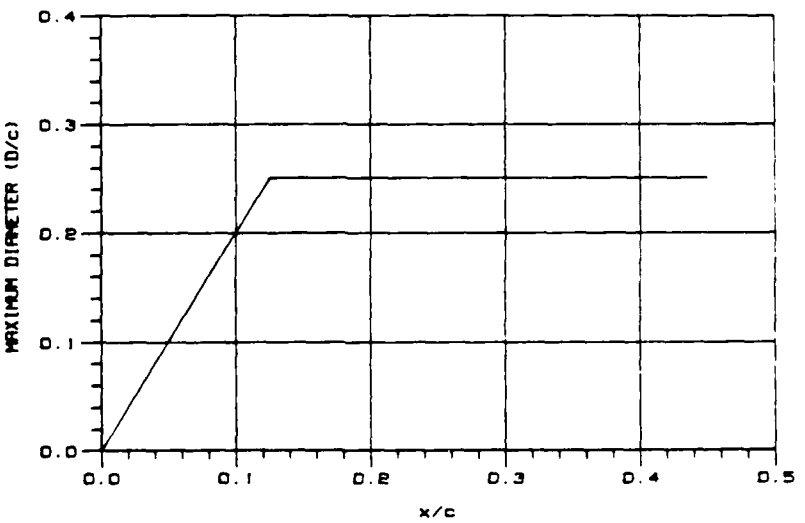

Fig. 4.3. Diameter of inscribed circles as a function of chord position.

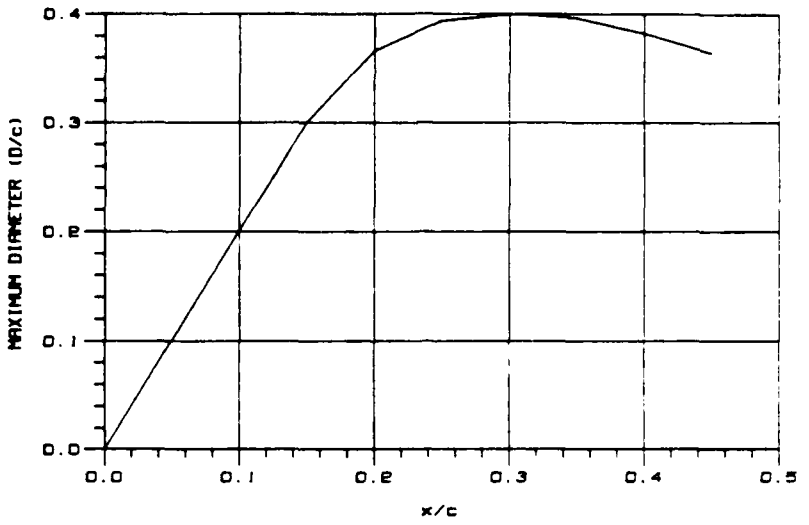

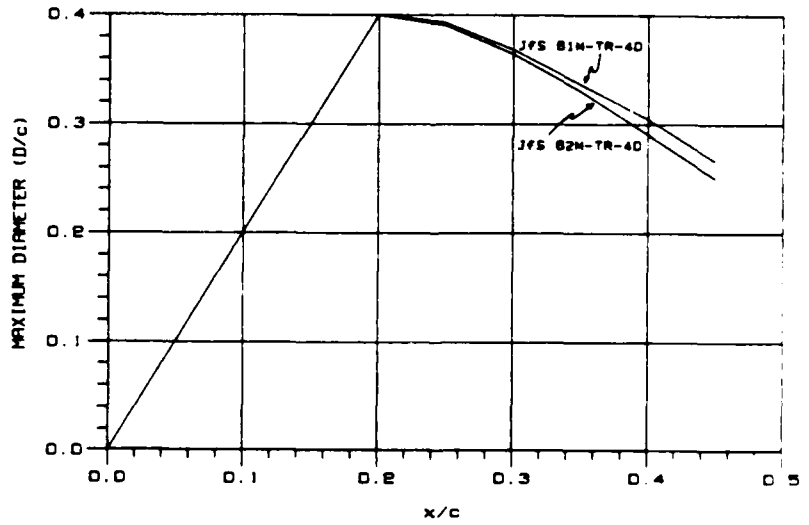

Fig. 4.3. Continued.

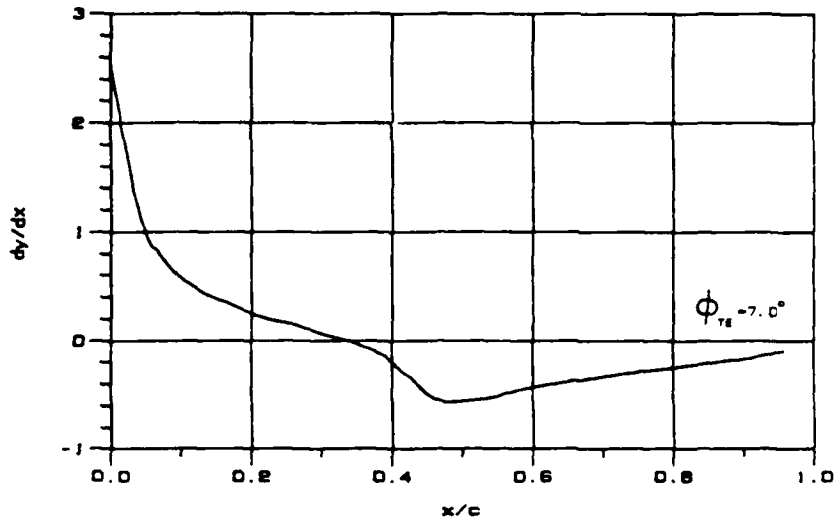

Liebeck Section

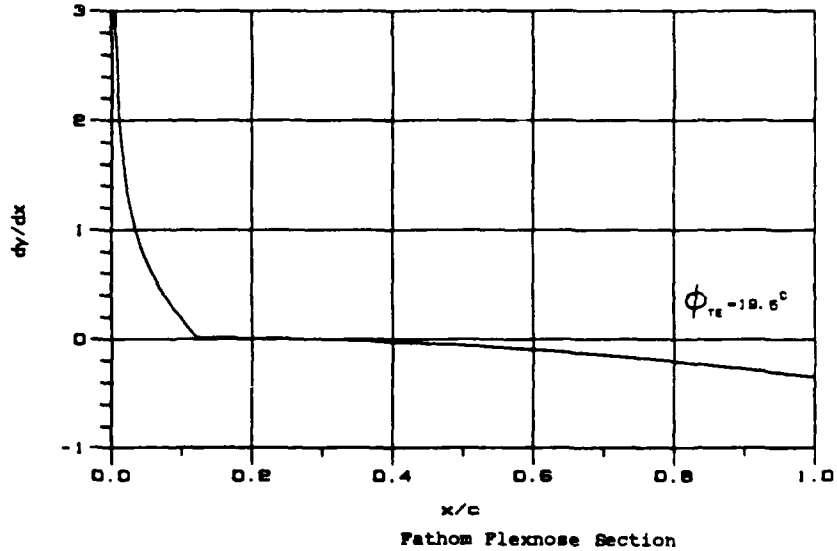

Fathom Flexnose Section

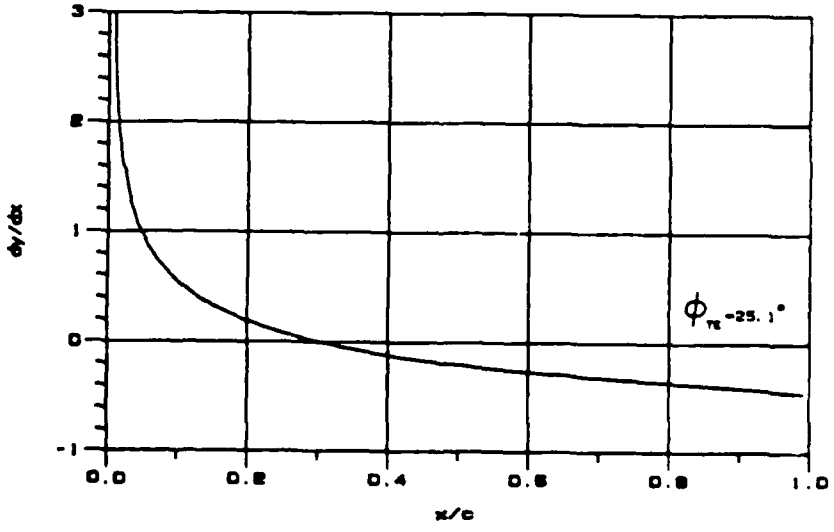

NACA 0040 Section

Fig. 4.4. Section surface slopes.

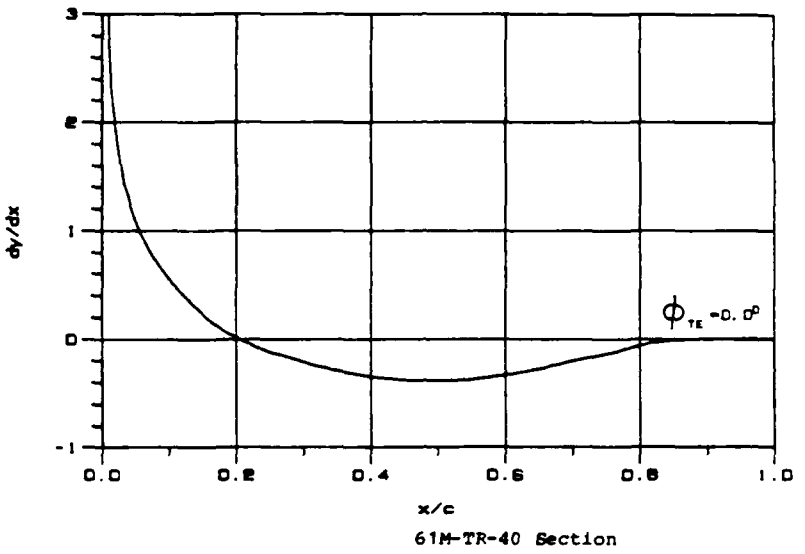

61M-TR-40 Section

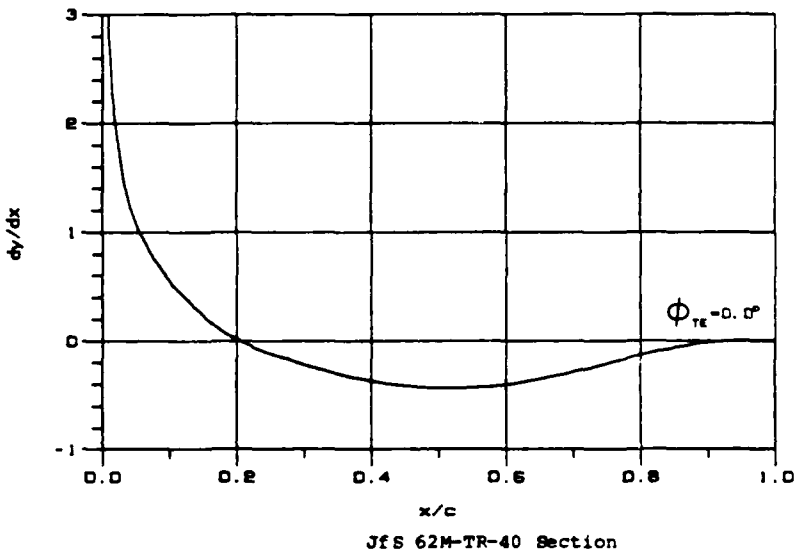

JfS 62M-TR-40 Section

Fig. 4.4. Continued.

5.0. EXPERIMENTAL EQUIPMENT

5.1. Wind Tunnel

The use of a wind tunnel for characterizing the fairing section hydrodynamics is appropriate, as long as Reynolds number equivalence is maintained. If it is assumed that the fairing section is being operated at depths great enough to avoid cavitation, the aerodynamic characteristics will be the same as the hydrodynamic characteristics. The tests were conducted in the University of Washington "Venturi" open return wind tunnel, which has an octagonal cross-section of 0.9 m across vertices and 0.79 m across flats. With a maximum speed of 27 m/s, a fairing section model with a 30.5 cm chord may be operated at a Reynolds number up to 5×10^5. The operational Reynolds number range for faired cables is from 5×10^4 to 1×10^6, while it is about 2 to 5×10^6 for faired riser pipes.

5.2. Tunnel Turbulence Intensity

The wind tunnel turbulence intensity was measured using the sphere drag coefficient method outlined in Pope [15], "Wind Tunnel Testing." The sphere drag coefficient was measured as a function of diameter Reynolds number. The Reynolds number at which the drag coefficient equals 0.30 is termed the "critical Reynolds number," R_{cr}, which has a value of 385,000 in free air. The turbulence factor is then defined as

$$TF = 385{,}000./R_{cr}. \tag{5.1}$$

For the Venturi Wind Tunnel, R_{cr} was equal to 1.5×10^5, which is equivalent to a TF equal to 2.85. The turbulence intensity level, T_u, is defined as

$$T_u = \tilde{u}/U_\infty \tag{5.2}$$

where $\tilde{u}$ = root mean square (rms) velocity fluctuations

U_∞ = free stream mean velocity.

The turbulence intensity is related to the turbulence factor so that T_u = 2.15 percent for the Venturi Wind Tunnel.

Since atmospheric turbulence levels in free flight are very much less than one percent, it is common to take means to reduce T_u to values below this. However, this problem must be reassed for conditions in the ocean. In general, the turbulence intensity will vary with location and depth. Because of the difficulties of measuring the ocean turbulence level, it is common to use a parameter, ε, which is the rate of viscous dissipation of velocity fluctuations Hinze, [16]. The rms velocity fluctuations are then defined as

$$(\tilde{u})^2 = \int_{k_1}^{k_2} [A(\varepsilon)^{2\backslash 3}(k_i)^{-5\backslash 3}]dk \qquad (5.3)$$

where k_i = wave number

k_1 = 0.1 cycle/m

k_2 = 5.0 cycle/m

A = constant = 1.5

$$(\tilde{u}) = \{[A(\varepsilon)^{2\backslash 3}(k_i)^{-2\backslash 3}]_{k_1}^{k_2}\}^{1\,2}$$

and the turbulence intensity, T_u, is then calculated using the towing velocity for U_∞. Measured values for two ocean locations, References [17] and [18] are presented in Table 5.1.

Table 5.1 - Ocean Viscous Dissipation Rates

Location	ε = W/m	Depth = m
Continental Shelf off Nova Scotia	10×10^{-6} to 3×10^{-3}	0 to 23.
Santa Maria Azores Atlantic Ocean	3×10^{-6} to 96×10^{-3}	0 to 750.

Figure 5.1 shows the ocean turbulence intensity levels, T_u, for these two locations and depth ranges as a function of towing speed. The resulting turbulence intensities, for a towing speed of 5 m/s, vary between 0.09 and 0.27 percent over a depth range from 0 to 750 m in the first location, while it varies from 0.6 to 8.7 percent over a depth range from 0 to 23 m in the second location.

The wind tunnel turbulence level could have been reduced by the addition of screens at the inlet; however, this would have been at the expense of a decrease in tunnel maximum operating speed (maximum Reynolds number). Because of the wide range of variation in ocean turbulence intensity, and since maximum Reynolds number in the tunnel was considered more important, the tunnel was left in its present condition and the wind tunnel data are presented as measured. If desired, a correction for turbulence intensity on the skin friction coefficient is available from Raghunathan [19]:

$$\Delta C_f/C_{f_o} = 12.6(T_u)^{1.4} \qquad (5.4)$$

for $0 < T_u < 0.04$

where C_{f_o} = skin friction coefficient at zero turbulence.

5.3. Wind Tunnel Models

All five of the fairing models were of the same size and

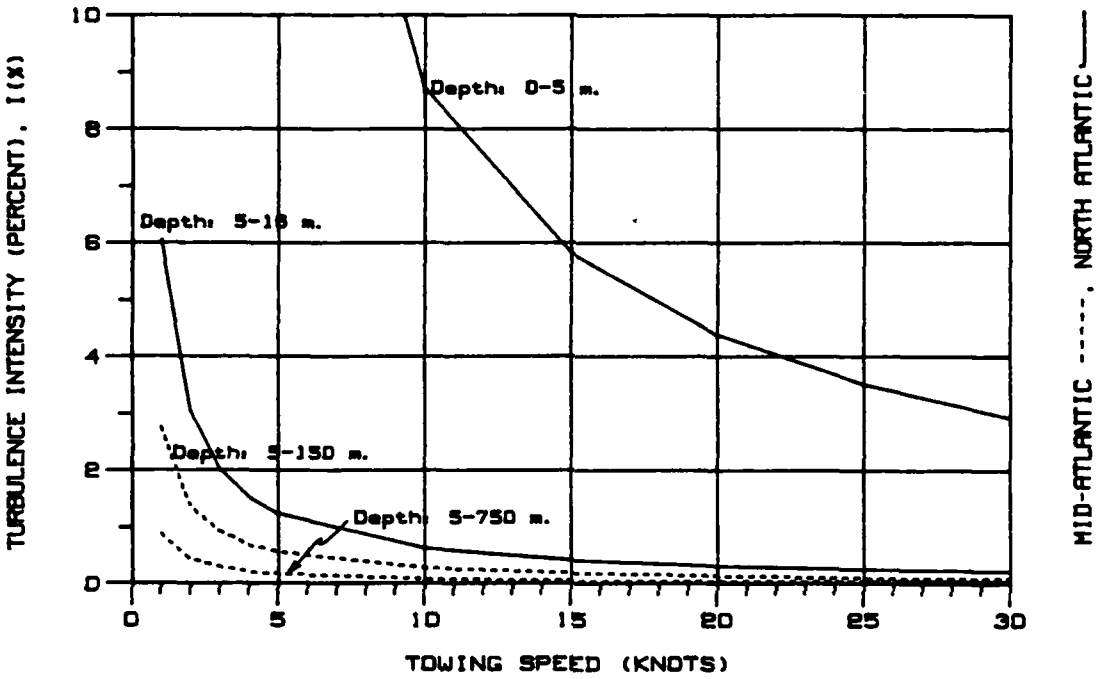

Fig. 5.1. Measured ocean turbulence intensity levels at two Atlantic Ocean locations.

construction. Each model had a chord length of 30.5 cm, a span of 78.11 cm and thicknesses of 7.6 cm for the Fathom fairing and 12.2 cm for the other four sections. The models were made using a urethane foam core with a birch plywood and fiberglass skin. The urethane foam core was cut to the fairing shape on a numerically controlled milling machine. The foam core was then cut to accept mahogany supporting members that formed the leading edge, trailing edge, and side supports at mid-chord. Profiled birch plywood with a recessed brass plate acted as a mount for the pivot pin bearings, Fig. 5.2.

The five models are shown in Fig. 5.3. Sixteen pivot points along the chord at five percent chord intervals were available for each model. The Liebeck model was also tested in two additional configurations, the trailing edge wedge and the vortex generator strip. The trailing edge wedge, Fig. 5.4, had a length of 0.05 chord with an included angle of 90 degrees and a $(t/c)_{base} = 0.105$. The vortex generator configuration, Fig. 5.5, was based on the recommendations of Pearcey [20], where the length l, height, h, and spacing, d, were 0.01, 0.025 and 0.1 chord. The vortex generators were fabricated in the form of a continuous strip which could be positioned at any station along the chord. The tests were conducted with the strip at $x/c = 0.35$.

The two-dimensional models were mounted in a vertical position between the top and bottom of the wind tunnel, Fig. 5.6, and were free to rotate about a pivot aligned with the leading edge. The pivot position was variable along the section chord, with the center of rotation positions at five percent chord stations along the chord. Brass pivot pins were positioned in the top and bottom plates of the tunnel test section and were fitted into the brass plates that were

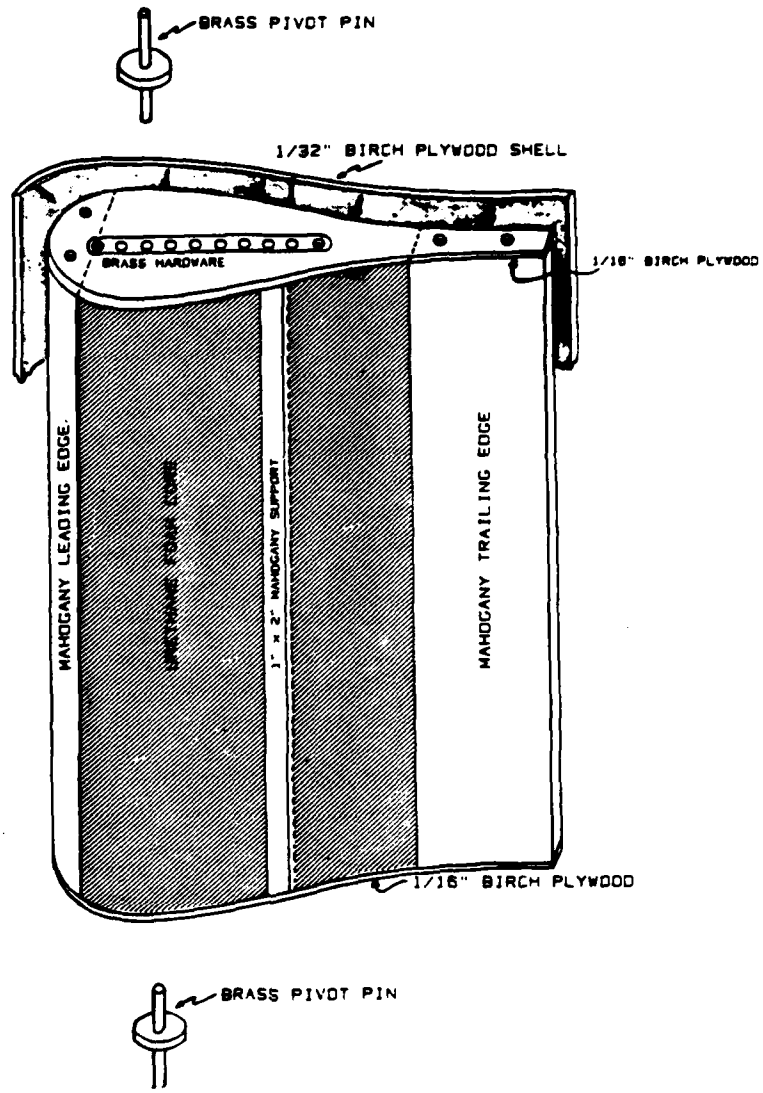

Fig. 5.2. Fairing model construction details.

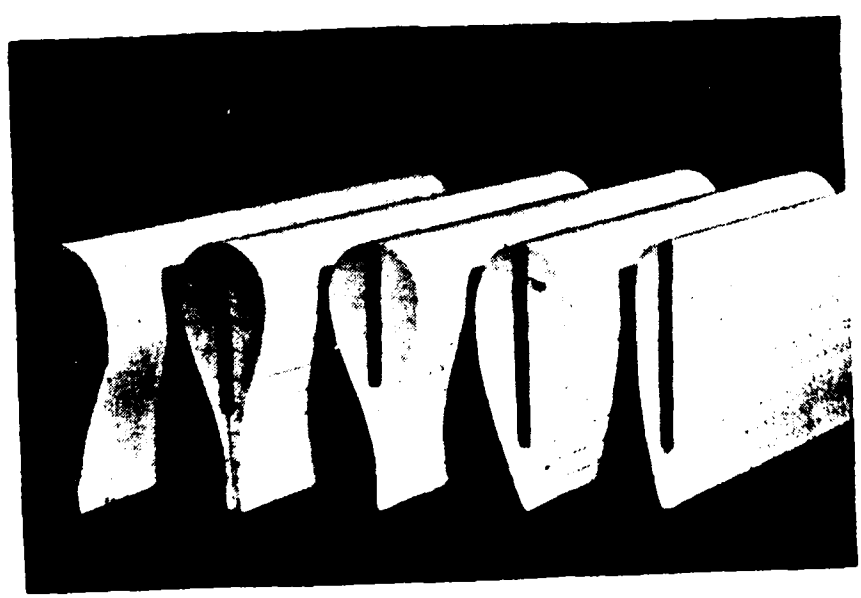

Fig. 5.3. Fairing section models.

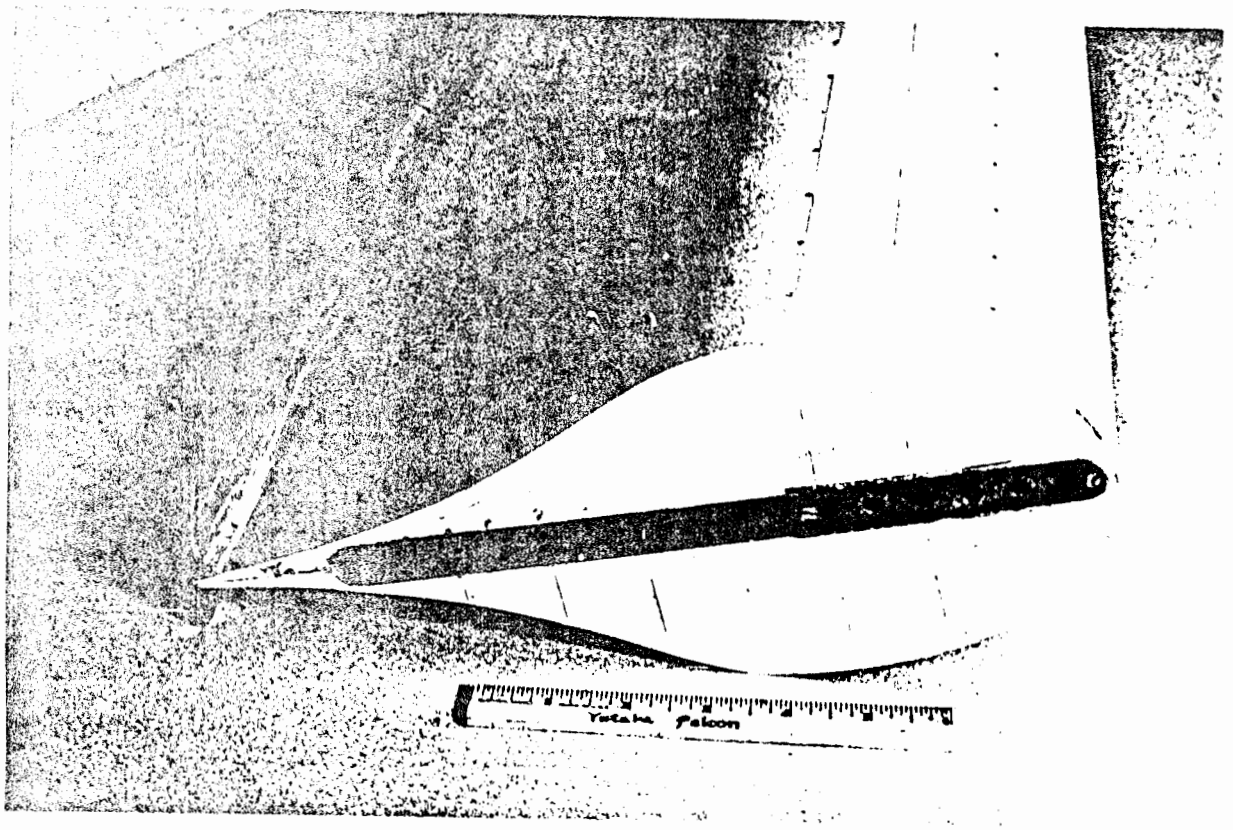

Fig. 5.4. Liebeck section with trailing edge wedge.

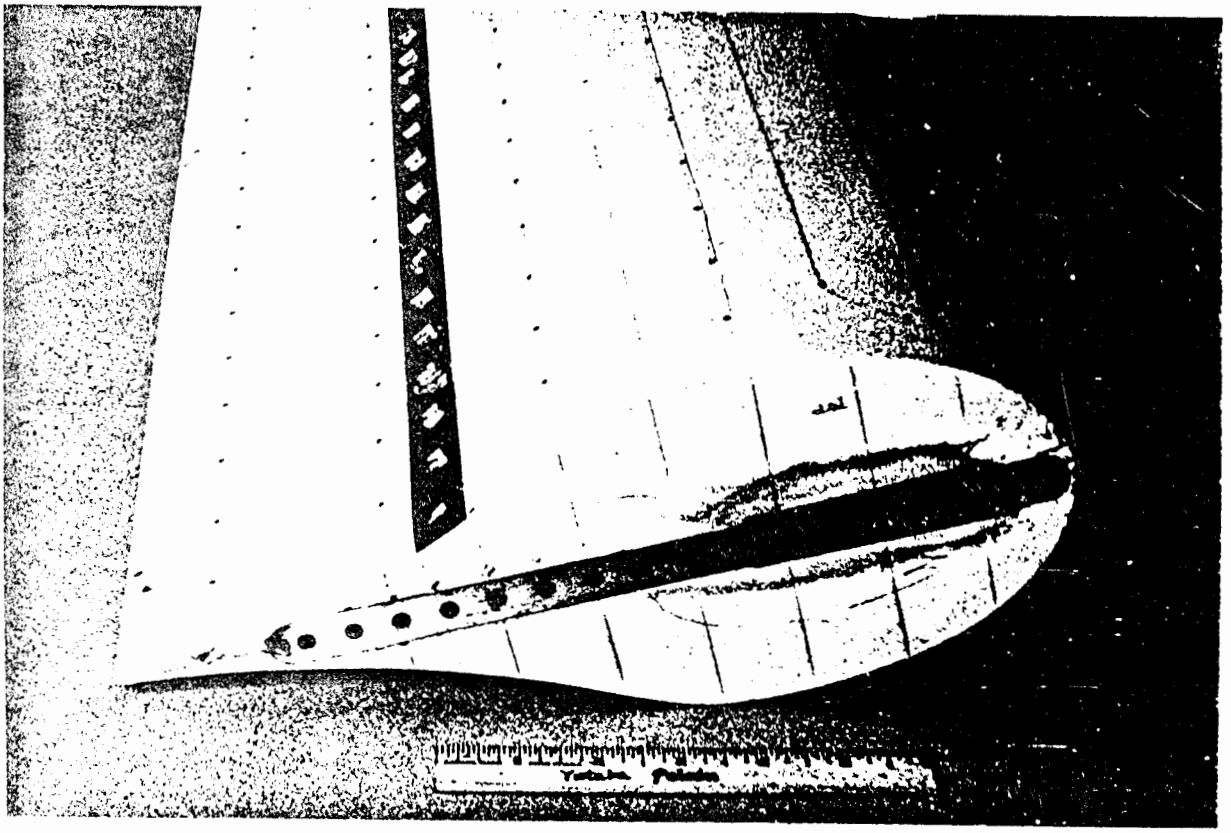

Fig. 5.5. Liebeck section with vortex generator strip.

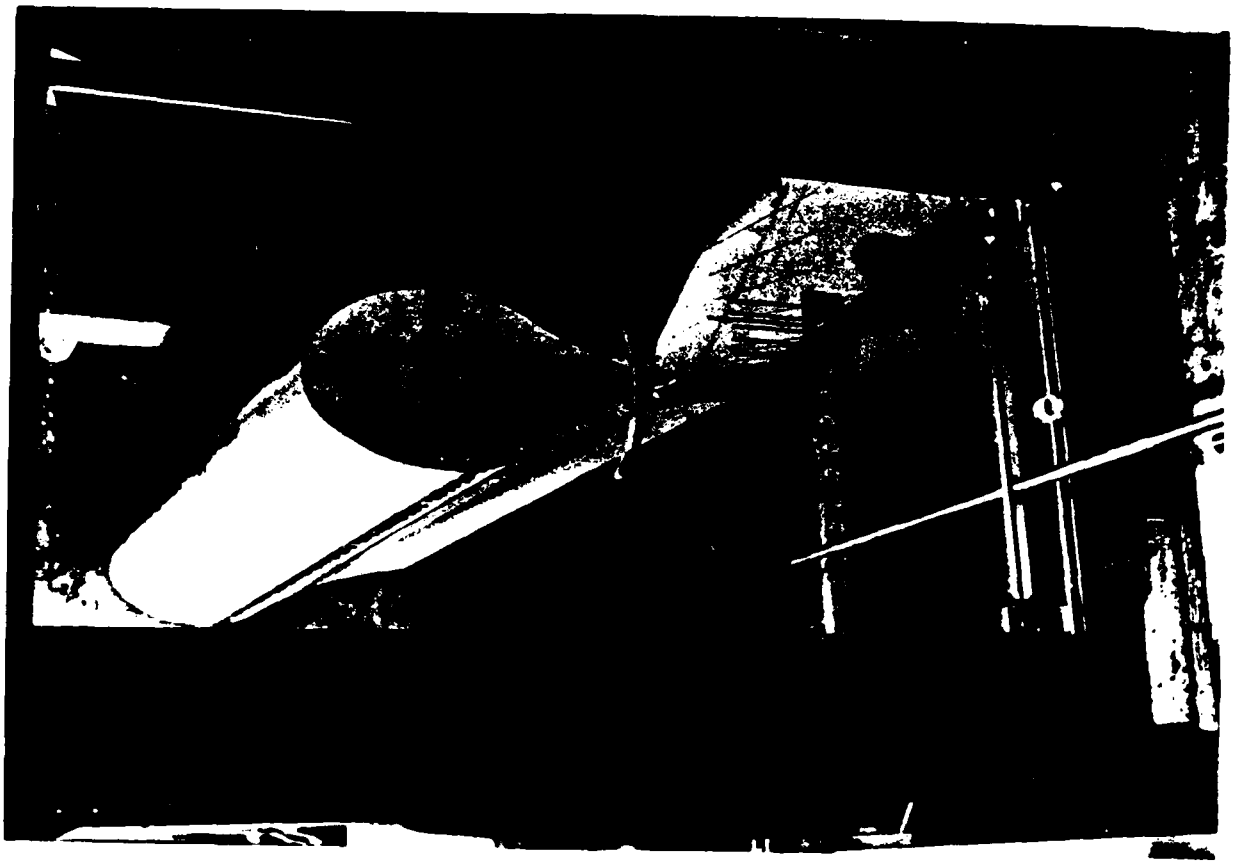

Fig. 5.6. Wind tunnel installation.

recessed into the top and bottom faces of the models. A clear plexiglass plate acted as the top viewing window for the wind tunnel test section. Several holes and a curved slot were cut in the plexiglass window to hold the pivot pin and locking pin and to mount the moment arm for torque measurements. A protractor was etched into the plexiglass so that the yaw angle of the model could be measured. The locking pin was used to prevent the rotation of the model and to align it with the flow when the wake survey was being conducted.

5.4. Data Acquisition System

An Apple II computer was used as the data acquisition system, Fig. 5.7. This system was chosen in part because of the availability of expansion hardware and software, and partly for the ease with which it could be transported to the non-instrumented wind tunnel. Table 5.2 lists the expansion cards that were added to the Apple II to render it capable of handling the acquisition, reduction, storage, and output of the data. The slot number indicates the card's location on the Apple bus.

Table 5.2 - Apple II Computer Expansion Hardware

Apple II Bus	Card Name	Manufacturer	Function
Slot 0	Ramcard	Microsoft	64K Memory
Slot 1	Grappler +	OrangeMicro	Printer Interface
Slot 2	SuperSerial Card	Apple	Serial Communictions
Slot 3	Videoterm	Videx	80-Column Display
Slot 4	AD 213	Tec-Mar	A/D Motherboard
Slot 5	Digisector DS-65	MicroWorks	Digitizer
Slot 6	Disk II Interface	Apple	DOS of 2 Disk Drives
Slot 7	Softcard	Microsoft	Z80A CPU

Peripherals included a Zenith monochrome video monitor, a Tec-Mar 12-bit A/D daughter board, a C.Itoh Model 8510A dot matrix printer, and an HP 7470A graphics plotter. The A/D converter was used for the

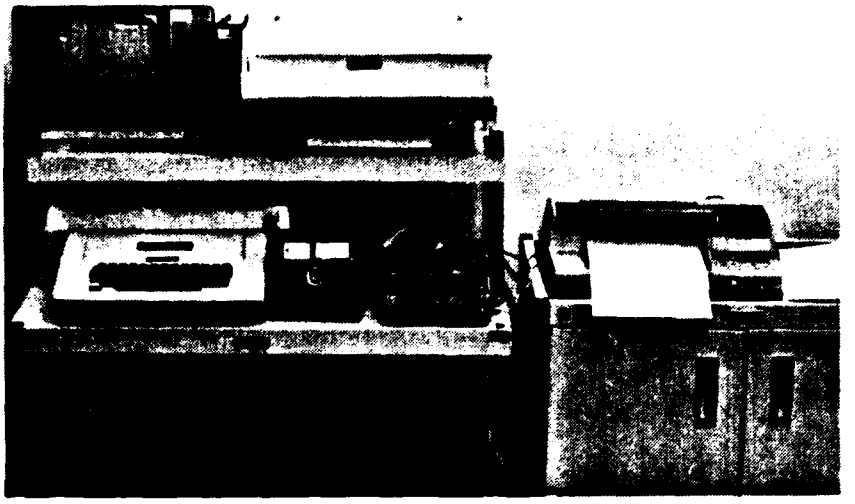

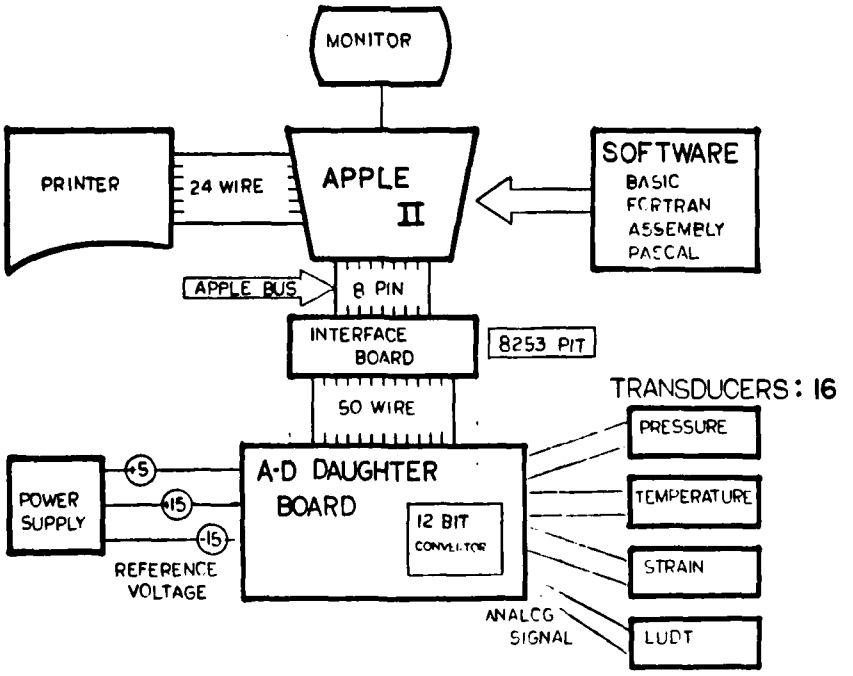

Fig. 5.7. Apple II microcomputer data acquisition system.

collection of the pressure and force data during the wind tunnel tests. Pressure measurements were made for the determination of the fairing drag and for recording upstream dynamic pressure. Force data were taken to determine the restoring moment coefficients. These measurements were not made simultaneously. The wake pressure survey was done with the fairing model pinned to prevent rotation. The models were free to pivot for the measurement of the restoring or destabilizing moments.

The analog output of the pressure or force transducers was input to the A/D conversion circuitry. The A/D board was manufactured by Tec-Mar, Inc. The signal conversion was handled with 12-bit accuracy at a rate of 30 kHz. The A/D daughter board included an Intel 8253 programmable interval timer (PIT) for timing and interrupt control. The analog input range was ± 10 volts. The digital output was in twos complement binary format. A Tec-Mar manufactured mother board handled the interfacing between the A/D and the Apple bus. Fig. 5.7 shows a schematic of the A/D conversion system.

Software for data acquisition was written in FORTRAN. The programs were compiled with a Microsoft compiler written for the Apple II. Copies of the data acquisition and reduction programs are contained in Appendices A and B. For both pressure and force signals, only the average value at each station was required. Thus the data reduction programs did not save each conversion, but summed the data and divided by the total number of conversions to determine the average signal. Five hundred conversions were made at the maximum frequency. Allowing for software handling, the signal was averaged over a period of 5 seconds. No analysis was done on the signal fluctuations nor frequency components.

The average digital signal was converted to pressure or force units using calibration constants that were calculated by a separate A/C conversion program. The balance of the data reduction programs handled the operator interaction and interrogation, the data integration, the nondimensionalization, the plotting, and the data output functions.

6.0. EXPERIMENTAL MEASUREMENTS

The following measurements were made:

(1) boundary layer visualization to determine positions of laminar to turbulent transition, and laminar or turbulent boundary layer separation

(2) wake survey to determine two-dimensional section drag coefficient

(3) determination of position of hydrodynamic center, or neutral stability point

(4) torque about the center of rotation as a function of yaw angle.

6.1. Boundary Layer Visualization

Two techniques were used for flow visualization, including fluorescent mini-tufts and an oil/ultraviolet light method. The fluorescent mini-tuft technique, developed by Crowder [21], utilizes extremely thin fluorescent nylon monofilaments, about 0.018 mm in diameter, attached to the model with a drop of lacquer adhesive. The use of the mini-tufts results in negligible interference with the flow, as determined by wind tunnel tests [21,22]. Thus a large matrix of tufts may be used for flow visualization without changing the flow patterns. The tufts were used to map the areas of turbulent boundary layer separation. The tufts, approximately 2.5 cm in length, must be viewed under ultraviolet light to contrast them with the white model surface. A matrix of the tufts was applied at 10 percent chord stations along the chord, with approximately equal spacings along the span of the model. With a white model background viewed under ultraviolet light, the model surface disappeared and the tufts were illuminated.

The second technique, which involved the use of oil and ultraviolet light, was used to determine the position of transition

from laminar to turbulent flow in the boundary layer, the existence of a laminar separation bubble and turbulent separation. The latter thus serves as a check on the fluorescent mini-tuft method. A mixture of kerosene (70 percent by volume), 104W0 motor oil (20 percent) and vinegar (10 percent) was used along with approximately four to five tablespoons of fluorescent yellow pigment per pint of the liquid. The kerosene provides the base for the mixture, the motor oil slows down the rate of evaporation of the kerosene in the wind stream, and the vinegar is used to keep the powdered fluorescent pigment in suspension. It has been found through experiments that a lemon yellow pigment used in combination with a white model background results in the highest contrast.

Both types of flow visualization were viewed under 100-watt ultraviolet lights approximately 0.5 to 1.0 m from the model. Photography was accomplished with settings of f/2 to f/4 at 1/15 to 1/30 of a second, using a Minolta ultraviolet light filter over a Griffin 1-A skylight filter.

6.2. Drag Coefficient

Two wind tunnel methodologies are available for determining the drag coefficient of streamline shapes. One technique requires the use of mechanical or electrical balances to which the model is attached, for direct measurement of the lift, drag, and pitching moment aerodynamic forces. The other technique is indirect. The profile drag is determined from the velocity distribution in the wake of the fairing. This method was chosen for this study because it was believed that the position of the hydrodynamic center could be determined with greater accuracy using the free pivoting technique. This precluded the use of models that would fit on the available wind

tunnel balance.

The momentum loss method for determining the profile drag is well known, Pope [15]. When the momentum equation is integrated around a control volume that includes the wake, it can be shown that the drag force on the body is given by the expression:

$$D = b\rho \int_{-\infty}^{\infty} U(U_\infty - U)\,dy . \qquad (6.1)$$

6.2.1. Momentum Wake Rake

This integration must be done with the wake profile data taken far enough downstream from the body so that the static pressure at the measuring section is equal to that in the undisturbed stream. Pope [15] states that locating the wake rake at least 0.7 chord behind the trailing edge of the wing is sufficient.

The wake rake, shown in Fig. 6.1, was positioned at mid-tunnel height and 0.678 chord, 20.3 cm, length downstream of the model trailing edge. The wake rake was fixed in this position and was not adjustable to port or starboard. Thirty-one total head probes were spaced at 0.5 in. (1.27 cm) intervals along the wake rake. The center 5 probes were spaced 38.1 cm apart. The total width of the wake survey was 38.1 cm. The probes, 0.16 cm o.d. rigid stainless steel tubing, extended 7.62 cm from the body of the rake. Static pressure probes were made from the same tubing. These tubes extended 10.16 cm from the rake body and the ends were sealed and rounded. Four 0.08 cm holes were drilled perpendicular to the axis of the tubing, 2.54 cm downstream from the leading edge. The static probes were spaced at 5.08 cm intervals over the center 31.75 cm of the wake rake. The static pressures were taken in the same plane and the same

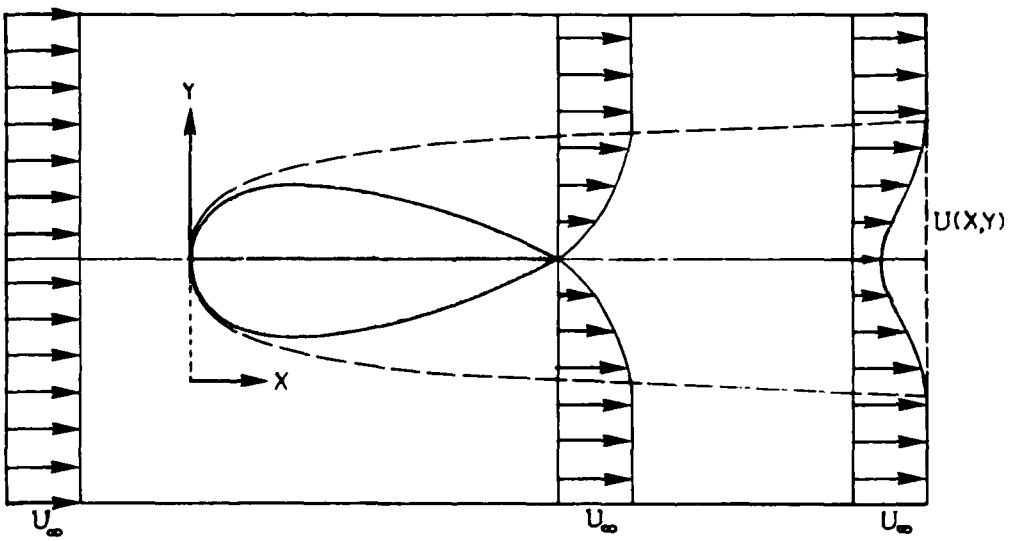

Fig. 6.1. Wake rake and geometry of the momentum deficit calculation.

distance downstream from the model as the total head measurements.

Flexible, multi-colored "strip-a-tube" was lead through the body of the wake rake, down through the faired supporting struts, and out to a distribution panel. Each pressure tap of the wake rake was individually connected by way of a valve system to a differential pressure transducer. Six of the ten static pressure probes from the central region of the wake were attacked to one side of the transducer, thus providing the average static pressure in the wake. The total head probes were then individually input to the other side of the transducer. The output signal was the dynanic pressure at each station in the wake, ($q = H - P_s$).

The transducer was a Dynasciences model P109D 0 to ±15 PSID variable reluctance type differential pressure transducer. The transducer was driven by a Dynasciences model CD10 DC output Carrier-Demodulator operating at 10 DC volts full scale. The wake dynamic pressures varied from 0.003 PSIG to 0.1 PSIG. The output voltage ranged from 1.0 to 3.0 volts. Calibration curves were calculated before each set of wake surveys using a kerosene manometer. The calibrations were linear to ±0.1 percent of best straight line fit. The output voltages from the transducer were input to the A/D circuit described in Section 5.4.

The data reduction program prompted the operator to open each probe valve in sequence, and then collected, converted, and stored the pressure data. The data collected from the port and starboard side of the wake were folded and averaged so that the wake was forced to be symmetrical. The integration required by Eqn. 6.9 was accomplished using the Fritsch-Carlson [23] formulas for piecewise cubic data interpolation and Gauss-Legendre Quadrature numerical

integration [24]. The limits of the integration (the wake width) were determined by operator inspection of the wake profile shape. The program plotted the wake profile and the operator would then choose and input the integration limits. A sample wake survey profile for the Liebeck section is shown in Fig. 6.2 for $R_c = 0.511 \times 10^6$. The symmetry of the wake profile was due to the folding and averaging described above.

The experimental parameters (model name and configuration, date, model dimensions, rake position, and probe locations) were read into the program from a special parameter file. The wind tunnel operating conditions of temperature and upstream dynamic pressure were input by the program operator. The program then calculated the downstream R_c, the blockage correction factor used in Eqn. 6.9, and the drag coefficient.

The drag coefficient may be based on planform area (bc) as is common in aeronautical work, or on frontal area (bt), as is common practice among marine engineers. Thus

$$C_{d_{(bc)}} = D/\tfrac{1}{2}\rho U_\infty^2 bc \tag{6.2}$$

or

$$C_{d_{(bc)}} = D/\tfrac{1}{2}\, U_\infty^2 bt\ . \tag{6.3}$$

Throughout this paper the drag coefficients will be given based on frontal area. Using Equation 6.2, the drag coefficient equation becomes:

$$C_{d_{(bc)}} = \frac{2}{c}\int_{-\infty}^{\infty}[(q/q_\infty)^{1/2} - (q/q_\infty)]dy. \tag{6.4}$$

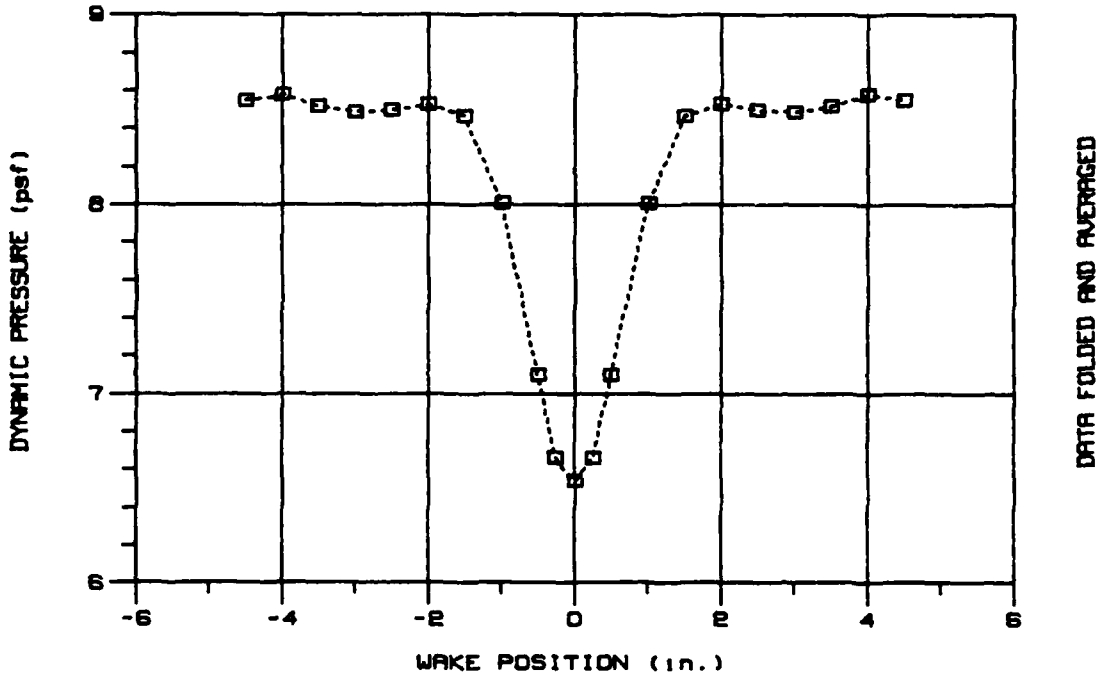

Fig. 6.2. Wake profile for Liebeck section at $R_c = 0.511 \times 10^6$.

6.2.2. Blockage Correction

The flow conditions that the model experiences in a wind tunnel are not the same as those in free air or the open ocean. The presence of the wind tunnel walls changes the velocity of air flow over the model. The two corrections that are important in the calculation of drag coefficients are "solid blockage" and "wake blockage." Pope [15] defines the total blockage as

$$E = E_{sb} + E_{wb} \tag{6.5}$$

where E is the sum of the solid blockage, E_{sb}, and the wake blockage, E_{wb}. Or, in terms of the change in freestream velocity due to the presence of the model

$$E = (U_o/U_\infty) - 1 \tag{6.6}$$

or

$$E = \sqrt{q_o/q_\infty} - 1 \tag{6.7}$$

where U_o and q_o are the velocity and dynamic pressure downstream of the model at the edge of the wake.

The correction of the wake survey drag coefficient for blockage by the method proposed by Shaw, Sotos and Solano [23] of NACA Lewis Research Center. They employed the following procedure to correct for the effects of blockage.

(1) The original wake survey is examined to determine the endpoints of the viscous wake.

(2) The values of the velocity ratio (U_o/U_∞) for the two wake endpoints are compared, and the larger volume used to calculate a velocity ratio correction factor by subtracting 1.0 from this

value.

(3) All velocity ratio values contained within the viscous wake are adjusted by subtracting the velocity ratio correction factor prior to computing the section drag coefficient.

The wake data were corrected for blockage in the following manner. The blockage correction factor was first determined experimentally as

$$E = (U_o/U_\infty) - 1 = \Delta U/U_\infty \tag{6.8}$$

where: U_∞ = upstream velocity

U_o = downstream velocity at edge of wake.

The drag coefficient was then computed using the NASA method described in Shaw, et al. [24], which includes the blockage correction factor.

$$C_{d_{(bc)}} = \frac{2}{c} \int_{-y_o}^{y_o} [(U/U_\infty - E)(1 - \frac{U}{U_\infty} + E)]dy \tag{6.9}$$

where: U = wake velocity

dy = distance across wake.

6.2.3. Base Drag Coefficient

Static pressures at the blunt trailing edge were measured for three of the fairing section shapes. A static pressure probe was mounted along the centerline of the trailing edge. Pressure taps were drilled in this probe at six-inch intervals over the center 18 inches of the fairing span. The static pressures were measured relative to the free stream static pressures which were measured downstream from the model at the wake rake.

The contribution to the total drag of the blunt trailing edge was calculated from the following equations.

$$C_{d_{te}} = P_s A/qbc \qquad (6.10)$$

where:

$C_{d_{te}}$ = base drag coefficient,

P_s = base static pressure

A = bt_{te} = base area of trailing edge,

q = downstream dynamic pressure corrected for blockage effects,

bc = fairing planform area.

The ratio $C_{d_{te}}/C_{d_{(bc)}}$ is the fraction of the total drag due to the blunt trailing edge.

6.3. Hydrodynamic Center

6.3.1. Definition

The aerodynamic center is defined as the position along the airfoil chord for which the moment coefficient , C_{mac}, is constant, that is, independent of C_L.

$$a.c. = n - dC_{m_n}/dC_L \qquad (6.11)$$

where

$C_{m_{a.c.}}$ = constant (= 0. for symmetrical section)

n = moment center location along chord

C_{m_n} = moment coefficient about n

C = M_n/qSC

C_L = lift coefficient.

For symmetrical sections, the value of the pitching moment coefficient, C_{m_n}, is zero.

The neutral point is defined as that point along the chord where the slope of the pitching moment versus lift coefficient curve is equal to zero, i.e.,

$$dC_{m_n}/dC_L = 0 \qquad (6.12)$$

and

n = neutral point location.

Thus for a symmetrical section,

$$\text{a.c.} = n - dC_{m_n}/dC_L \qquad (6.13)$$
$$= n - 0$$

and

$$\text{a.c.} \equiv n.$$

Therefore, for symmetrical sections, the neutral point and the aerodynamic center are one and the same. In this study the terms aerodynamic center and hydrodynamic center are used interchangeably.

6.3.2. Free Pivot Technique

Two methods were used to find the chordwise position of the hydrodynamic center. In the first method, a visual measurement was made of the equilibrium angle of attack of the fairing as a function of the mechanical pivot location. When the pivot point is forward of the hydrodynamic center, the fairing will remain aligned with the flow, exhibiting "weathervane" stability and the angle of attack will be zero degrees.

The pivot location was moved progressively aft in steps of 0.05 c. At each pivot position the equilibrium angle of attack was recorded. The angles were measured using the protractor that was inscribed in the plexiglass top of the wind tunnel. The accuracy of the readings was ±0.5 deg. When the pivot position is moved aft of the hydrodynamic center, the fairing will assume an equilibrium angle of attack other than zero degrees. This equilibrium angle will be positive or negative, depending on the direction of the initial

disturbance. Because the step size between pivot positions was 0.05 c, the hydrodynamic center was located by this technique with an accuracy of +0.025 c.

6.3.3. Pivot Point Torque Technique

Restoring or destabilizing moments were measured about several pivot points as an alternative method of locating the hydrodynamic center. When the mechanical center is forward of the hydrodynamic center, the moments tend to align to fairing with the flow. When the mechanical center is aft of the aerodynamic center, the moments are destabilizing and cause misalignment with the flow. Thus the sign of the moment coefficient changes from negative to positive as the pivot location moves aft past the hydrodynamic center.

The moments were measured using a free pivot technique. The fairing model, free to to pivot about a selected chordwise position, was rotated to an equilibrium angle of attack to the flow with a force transducer to measure the restoring or destabilizing moment about the pivot location.

The output signal from the force transducer was connected to an A/D converter driven by the Apple computer. Moment data were taken for each fairing, at pivot locations ranging from 5 to 35 percent of the chord length, and for geometric angles of attack ranging 0 to 20 degrees in increments of two degrees. The upstream dynamic pressure was approximately 8.0 psf (Reynolds number 0.5×10^6).

The data reduction program calculates and prints the moment coefficient as a function of angle of attack for each pivot location. The moment coefficient is

$$C_m = Fr/qbc^2 \qquad (6.14)$$

where r is the moment arm and F is the measured force.

Because of the presence of the wind tunnel walls, the measured moment coefficients differ from the moments that would be experienced by a fairing in the open ocean. A correction is necessary due to the effects of blockage and streamline curvature that results from the presence of the walls. The measured moment coefficients are greater than they would be in the freestream environment.

Pope [15] gives the moment coefficient correction as

$$C_m = C_{m_n}(1 - 2E) + \sigma C_l/4 \qquad (6.15)$$

with

$$\sigma = (\pi^2/48)(C(h)^2 = 0.04.$$

The subscript, u, indicates the uncorrected coefficient. The correction to the moment coefficient is a function of blockage, E, and the lift coefficient, C_l. The lift coefficient is a function of angle of attack, α. Likewise, the measured angle of attack must be corrected for the effects of streamline curvature. Pope gives this correction as

$$\alpha = \alpha_u + \frac{57.3}{2\pi}\alpha(C_{l_u} + 4C_{m_n}). \qquad (6.16)$$

With the free pivot technique used in this project, it was not possible to measure the lift coefficients and the blockage factor upon which both these corrections depend. Thus the presented moment data are uncorrected for wind tunnel boundary conditions and can only be used as indications of the location of the hydrodynamic center. For small angles of attack, less that ±60 deg., the moment data have been

corrected for the effects of blockage. For these small angles, was taken from the drag measurement data and C was assumed to be near zero. Thus Equation 6.15 becomes

$$C_m = C_{m_u}(1 - 2E_o) \tag{6.17}$$

where E_o is the blockage measured at zero angle of attack.

Corrections to the measured angles of attack, α_u, were not calculated. The resulting error in C_m ranges from 0 to 5 percent as ranges from 0 to 20 deg., assuming a maximum lift coefficient of 1.0. and maximum moment coefficient of 0.5.

7.0. EXPERIMENTAL RESULTS

7.1. Liebeck Section

7.1.1. Boundary Layer

The results of both boundary layer visualization surveys for all three Liebeck model configurations are shown in Figs. 7.1, 7.2., and 7.3 as a function of Reynolds number. Noted are the chordwise position of the transition from laminar to turbulent boundary layer, the existence of a laminar separation bubble and turbulent boundary layer separation. A laminar separation bubble was found to exist at the transition from laminar to turbulent flow. The position of this laminar separation bubble coincided approximately with the point of minimum pressure coefficient, which is at approximately 40 percent of the chord. It is seen from Fig. 7.1 that past a Reynolds number of 4.0×10^5, the turbulent separation over the aft portion of the section has completely disappeared. At the lower Reynolds numbers, approximately 1×10^5 to 2.7×10^5, the aft portion was separated from about 40 percent chord on. The boundary layer studies were conducted simultaneously on either side of the model.

The vortex generators, which were fixed at 0.35 c, eliminated the turbulent separation at all but the lowest Reynolds number, Fig. 7.2. The addition of the trailing edge wedge, Fig. 7.3, had no effect except at the higher Reynolds numbers. A standing vortex flow was generated in the region of the wedge, such that a turbulent boundary separation condition was initiated. In all three cases, the transition from laminar to turbulent flow occurred at the same location. Transition occurred at 0.30 c for the low Reynolds number of 1.2×10^5 and moved progressively aft to 0.47 c at 5.5×10^5. The effect of the massive turbulent separation from 1.0 to

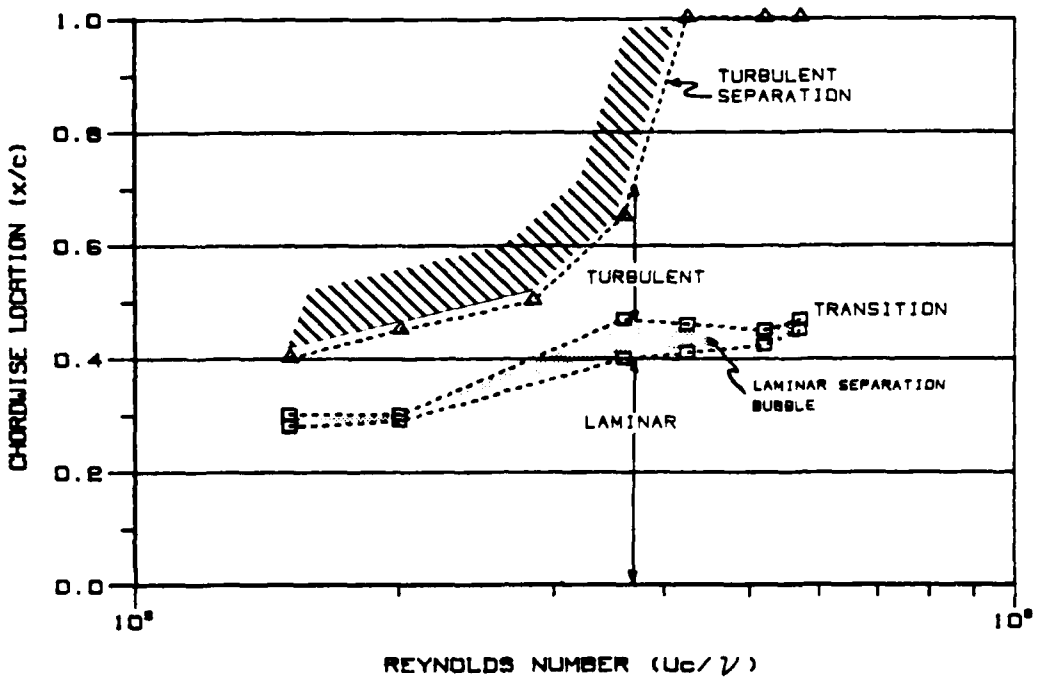

Fig. 7.1. Results of the boundary layer survey of the Liebeck section.

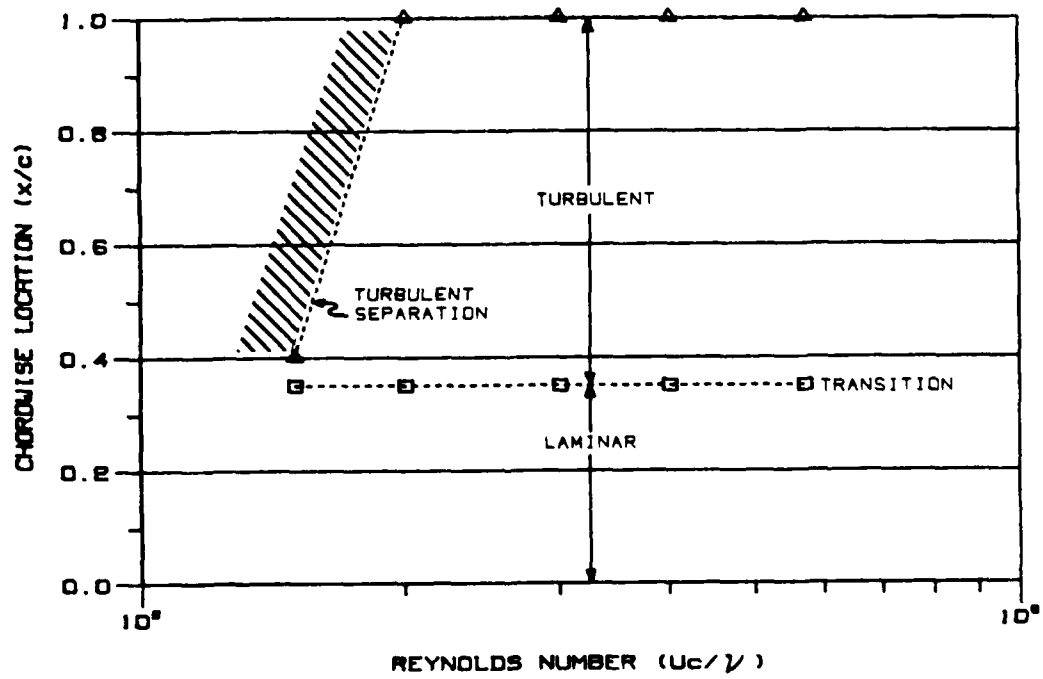

Fig. 7.2. Results of the boundary layer survey of the Liebeck section with vortex generators.

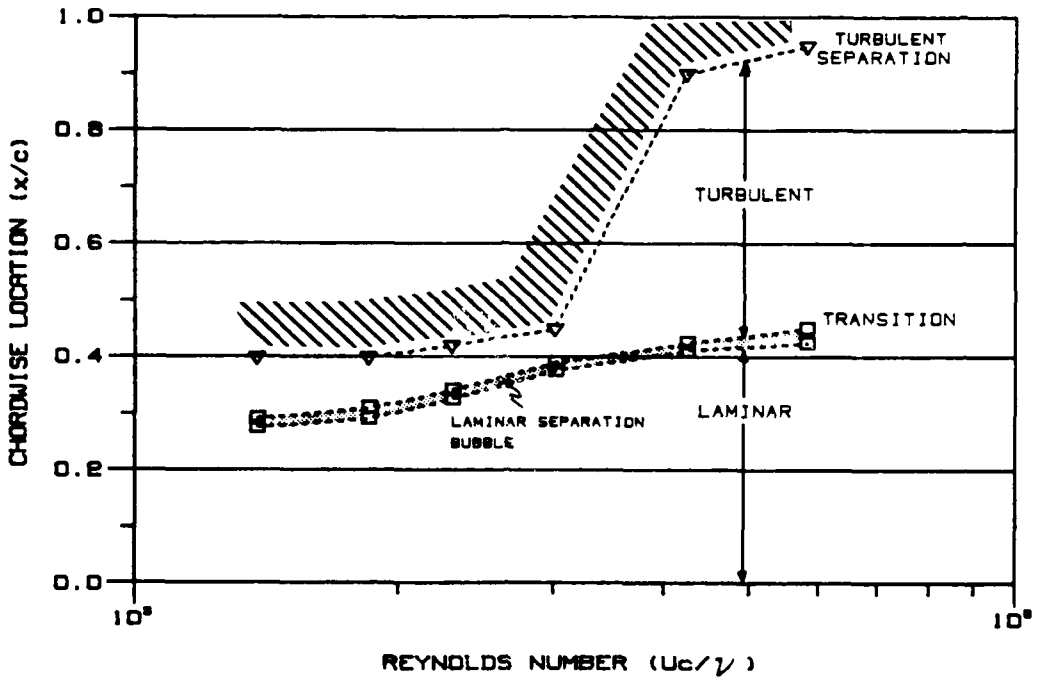

Fig. 7.3. Results of the boundary layer survey of the Liebeck section with trailing edge wedge.

2.7×10^5 apparently caused this migration forward.

The results of the fluorescent mini-tuft survey, Figs. 7.4 and 7.5, show the fully attached flow for the baseline configuration at a Reynolds number of 3.9×10^5, and the effect of the standing vortex on the trailing edge wedge flow pattern. The separated flow condition which existed for a Reynolds number of 1.5×10^5 is shown in Fig. 7.6. Separation starts at approximately the 45 percent chord position, after which the motion of the mini-tufts is quite dramatic. The oil technique results are shown in Fig. 7.7 for a Reynolds number of 4.0×10^5. The beginning of the laminar separation bubble can be seen at the 40 percent chord station. The fully attached turbulent boundary layer aft of this location can be distinguished from the laminar boundary layer forward of this location by the relative contrast between the pigment coating which remains on the surface. Since the shearing stress levels are lower in the laminar boundary layer, less of the oil is scrubbed away, and consequently the yellow pigment has a much higher contrast in this area. In the turbulent boundary layer, the shearing stress levels are higher and consequently more of the liquid is scrubbed away, resulting in a darker area.

7.1.2. Drag Coefficient

The blockage correction factors are shown in Fig. 7.8 as a function of Reynolds number based on U_o. Blockage over the Reynolds number range tested varies from 57 down to 2 percent for the baseline model, while it was constant at about 13 percent for the trailing edge wedge configuration. The addition of the vortex generators to the baseline model decreased the blockage due to modification of the boundary layer. A typical baseline model wake profile for a Reynolds number of 0.511×10^5 is shown in Fig. 6.2. The symmetry of the

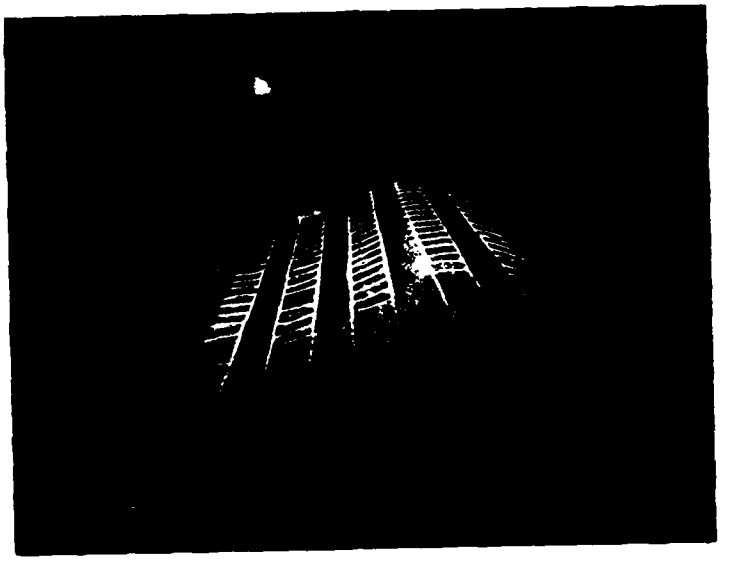

Fig. 7.4. Liebeck section with mini-tufts ($R_e = 3.9 \times 10^5$).

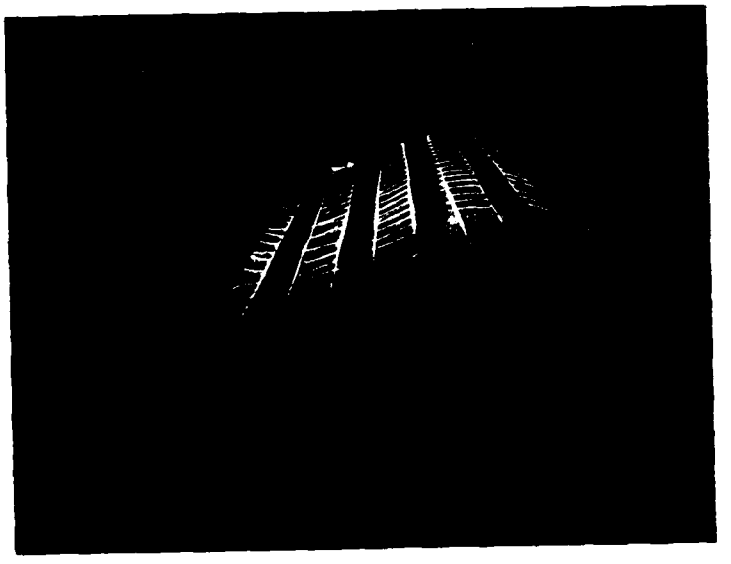

Fig. 7.5. Liebeck section with trailing edge wedge and mini-tufts ($R_e = 3.9 \times 10^5$.

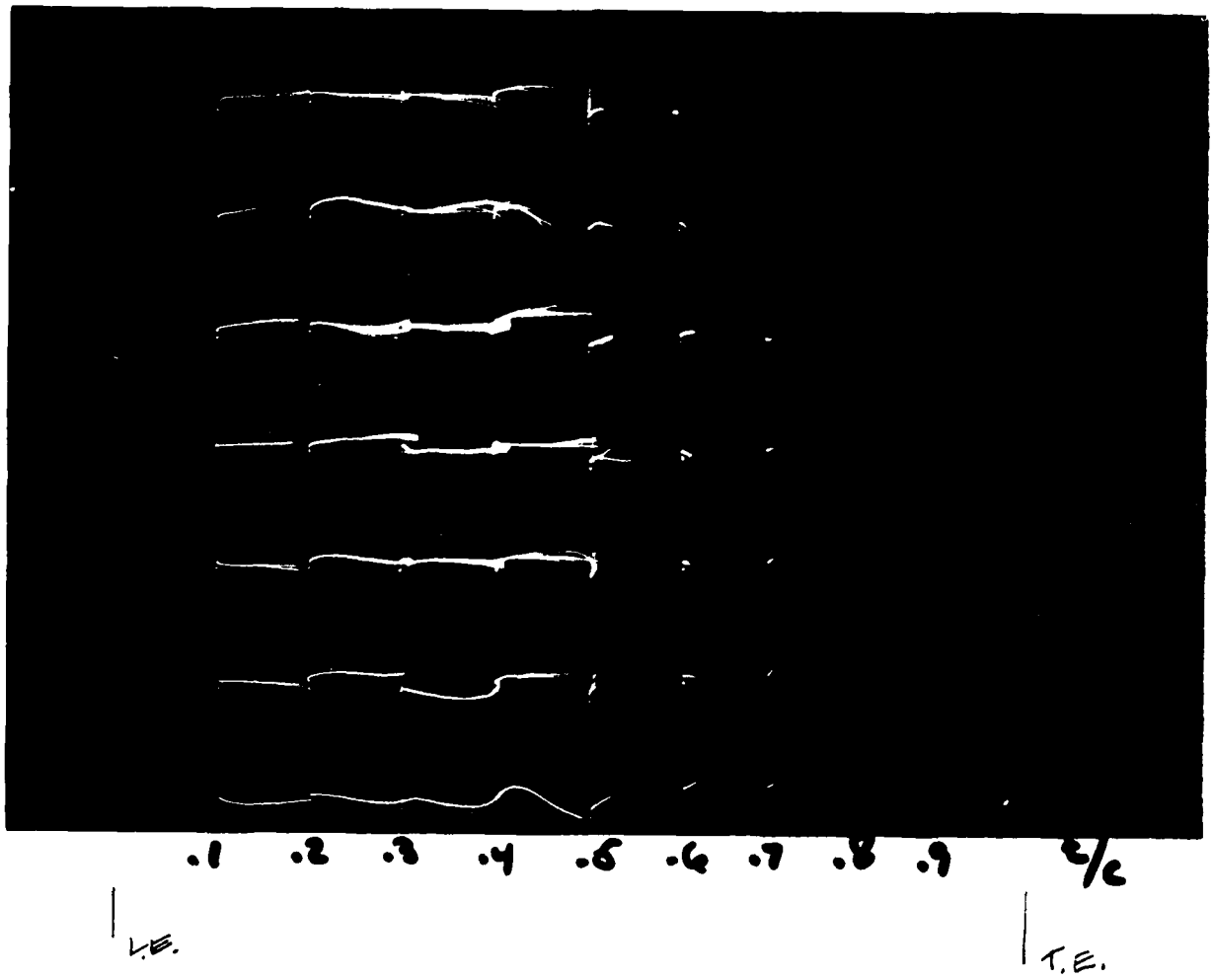

Fig. 7.6. Baseline/mini-tufts ($R_e = 2.5 \times 10^5$).

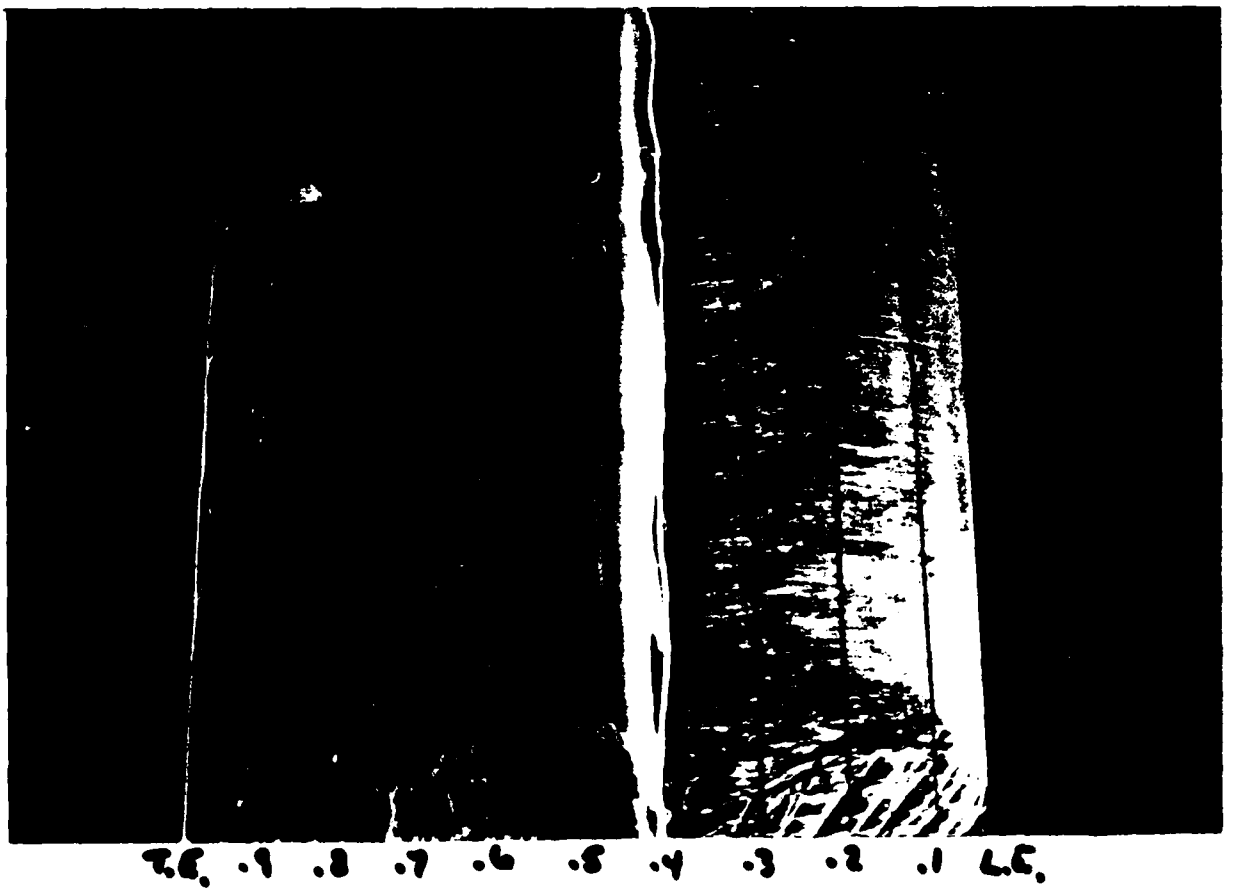

Fig. 7.7. Baseline/oil-ultraviolet light ($R_e = 4.0 \times 10^5$).

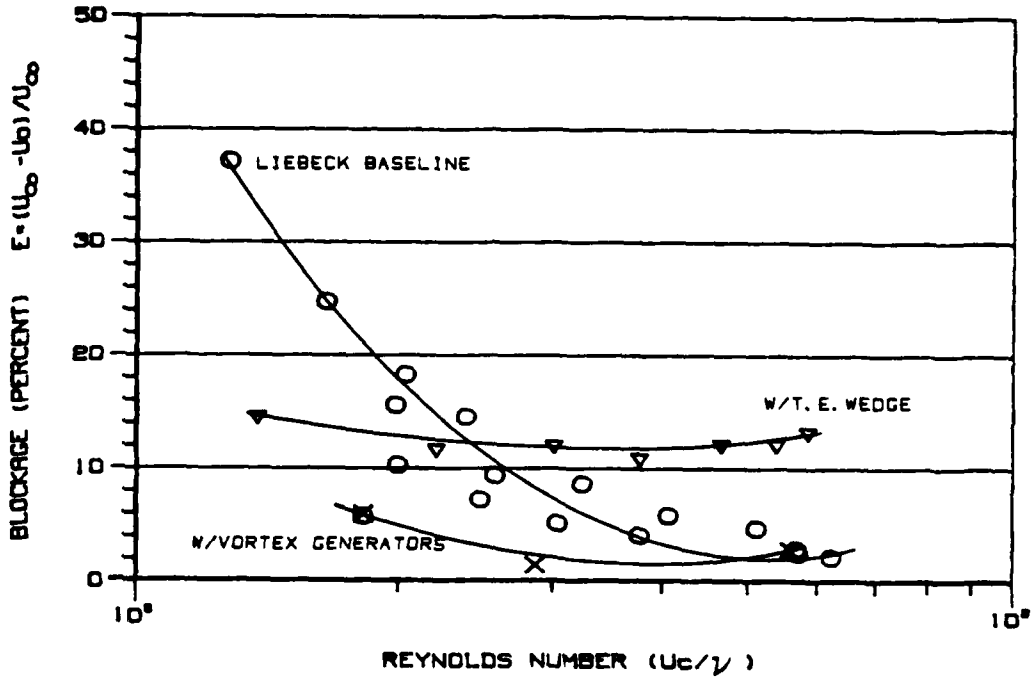

Fig. 7.8. Measured blockage of the Liebeck sections.

profile is due to port and starboard averaging of the data.

The two-dimensional drag coefficient corrected for blockage for the three configurations tested is shown in Fig. 7.9 as a function of the Reynolds number based on chord. In order to provide a comparison, the results from Hoerner [11] are included for symmetrical sections with thickness/chord ratios of 37 and 50 percent. It should be noted that the drag coefficient is based on the projected frontal area rather than the planform area. The shape of the baseline section curve is seen to agree well with the Hoerner curve. The drag coefficient decreases down to a Reynolds number of 4×10^5, after which it is approximately constant.

The addition of the vortex generators, which eliminated the boundary layer separation at the low Reynolds number, is shown to decrease the drag coefficient in this region. The crossover point occurs at a Reynolds number of about 3.0×10^5, which agrees with the results shown in Fig. 7.1, where the turbulent separation disappeared on the baseline model. At Reynolds numbers above this point, the model with the vortex generators had a higher drag coefficient, indicating that the drag of the vortex generators themselves was quite large when working in a range where they had no effect on the boundary layer.

The addition of the trailing edge wedge is seen to increase the drag coefficient over most of the Reynolds number range. At the higher Reynolds numbers, the drag coefficient is higher by a factor of three.

For the Liebeck 40 percent section with the trailing edge wedge, the percentage of trailing edge drag, Fig. 7.10, varied from 15 to 56 percent for the Reynolds numbers tested. For this case, the

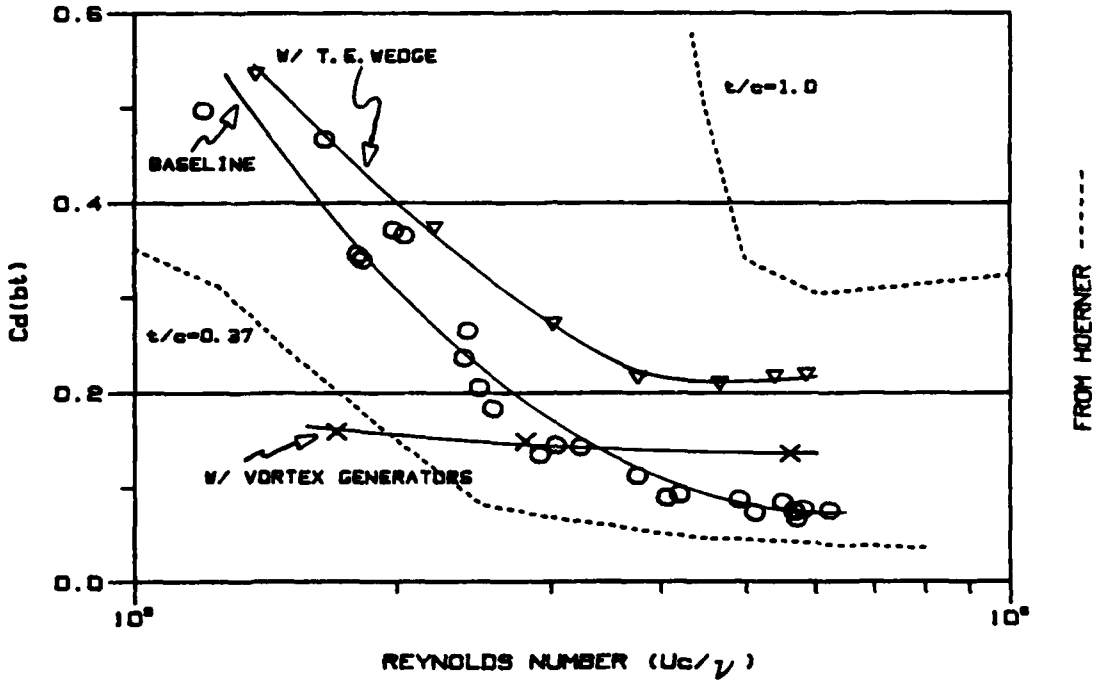

Fig. 7.9. $C_{d(bt)}$ vs. R_c for the Liebeck 40% section.

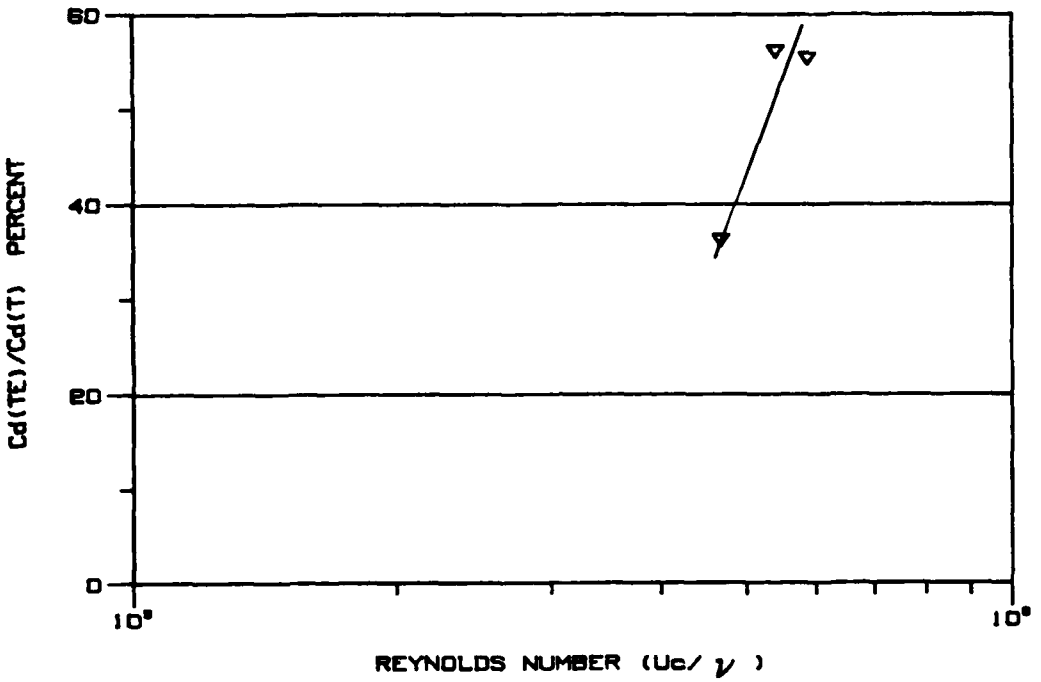

Fig. 7.10. Ratio of the base drag to total drag for Liebeck 40% section

contribution to the total drag of the trailing edge wedge was not constant but varied significantly with Reynolds number. At the low Reynolds number of 0.13×10^6, the static pressure was greater than the freestream static pressure, indicating separated flow at the trailing edge. The boundary layer visualization indicated that separation had occurred for all Reynolds numbers less than 0.35×10^6.

7.1.3. Hydrodynamic Center

The results of the hydrodynamic center (neutral point) location study are shown in Fig. 7.11 for a Reynolds number of 4.8×10^5. As can be seen for the baseline section, the hydrodynamic center is quite far forward, at about 20 percent of the chord. For pivot positions aft of this station, the model would assume a bistatically stable position at either a plus or a minus yaw angle, depending on which way the initial disturbance was directed. The unstable region increases until finally, past stations at approximately 30 percent of the section chord, it widely diverges.

The effect of adding the trailing edge wedge, Fig. 7.11, is dramatic. The model is seen to be stable for pivot positions all the way up to 35 percent of the chord, past which point it was bistatically unstable. This indicates that the addition of the trailing edge wedge would allow the use of a larger diameter cylinder. The penalty to be paid for this, of course, is the higher drag coefficient over the operating Reynolds number range.

The restoring torque coefficient is shown in Fig. 7.12 as a function of pivot location along the chord length for each yaw angle. The point where each curve crosses the zero moment axis corresponds to the neutral point position. At small angles of attack (≤ 2 deg.), this position corresponds with the data of Fig. 7.11.

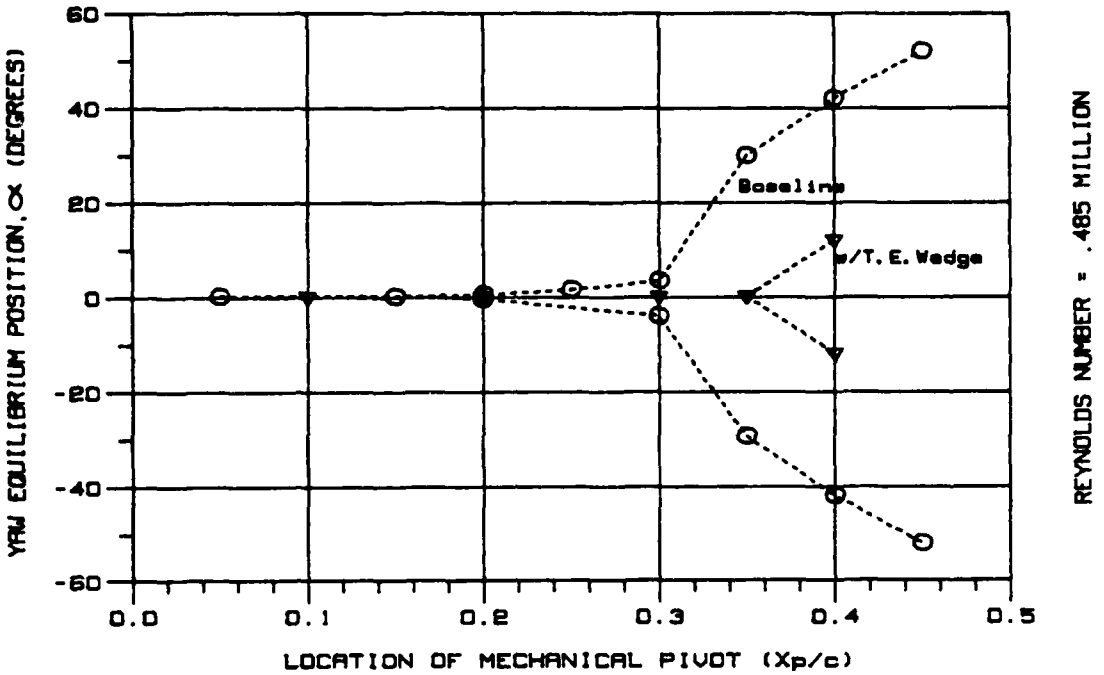

Fig. 7.11. Yaw equilibrium positions for the Liebeck sections.

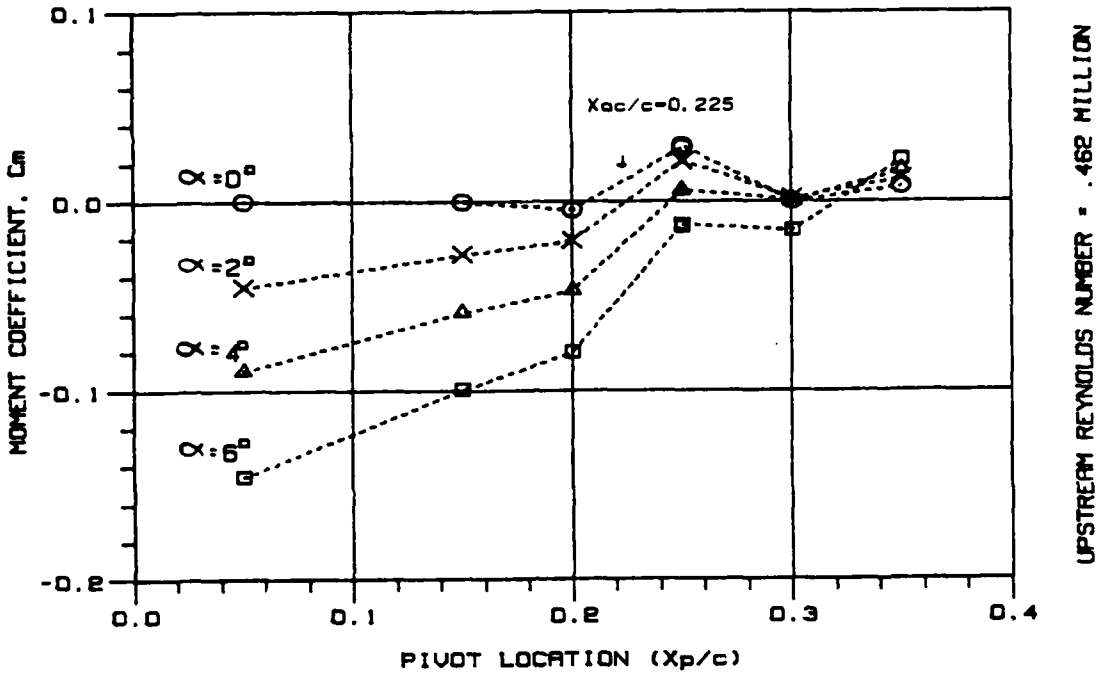

Baseline Section

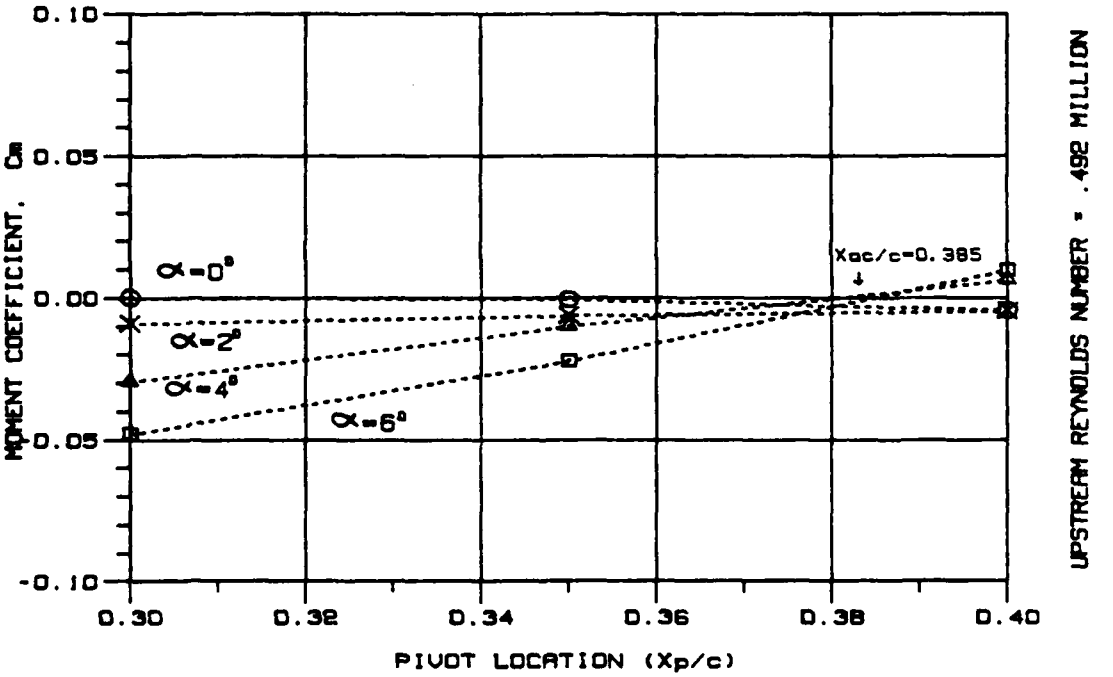

Trailing Edge Wedge

Fig. 7.12. c_m vs. pivot position for the Liebeck section.

7.2. Fathom Fairing Section

7.2.1. Boundary Layer

The boundary layer survey results for the Fathom section shown in Fig. 7.13. Transition occurred at the 20 percent chord position and moved forward with increasing Reynolds number to the 15 percent chord position. For this section the laminar to turbulent boundary layer transition occurred downstream of the minimum pressure point, which was located at the 9.8 percent chord position. A laminar separation bubble also occurred at the transition location. The bubble length, approximately 10 percent chord length at the lowest Reynolds number, decreased in length as Reynolds number increased.

Turbulent separation occurred just before the trailing edge at the 95 percent chord position for all Reynolds numbers tested. This was in agreement with the results of Henderson [2], who also found separation at the 95 percent chord position at a Reynolds number of 0.22×10^6.

7.2.2. Drag Coefficient

The measured blockage correction factors for the Fathom Flexnose section are shown in Fig. 7.14. Blockage ranges from a high of 40 percent at the lowest Reynolds number to 12 percent at the highest. The curve is quantitatively similar to the blockage found for the Liebeck sections. However, the blockage effect seems quite large considering the section t/c ratio.

Because there were no major changes in the behavior of the boundary layer throughout the Reynolds number range tested, the drag coeffients, Fig. 7.15, remained fairly constant. The measured drag coefficients are in good agreement with the one data point measured by Henderson.

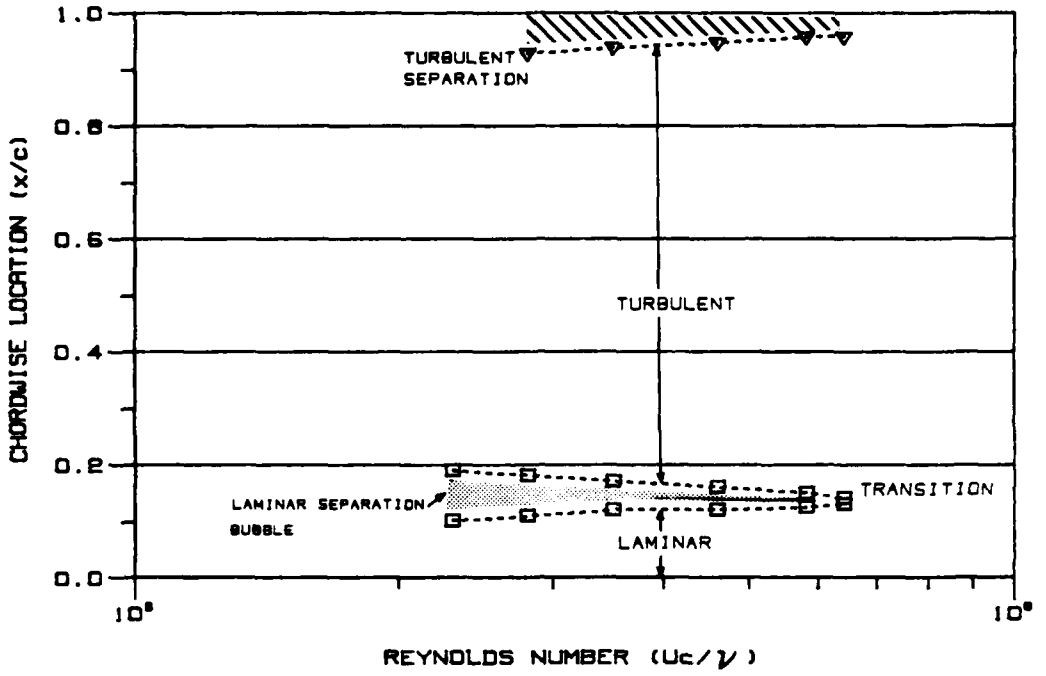

Fig. 7.13. Results of the boundary layer survey of the Fathom Flexnose section.

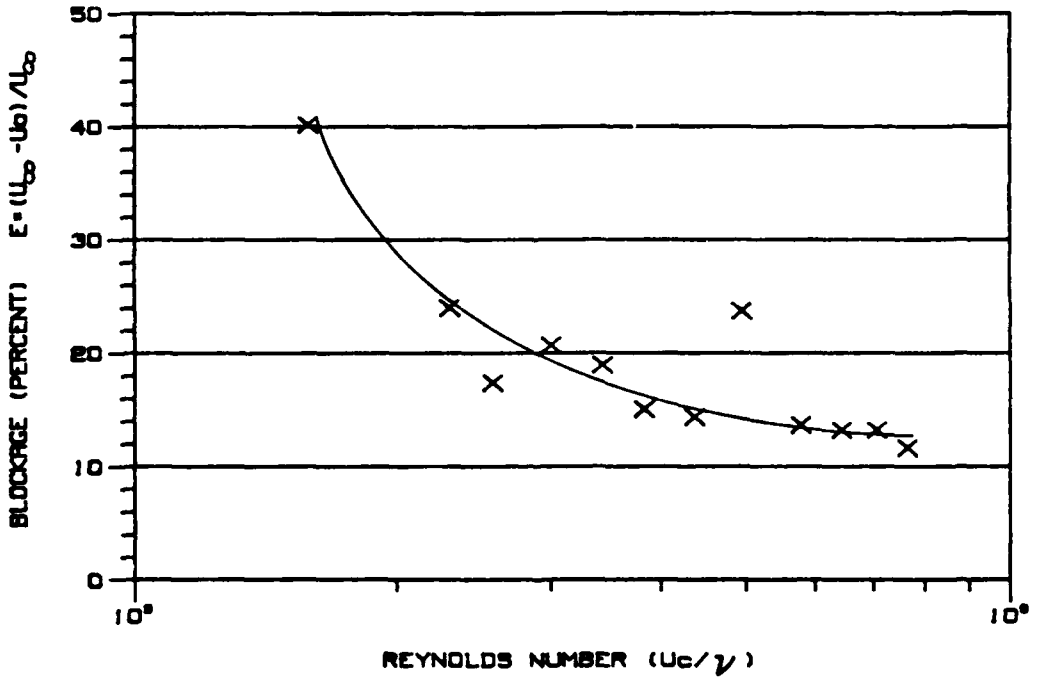

Fig. 7.14. Measured blockage of the Fathom Flexnose section.

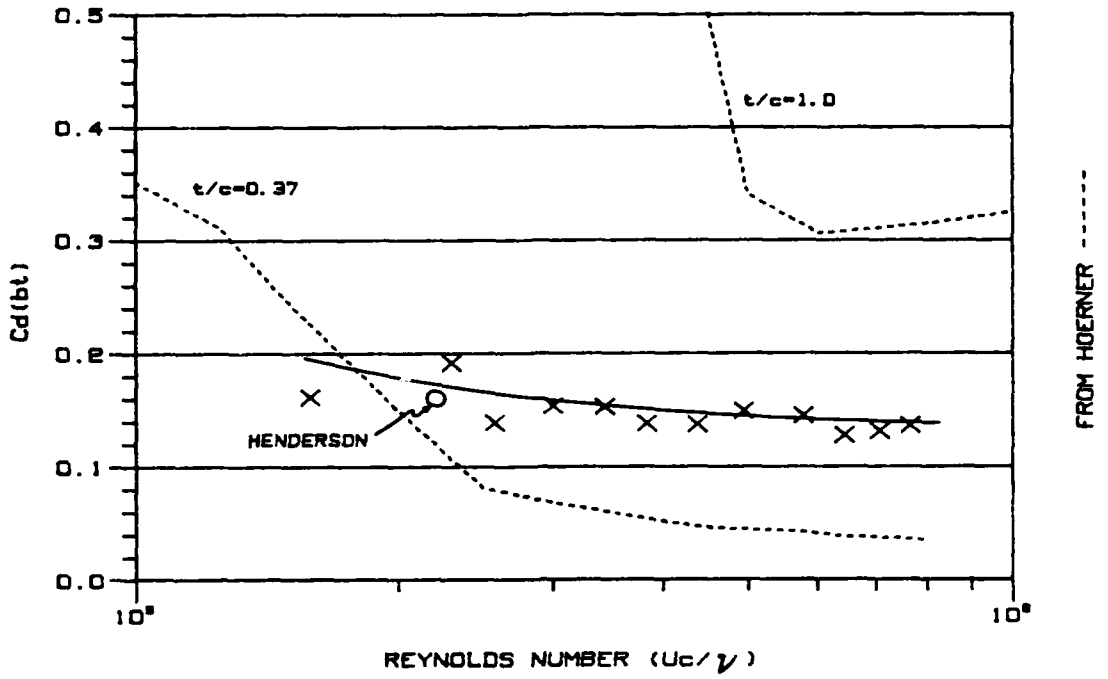

Fig. 7.15. $C_{d(bt)}$ vs. R_c for the Fathom Flexnose section.

7.2.3. Hydrodynamic Center

Figures 7.16 and 7.17 show the results of the stability experiment at two different Reynolds numbers for the Fathom fairing, 0.38 and 0.53 x 10^6. The hydrodynamic center is seen to be located at 15 percent chord at the low Reynolds number and 70 percent chord for the high one. Regions of dynamic instability occurred at certain pivot point locations at the low Reynolds numbers.

Moment coefficient measurements plotted in Fig. 7.18 were made at a Reynolds nubmer of 0.495 x 10^6. The hydrodynamic center was found to be located near the 21.5 percent chord position, which agrees with the free pivot results. The hydrodynamic center for the Fathom Flexnose fairing was found by Henderson from lift and moment data to be located at the 15.3 percent chord position at a Reynolds number of 0.22 x 10^6.

The design mechanical pivot position for the prototype Fathom Flexnose 25 percent fairing is the 12 percent chord position. The fact that the hydrodynamic center is located so closely behind the mechanical center can explain most of the unacceptable behavior of this fairing in sea trials. A complete description of the problems encountered with this fairing is given by Henderson [2].

7.3. NACA 0040 Section

7.3.1. Boundary Layer

The results of the boundary layer survey of the NACA 0040 fairing are shown in Fig. 7.19. The laminar to turbulent boundary layer transition location was found to move forward toward the leading edge with increasing Reynolds numbers between 0.2 and 0.3 x 10^6. At a Reynolds number of 0.3 x 10^6, transition occurs at the 30 percent chord position. The minimum pressure point determined from the

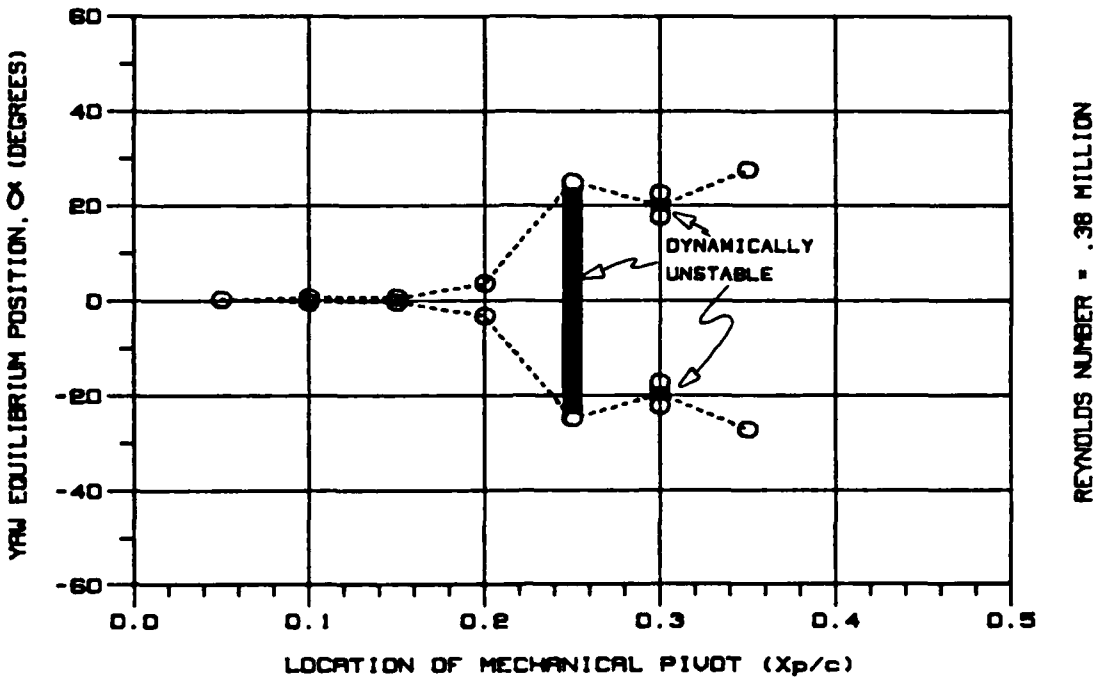

Fig. 7.16. Yaw equilibrium positions of the Fathom Flexnose section.

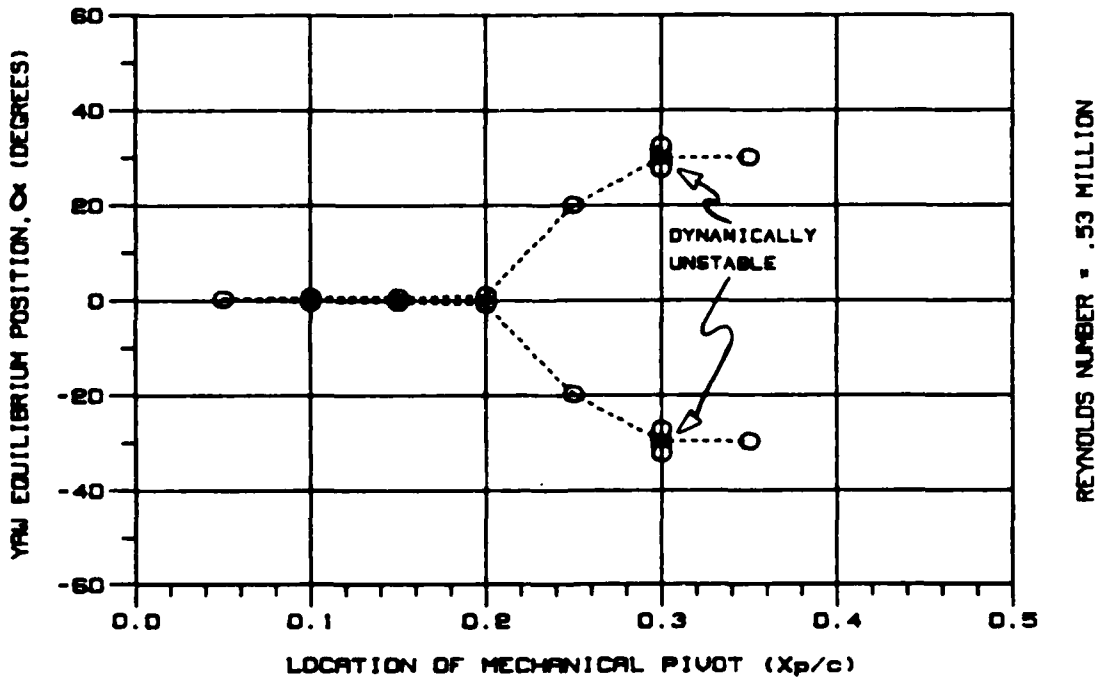

Fig. 7.17. Yaw equilibrium positions of the Fathom Flexnose section.

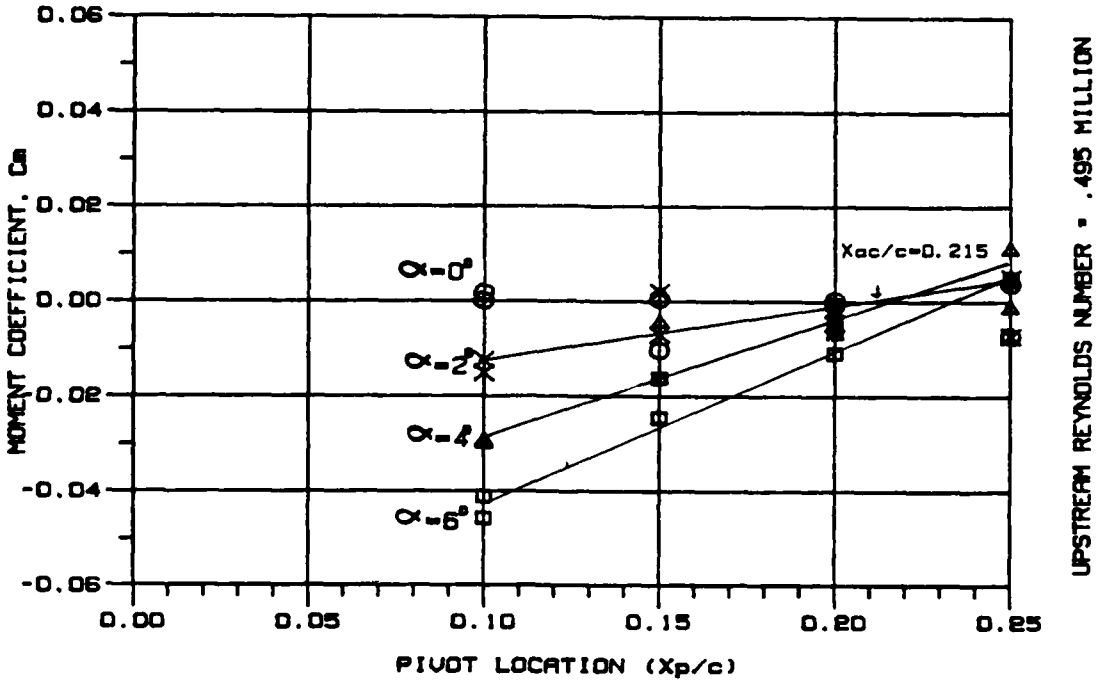

Fig. 7.18. c_m vs. pivot position for the Fathom Flexnose section.

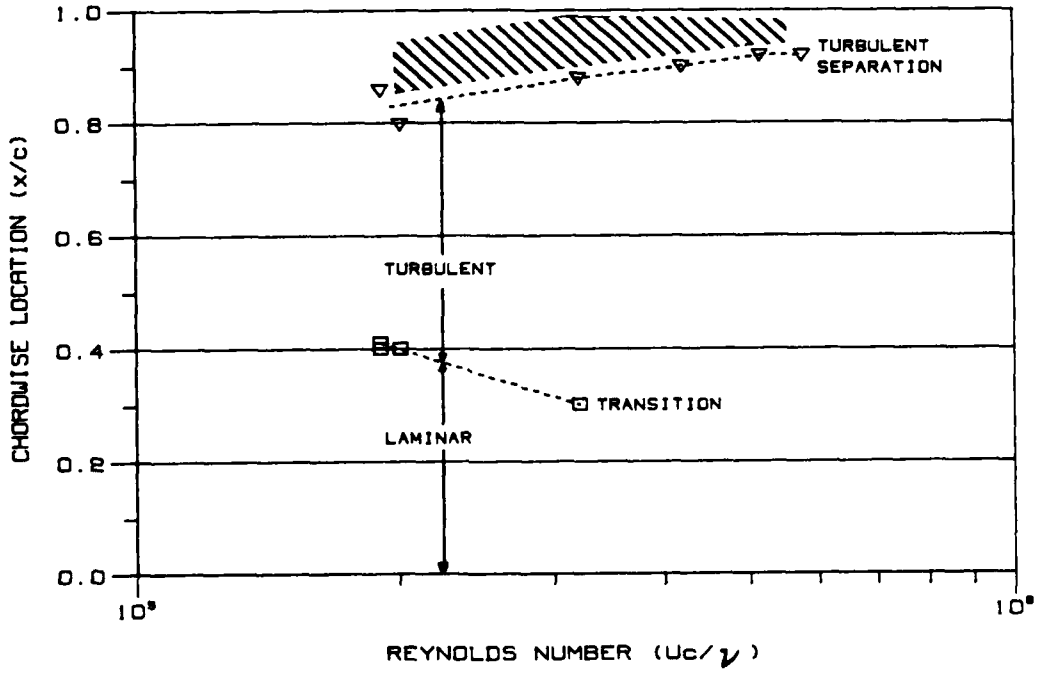

Fig. 7.19. Results of the boundary layer survey of the NACA 0040 section.

potential flow calculations is the 19 percent chord location. The maximum thickness for the NACA 0040 section is at the 30 percent chord location. Thus transition occurred aft of the minimum pressure point and just at the maximum thickness position. For Reynolds numbers greater than 0.3×10^6, the location of the boundary layer transition was not clearly indicated with the oil/dye technique. There was no laminar separation bubble visible and no apparent transition point. It was possible that transition occurred at the leading edge. This investigation was unable to determine its location with any certainty.

Transition locations as a function of Reynolds number are plotted in Fig. 7.20 for other NACA 00XX sections [8]. In each case, the boundary layer transition location moved forward toward the leading edge with increasing Reynolds number. There was no indication that transition might occur at the leading edge on any of the thinner NACA sections.

The turbulent boundary layer separation location varied slightly with Reynolds number, moving toward the trailing edge as the Reynolds numbers increased. Throughout the Reynolds number range tested, from 0.20 to 0.61×10^6, the boundary layer was never fully attached.

7.3.2. Drag Coefficient

The measured blockage correction factors for the NACA 0040 section are shown in Fig. 7.21. The blockage ranges from 26.5 percent at the low Reynolds number of 0.15×10^6 to 6.5 percent at Reynolds number 0.56×10^6. The results of the two-dimensional drag coefficient measurements for the NACA 0040 fairing are shown in Fig 7.22. Also shown are drag coefficients for a Joukowski 40 percent section, and a NACA 0033 measured by Fage, Falkner, and Walker [24] and Althaus [13].

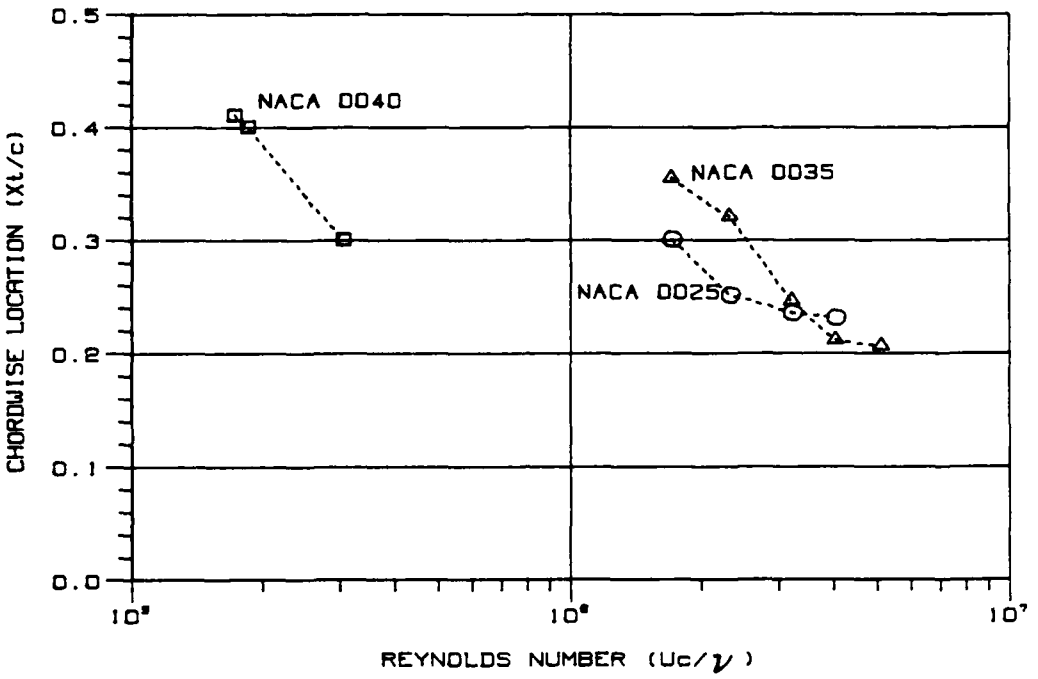

Fig. 7.20. Location of boundary layer transition vs. R_c for NACA 00XX sections.

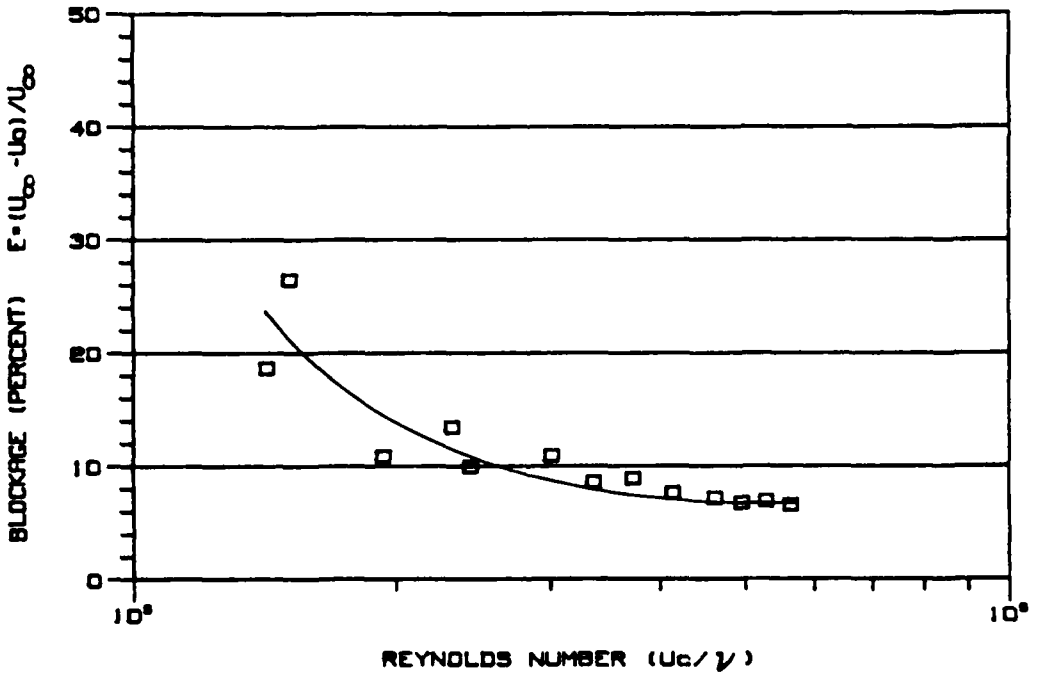

Fig. 7.21. Measured blockage of the NACA 0040 section.

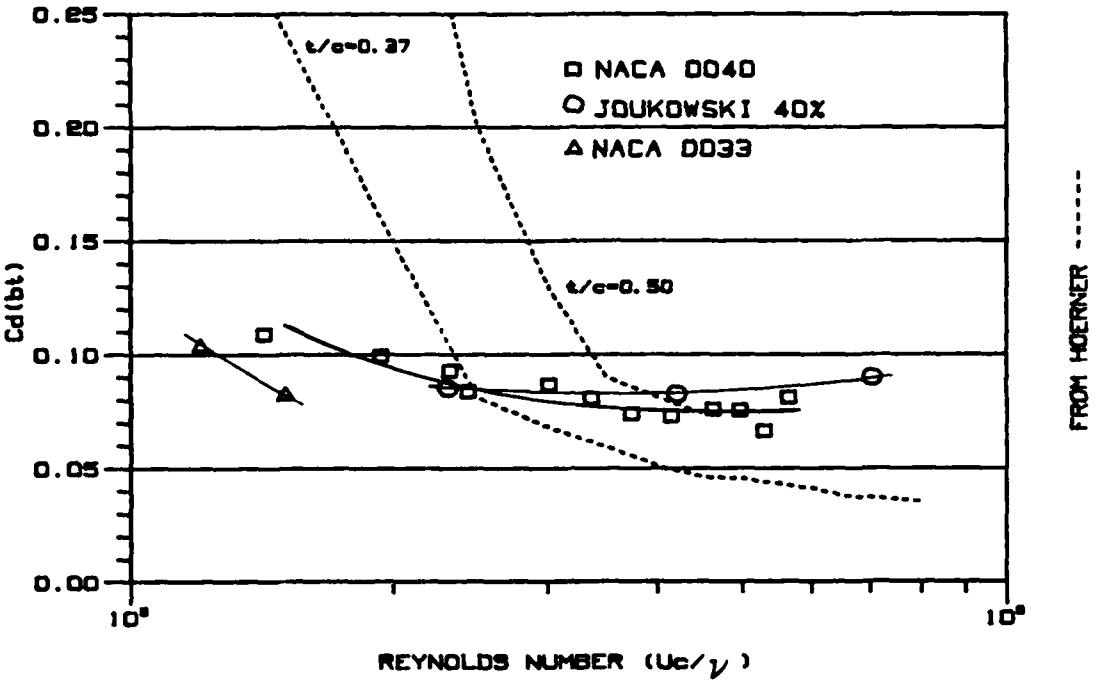

Fig. 7.22. $C_{d(bt)}$ vs. R_c for NACA 0040, NACA 0033 and Joukowski sections.

The drag of the NACA 0040 fairing decreased slightly over the Reynolds number range considered. The coefficient had a maximum value of 0.108 at a Reynolds number of 0.14×10^6 and a low of 0.08 at a Reynolds number of 0.56×10^6. The slight decrease in drag coefficient with increasing Reynolds number was related to both the decreasing portion of laminar boundary layer drag increase, and decreasing portion of separated turbulent boundary layer drag decrease. These two changes have opposite effects on the drag coefficient.

7.3.3. Hydrodynamic Center

Fig. 7.23 shows the results of the stability measurements for this section at a Reynolds number of 0.48×10^6. The location of the hydrodynamic center was found to be forward of the leading edge. With the pivot location at 5 percent of the chord length, the yaw equilibrium position was ±6 deg. The yaw equilibrium angle increased as the pivot location was moved aft. With the pivot location at 35 percent chord the fairing was in equilibrium at a yaw angle of ±41 deg.

Measurements of the moment coefficient, Fig. 7.24, also confirmed that the location of the hydrodynamic center was forward of the leading edge. Measured moments were positive for small angles of attack, up to 10 deg., for pivot positions at x_p/c = 0.05, 0.10, and 0.15. Positive moments are destabilizing, resulting in misalignment of the fairing with the flow.

Fig. 7.25 shows a plot of the location of the aerodynamic center vs. t/c ratio for NACA 00XX sections as given by Eastman [9]. The movement toward the leading edge with increasing t/c ratio is clearly indicated. For the NACA 0035 section the aerodynamic center was found

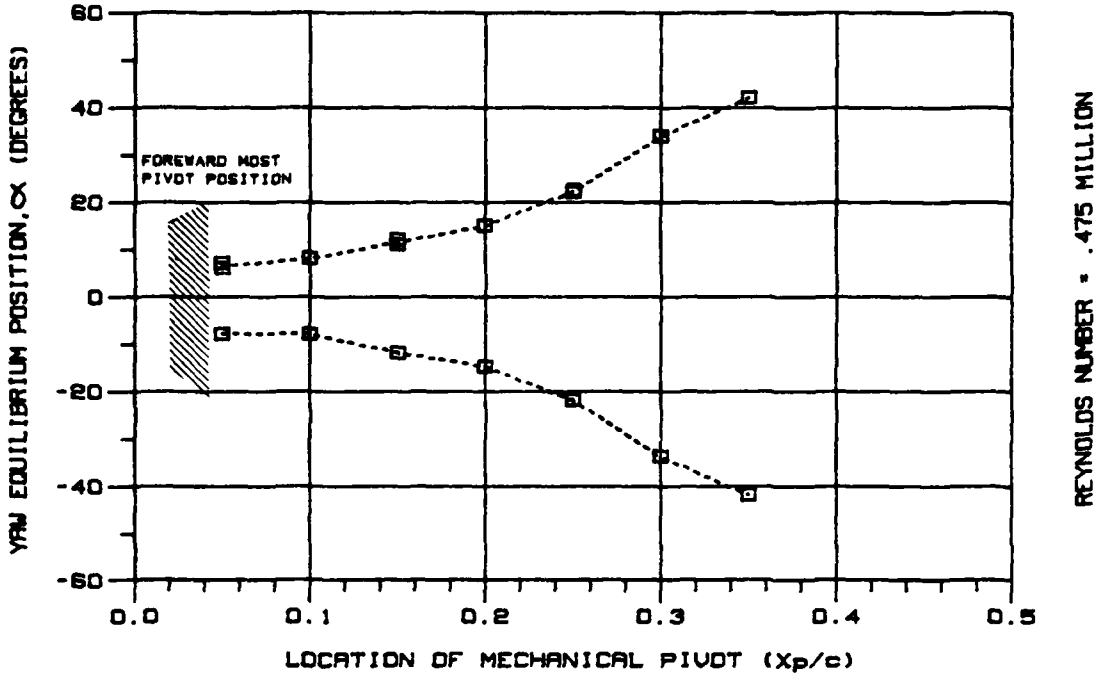

Fig. 7.23. Yaw equilibrium positions of the NACA 0040 section.

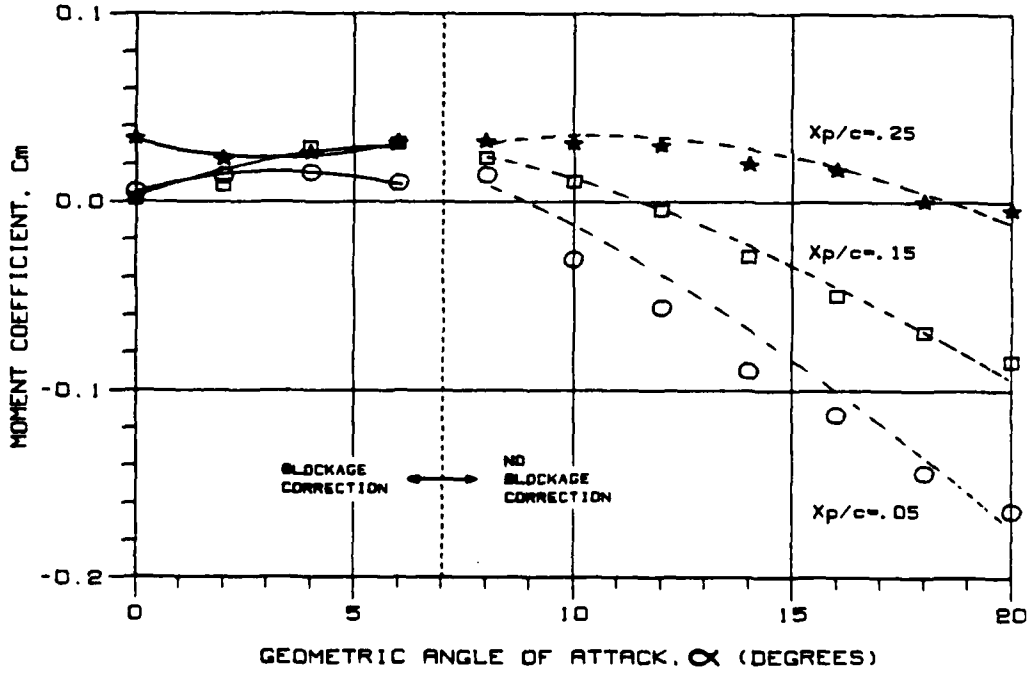

Fig. 7.24. c_m vs. α for the NACA 0040 section.

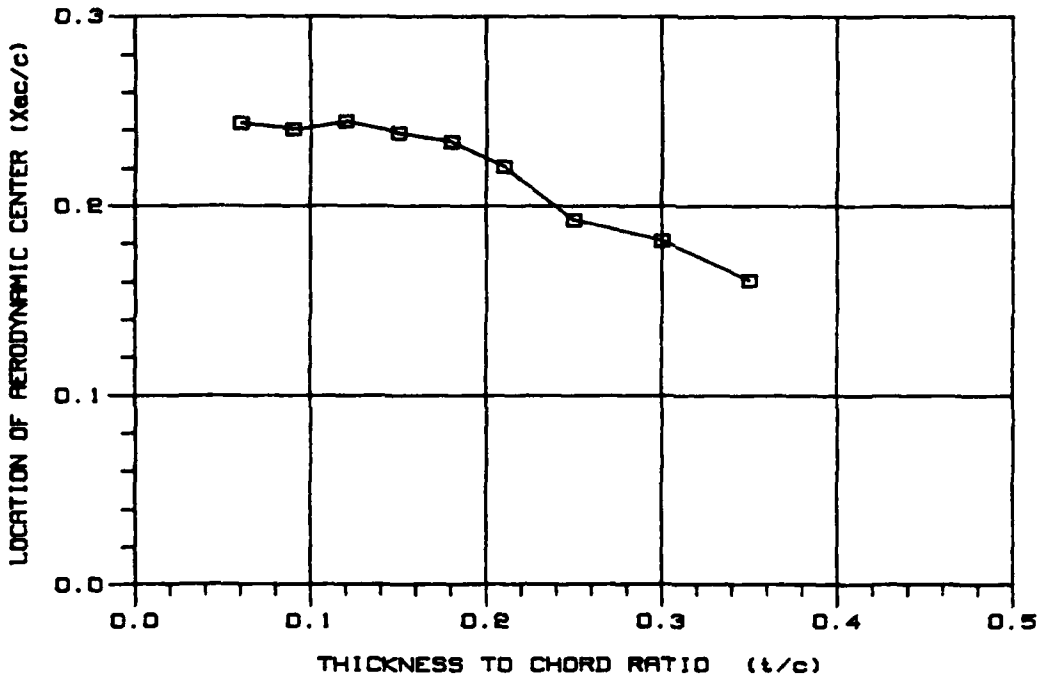

Fig. 7.25. Location of aerodynamic center vs. t/c ratio for NACA 00XX sections.

by Bullivant [8] to be at a.c. = 0.16. The location of the hydrodynamic center forward of the leading edge for the NACA 0040 was a significant phenomenon which could not have been predicted from the investigation of the other NACA 00XX sections.

The misalignment or lack of weathervane stability of the NACA 0040 section at all mechanical pivot locations precludes the possibility of using this section as a cable fairing. The large hydrodynamic lift and increase in drag due to the equilibrium angle of attack would cause significant problems. The addition of a trailing edge wedge as was fitted on the Liebeck 40 percent fairing would move the location of the hydrodynamic center aft to a more favorable location. No measurements were made to find the hydrodynamic center of the NACA 0040 section fitted with a trailing edge wedge.

7.4. JfS Section

7.4.1. Boundary Layer

Results of the boundary layer survey were similar for both sections. Figs. 7.26 and 7.27 show the boundary layer behavior as a function of Reynolds number. Transition occurred aft of the minimum pressure point and aft of the maximum thickness location at all Reynolds numbers. Transition occurred at the 30 percent chord position for the low Reynolds numbers and moved toward the leading edge to about the 20 percent chord position at the higher Reynolds numbers. Separation was visible only at Reynolds numbers less than 0.12×10^6 on the JfS 61M section and less than 0.165×10^6 on the JfS 62M section. The separation was of the laminar boundary layer and occurred at the 30 percent chord position. There was no sign that it reattached downstream. The boundary layer quickly became fully attached with a slight increase in Reynolds number and remained fully

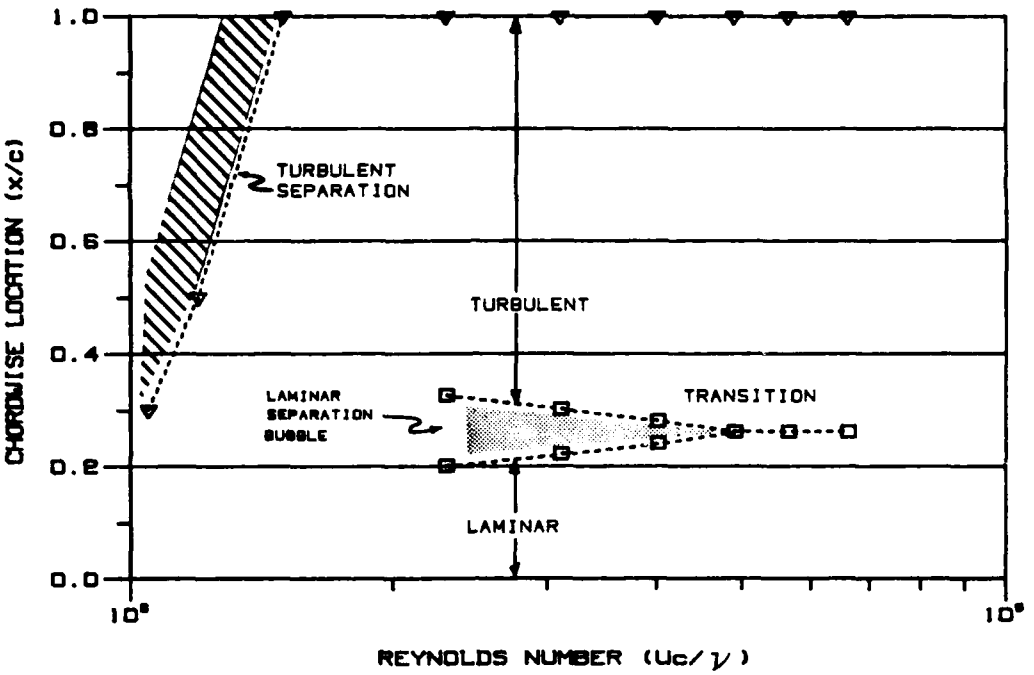

Fig. 7.26. Results of the boundary layer survey of the JfS 61M-TR-40 section.

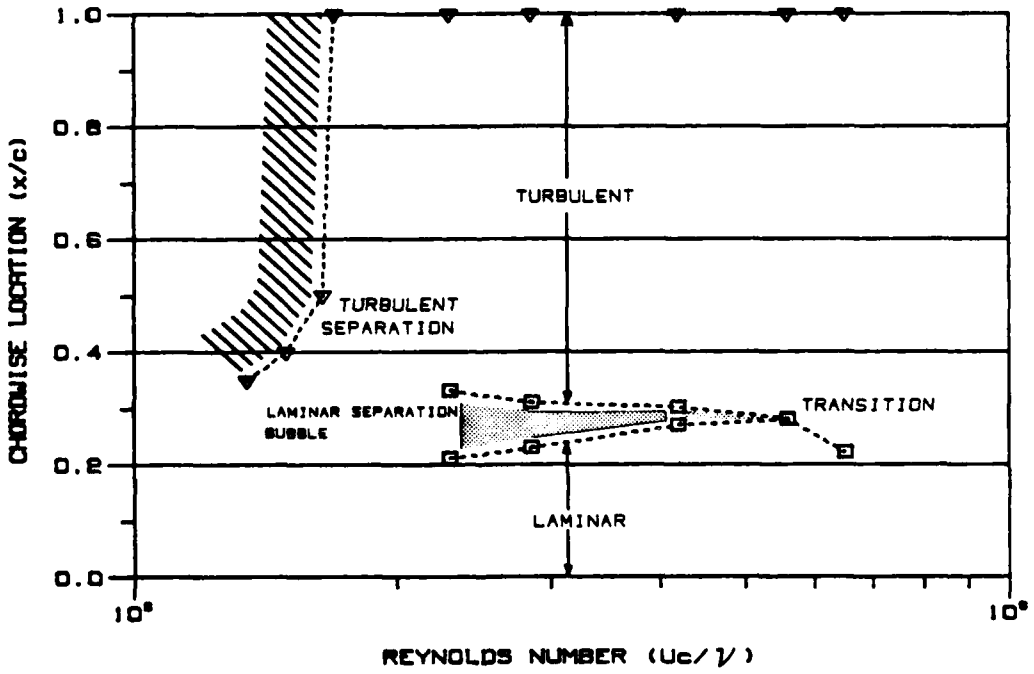

Fig. 7.27. Results of the boundary layer survey of the JfS 62M-TR-40 section.

attached at all higher Reynolds numbers.

7.4.2. Drag Coefficient

Fig. 7.28 shows a plot of the measured blockage correction factors for the two JfS modified 40 percent sections. The tunnel blockage ranges from 48 percent at a Reynolds number of 0.168×10^6 to 12 percent at a Reynolds number of 0.76×10^6. Blockage is lower for the JfS 62M-TR-40 section due to its thinner trailing edge.

The measured drag coefficients, shown in Fig. 7.29, show a marked decrease as the boundary layer became attached at Reynolds numbers between 0.1 and 0.2×10^6. Above a Reynolds number of 0.4×10 the drag coefficients remained approximately constant. As expected, the drag coefficients were higher for the JfS 61M section with the thicker trailing edge than they were for the JfS 62M section. The drag coefficient approaches an approximately constant value of 0.113 for the JfS 61M section and 0.088 for the JfS 62M.

Fig. 7.30 compares the drag coefficients of the JfS 61M-TR-40, JfS 62M-TR-40, JfS 61-TR-25 and JfS 62-TR-25 sections. The drag coefficients for the JfS 25 percent t/c sections were measured by Thieme [6], with models measuring 10 cm thick x 40 cm chord x 40 cm span (3.9" x 15.8" x 15.8"), at the JfS Wind Tunnel at the University of Hamburg, Germany. The drag coefficients of the 25 percent sections were only slightly less than those of the 40 percent modified sections. That there was such little difference indicates the penalty paid for the blunt leading edge of the unmodified 25 percent section as opposed to the circular leading edge of the modified 40 percent sections.

The base drag results are plotted in Fig. 7.31 for the two modified JfS sections. The fraction of the total drag due to the

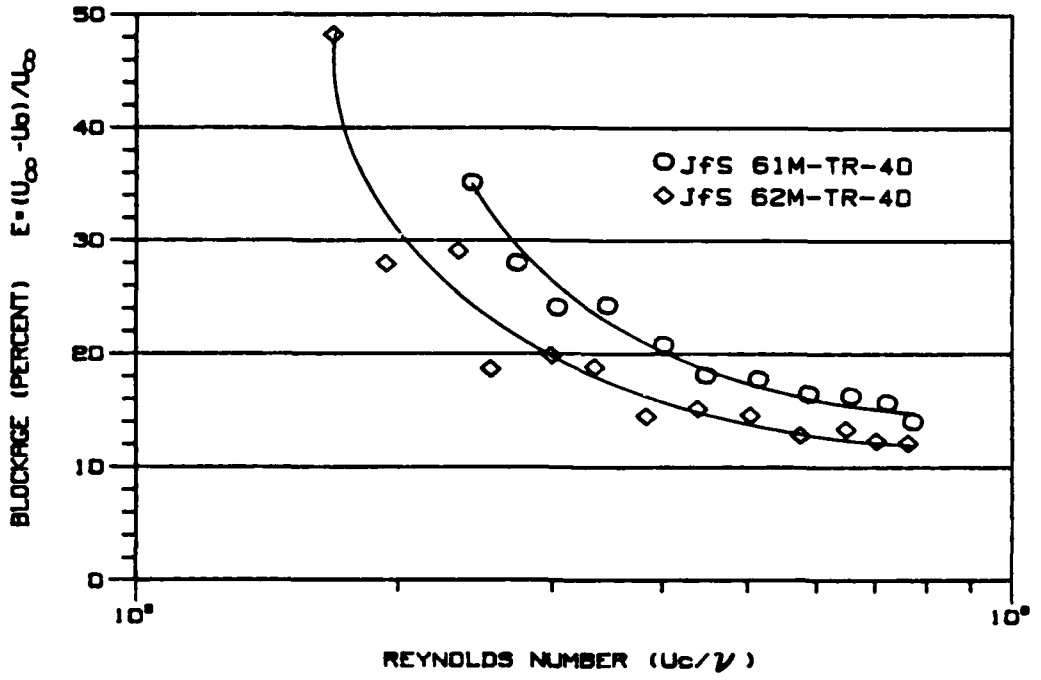

Fig. 7.28. Measured blockage of the JfS 40% sections.

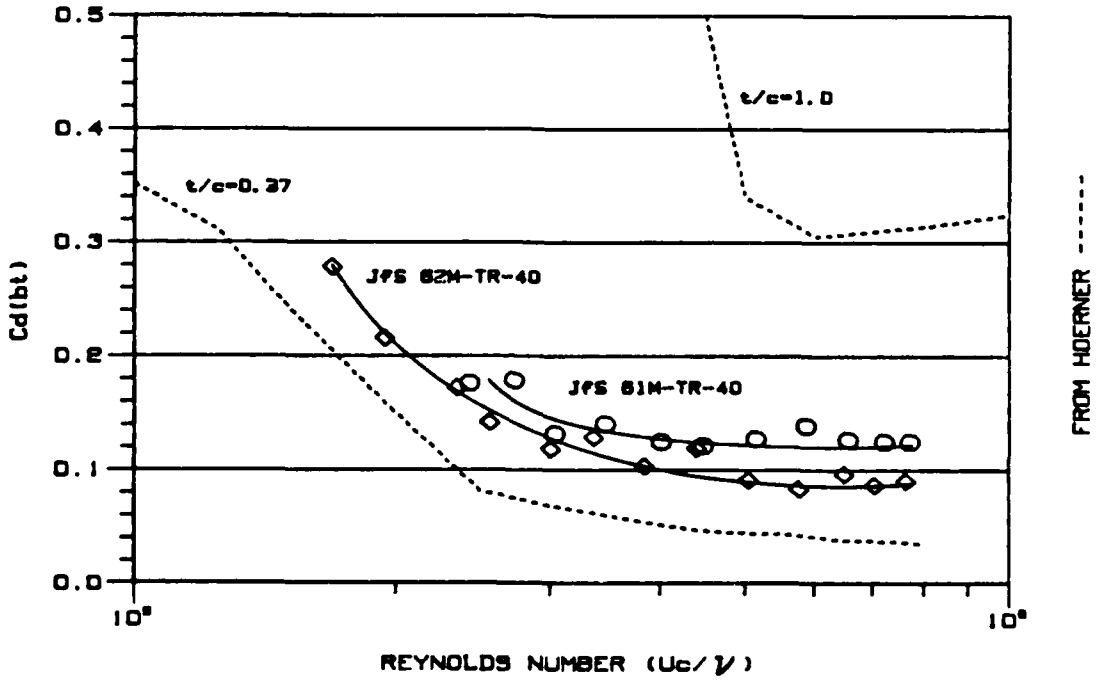

Fig. 7.29. $c_{d(bt)}$ vs. R_c for the JfS 40% sections.

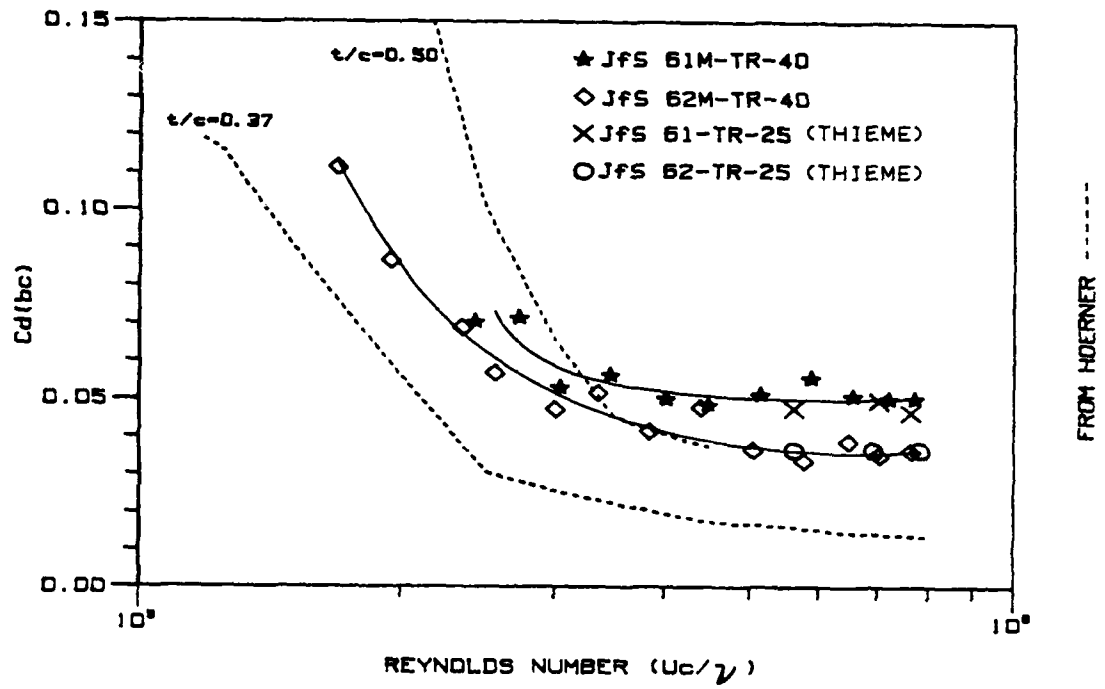

Fig. 7.30. $c_{d(bc)}$ vs. R_c for four JfS sections with thickness ratios of 0.25 and 0.40.

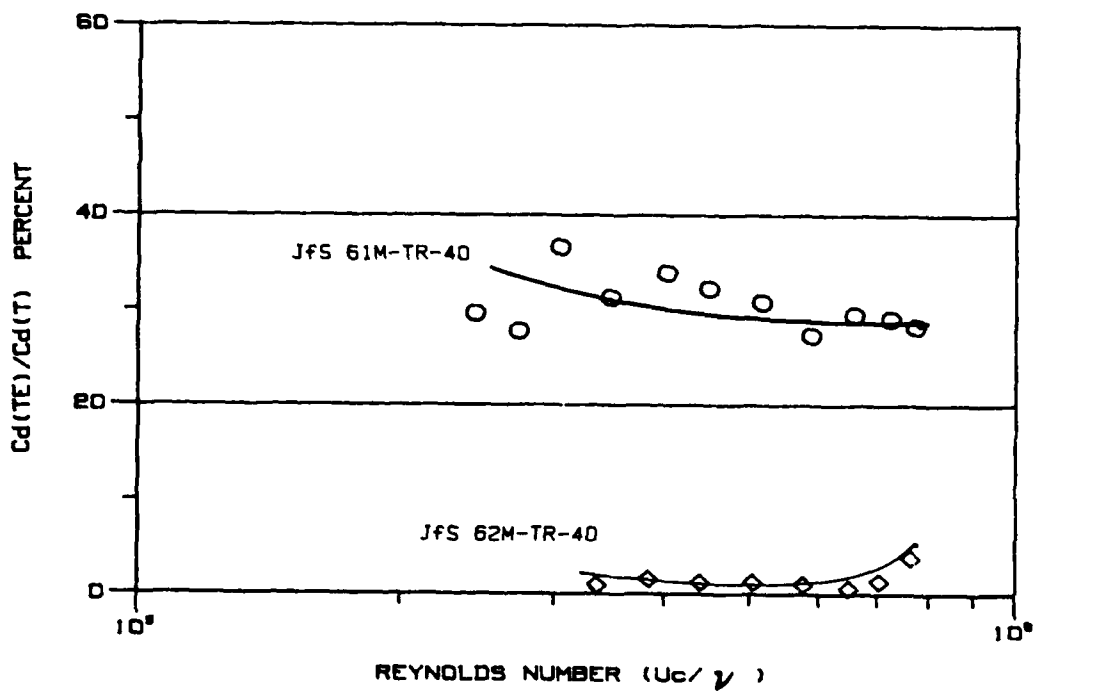

Fig. 7.31. Ratio of the base drag to total drag for JfS 61M-TR-40 and JfS 62M-TR-40 sections.

blunt edge ranged from 2 percent to 8 percent for the JfS 62M section. The ratio of the area of the blunt trailing edge to the projected frontal area is 0.06. For the JfS 61M section the ratio of trailing edge drag to total drag ranged from 27 percent to 37 percent. The ratio of the area of the trailing edge to the projected frontal area for this section is 0.20.

For both of the modified JfS sections, the fraction of the total drag due to the blunt trailing edge was approximately constant with Reynolds number. The average fraction was 30.5 percent for the JfS 61M and 15 percent for the JfS 62M. At all Reynolds numbers for which trailing edge static pressures were measured, the boundary layers were fully attached. The measured static pressures were negative, i.e. less than the freestream static pressure.

7.4.3. *Hydrodynamic Center*

The two JfS modified sections both show good weathervane stability. Figs. 7.32, 7.33, 7.34 and 7.35 show the results of the stability tests. The hydrodynamic center of both fairings was located at the 30 percent chord position, which is well aft of the best mechanical center located at the 20 percent chord position. The long, thick trailing edge of these two sections has the desired effect of moving the hydrodynamic aft from the 1/4 chord position predicted by thin airfoil theory. With the pivot located at the 35 percent chord position, both fairings were dynamically unstable.

Figs. 7.36 and 7.37 are plots of the moment coefficients for small angles of attack vs. pivot location. This method also confirmed that the hydrodynamic center for both sections was just aft of the 30 percent chord position but forward of the 35 percent chord position, approximately 0.34 chord for the JfS 61 and 0.33 chord for the JfS 62 section.

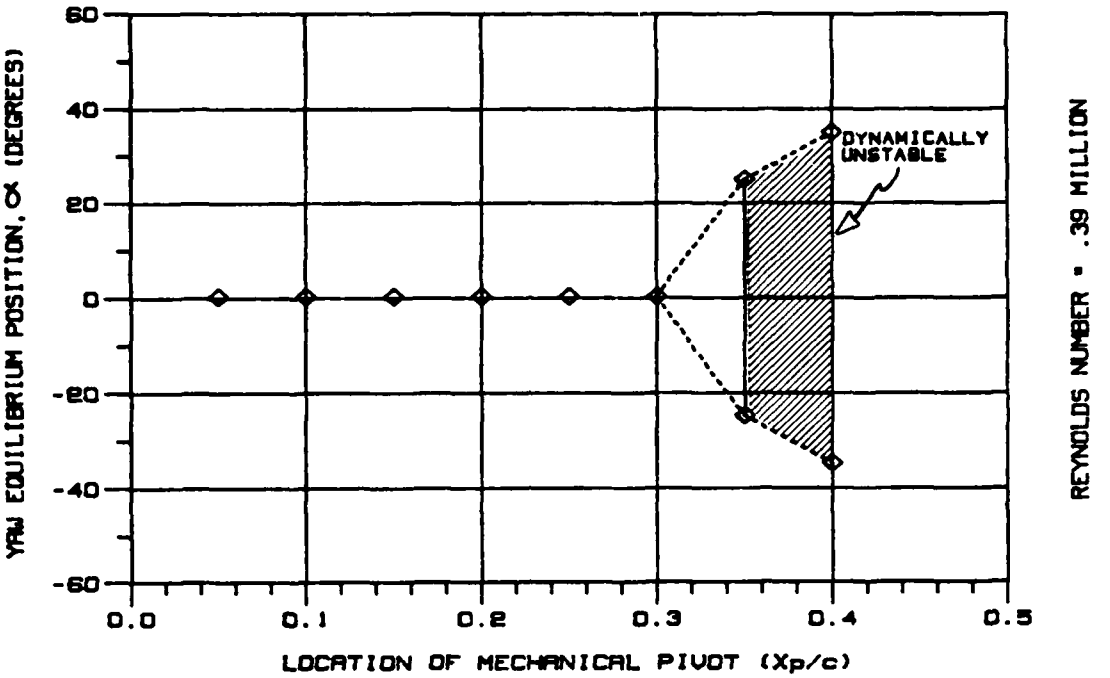

Fig. 7.32. Yaw equilibrium positions of the JfS 61M-TR-40 section.

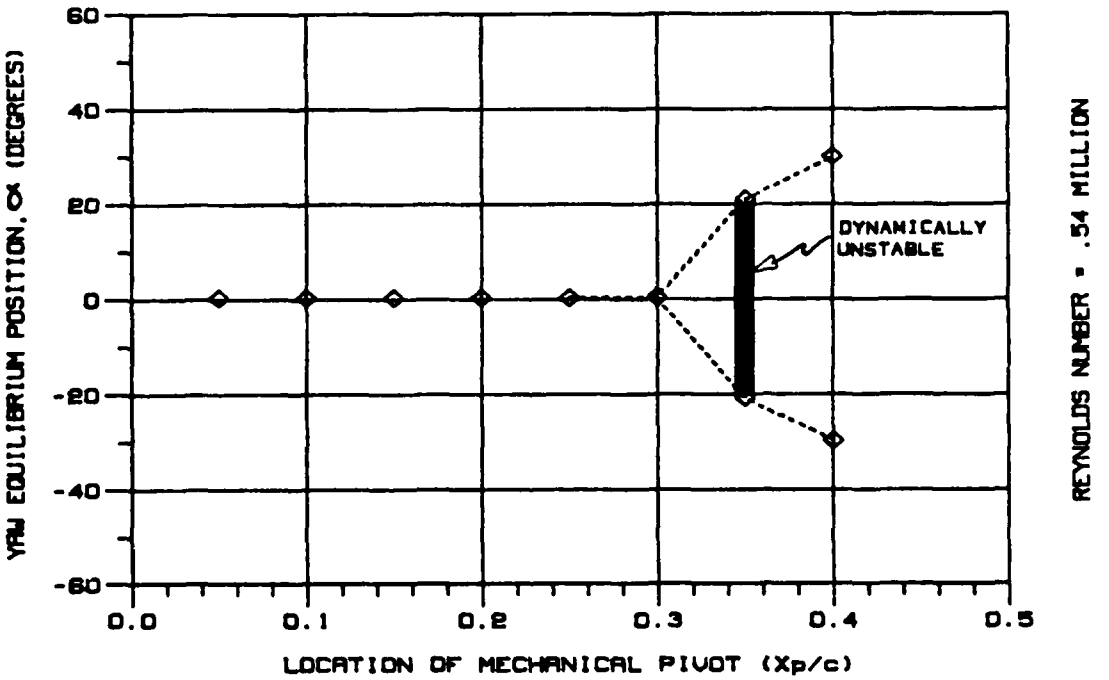

Fig. 7.33. Yaw equilibrium positions of the JfS 61M-TR-40 section.

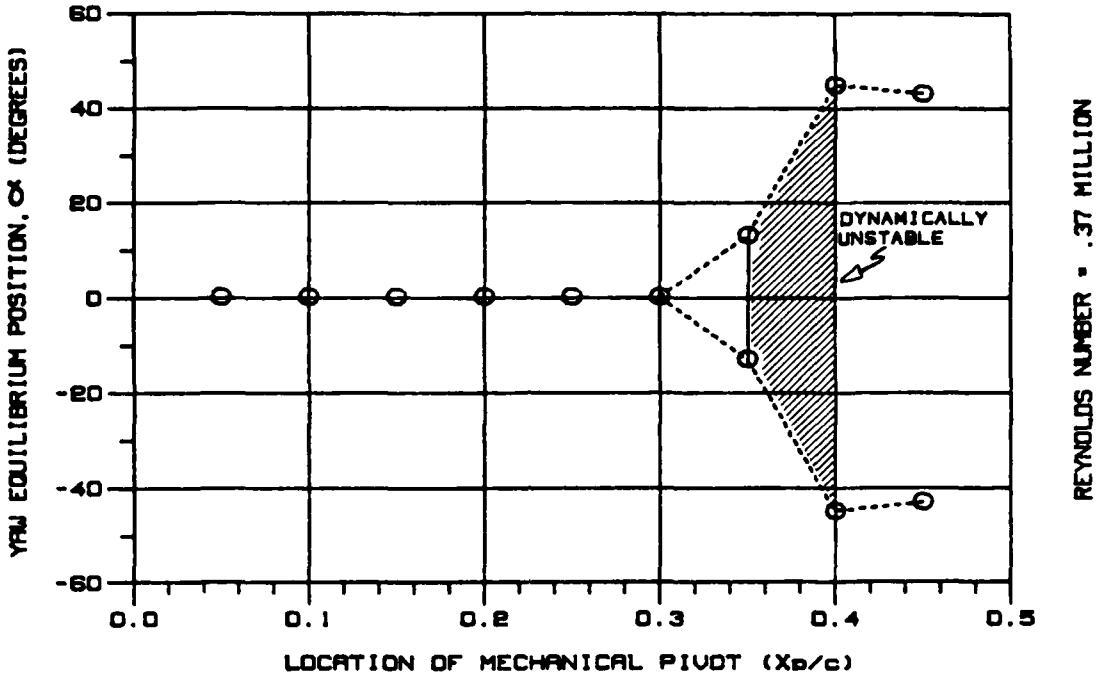

Fig. 7.34. Yaw equilibrium positions of the JfS 62M-TR-40 section.

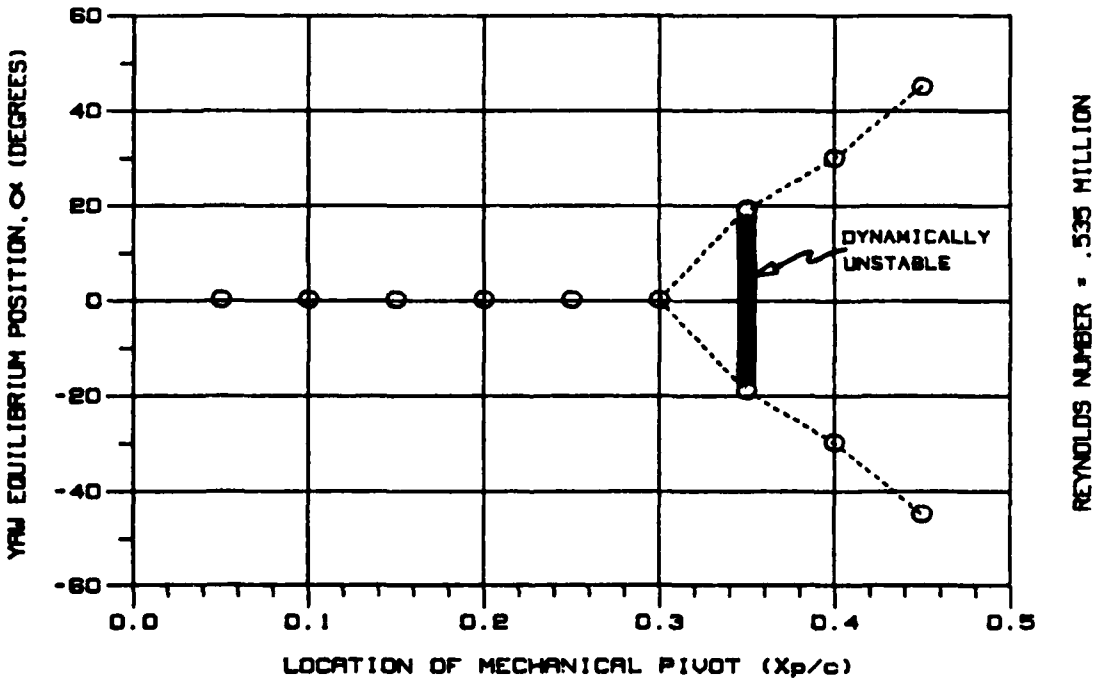

Fig. 7.35. Yaw equilibrium positions of the JfS 62M-TR-40 section.

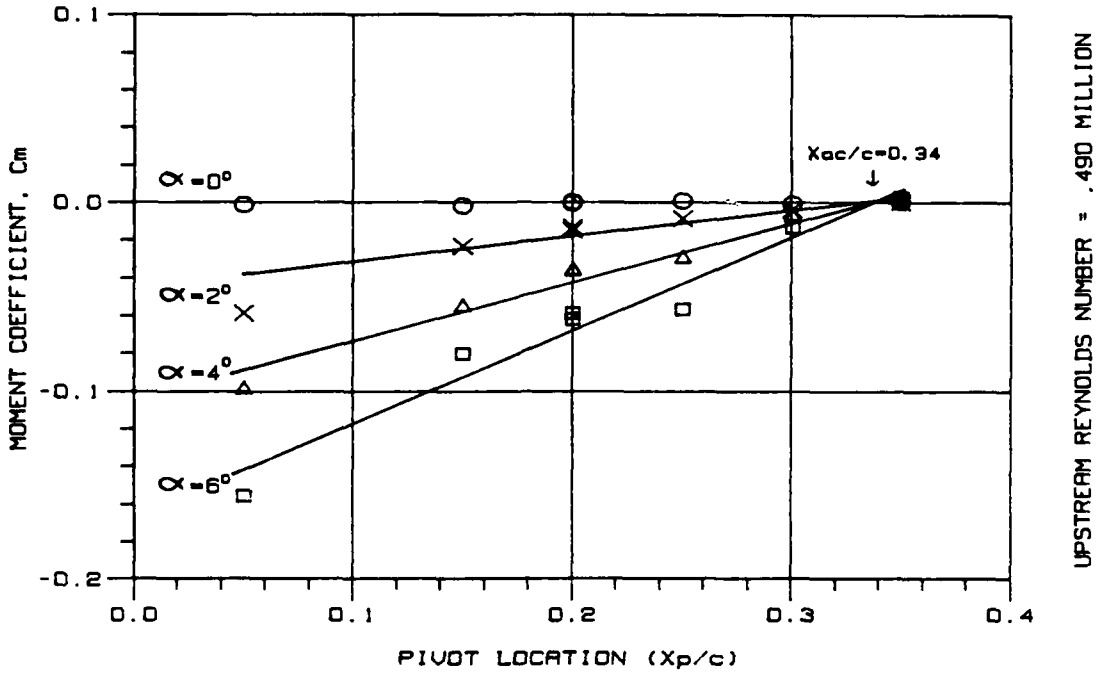

Fig. 7.36. c_m vs. pivot position for the JfS 61M-TR-40 section.

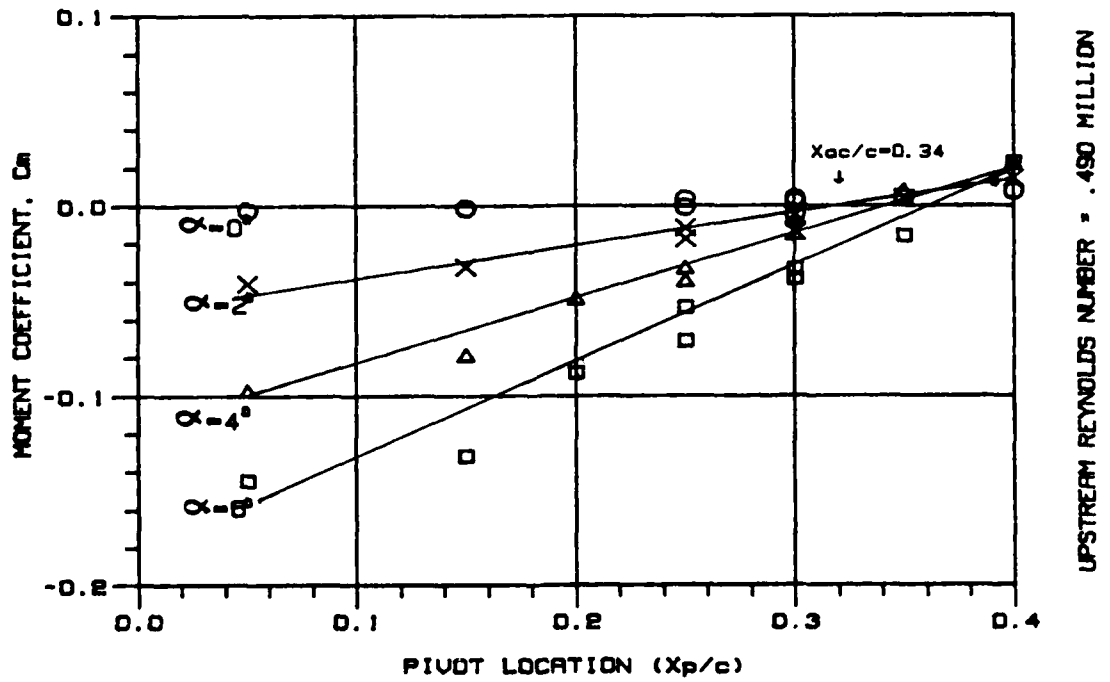

Fig. 7.37. c_m vs. pivot position for the JfS 62M-TR-40 section.

8.0. STUDY CONCLUSIONS

Each of the five sections tested has hydrodynamic characteristics that recommend its use as a fairing for marine applications. However none of the sections can be considered ideal. As in all engineering problems,, an acceptable solution arises from a compromise of the various criteria. This section will compare the experimental results of the five fairings and evaluate their performance in terms of the desired characteristics. Through this proceedure it is possible to recommend one of the fairings as most appropriate for further study.

8.1 Boundary Layer

Figures. 8.1 and 8.2 compare the boundary layer visualization results for all five sections at two Reynolds numbers. The boundary layer criteria for a successful fairing demands a large region of laminar flow extending from the leading edge and a separation free pressure recovery region aft of the maximum thickness point. The Liebeck fairing was designed specifically with these goals in mind. Of the five fairings the Liebeck section had the largest region of laminar flow. The laminar region was present for the leading 30 to 47 percent of the fairing depending on the Reynolds number. As the leading edge profiles increased in bluntness the extent of the laminar boundary layer decreased. The laminar boundary layer of the NACA 0040 section covered 30 to 41 percent of the fairing. Both of the JfS modified sections and the Fathom section have circular leading edges. The laminar to turbulent boundary layer transition occurred between the 14 and 19 percent chord positions for the Fathom section and between the 22 and 33 percent chord postions for the JfS sections. The Fathom section had the smallest extent of laminar flow.

Two approaches to the design of the pressure recovery profile of

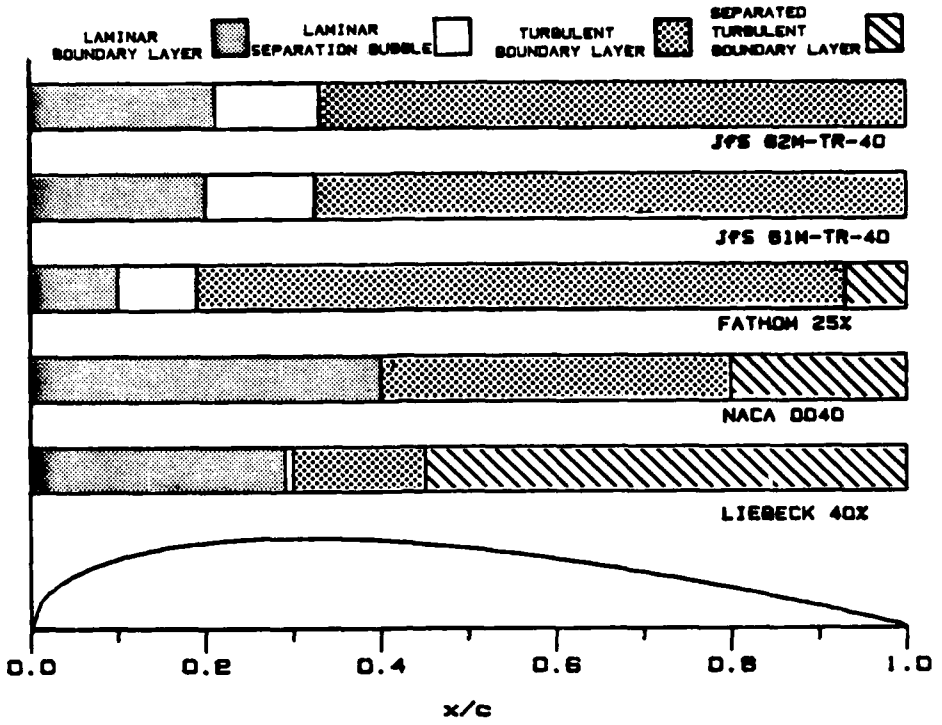

Fig. 8.1. Boundary Layer Visualization Results at $R_c = 0.23 \times 10^6$

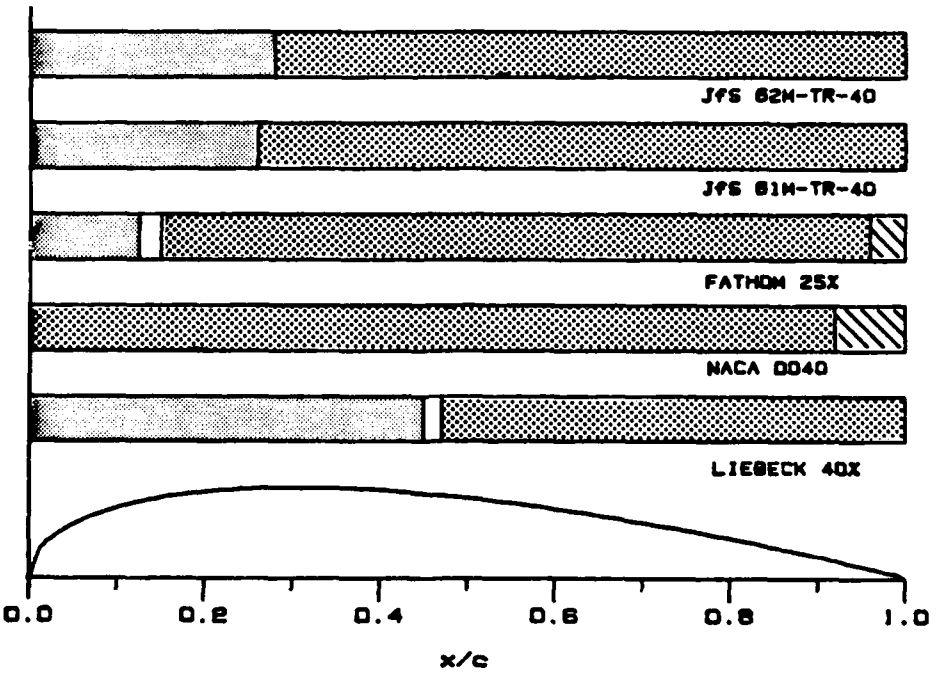

Fig. 8.2. Boundary Layer Visualization Results at $R_c = 0.56 \times 10^6$

the sections are incorporated. The NACA and the Fathom sections are convex in profile aft of their maximum thickness points, while the Liebeck section and both JfS modified sections are concave. Separation occurred at all tested Reynolds numbers on both convex profiles and varied little with changing Reynolds number. For all three of the concave profiles, massive turbulent boundary layer separation occurred at low Reynolds numbers but became fully attached as the Reynolds numbers were increased. The Liebeck section with the largest pressure recovery gradients stayed separated up to higher Reynolds numbers. The flow became fully attached at Reynolds numbers greater than 0.22×10^6 for the JfS 62M, greater than $.25 \times 10^6$ for the JfS 61M, and greater than 0.40 x 10 for the Liebeck section. The addition of the vortex generators improved the separation resistance of the Liebeck section. For this configuration the boundary layer became fully attached at Reynolds numbers greater than 0.17×10^6,

8.2. Drag Coefficient

The behavior of the boundary layer affects both the drag coefficients and the dynamic stability of the fairings. To satisfy the criteria for low drag coefficients, the fairing should have a maximum extent of laminar flow and be completely free from separation. An analysis of the measured drag coefficients indicates the importance of the boundary layer behavior. Figures. 8.3 and 8.4 show the measured drag coefficients of all five tested fairings normalized with respect to projected area at two different Reynolds numbers.

At low Reynolds numbers of less than 0.25×10^6, where the boundary layer was separated for the Liebeck and the two JfS sections, their drag coefficients were greater that those of the NACA and Fathom sections. The drag coefficients of the Liebeck section were the

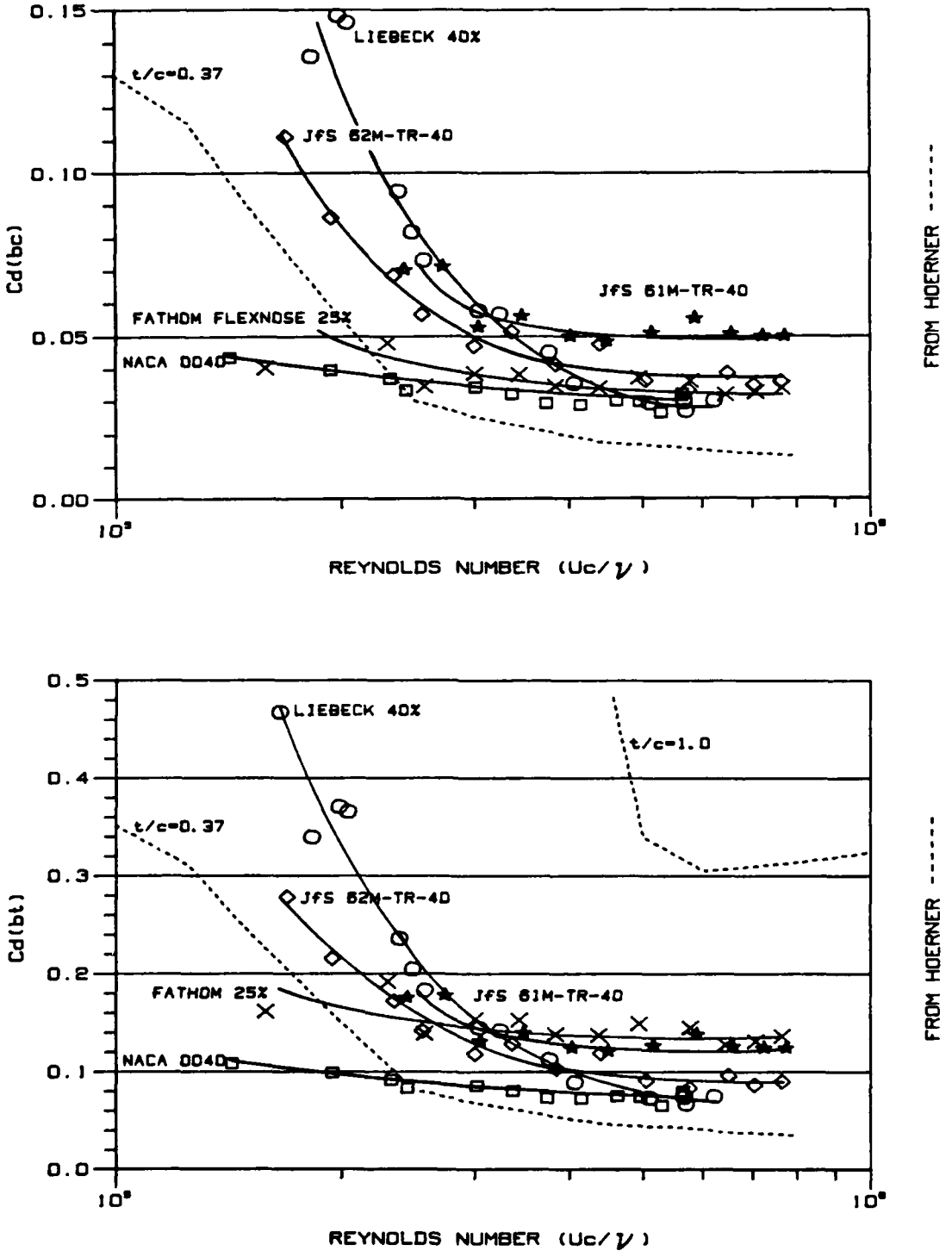

Fig. 8.3. Drag coefficient based on planform and frontal area for fairing sections.

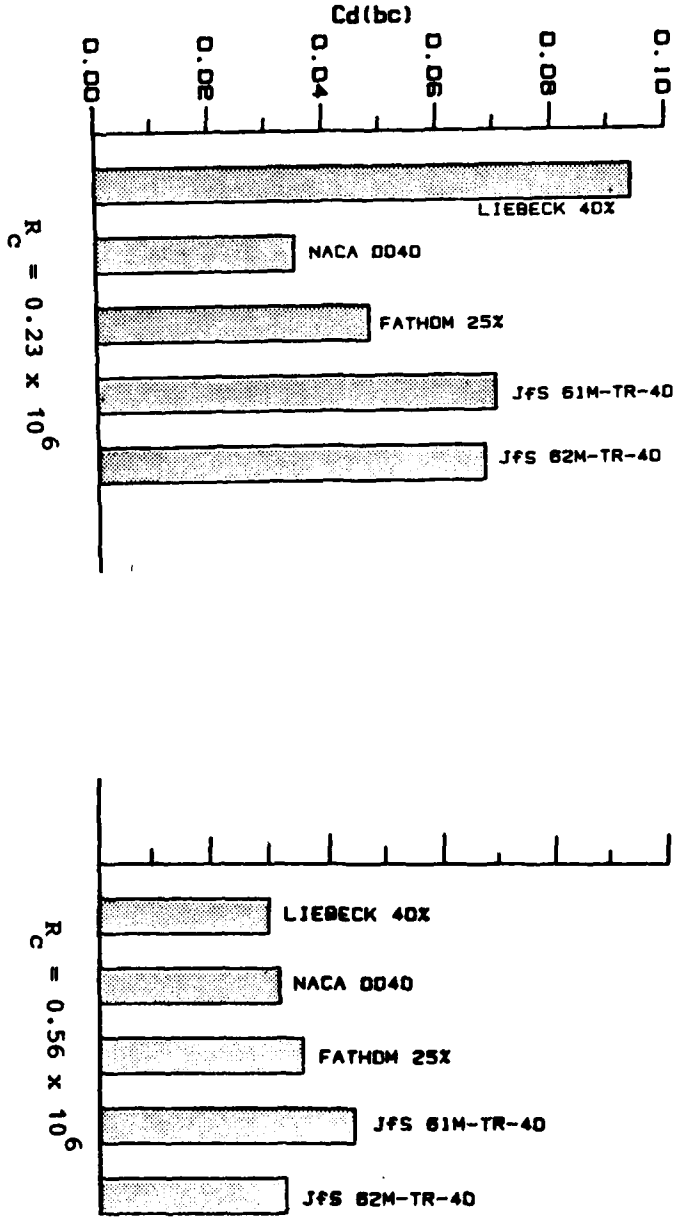

Fig. 8.4. Five drag coefficients of the five sections at two Reynolds numbers.

highest. The drag coefficients of the NACA section were the lowest due to its larger region of laminar boundary layer and small region of turbulent separation.

For Reynolds numbers greater than 0.5×10^6, when the boundary layers were completely attached for the Liebeck and JfS sections, the effects of the laminar region and the blunt trailing edge drag became important. The success of the Liebeck design is apparent. The drag coefficients for this section were less that those of all of the other shapes. Drag coefficients in this Reynolds number range were slightly higher for the NACA 0040 shape due to the small region of boundary layer separation, while the drag coefficients for the Fathom section were even higher. The small region of laminar flow and the additional drag effects of the blunt trailing edge were responsible. The two JfS sections had the highest drag coefficients in this Reynolds number range. Although they had a larger region of laminar flow then the Fathom section, their thickness ratios of 40 percent and their blunt trailing edges contributed to their higher drag. The JfS 61M section with its thicker trailing edge had a much higher drag than the JfS 62M section.

It is important to note the high drag coefficients of the Fathom section throughout the tested Reynolds number range. The Fathom section has a t/c of .25 while for all the others t/c = .40. The high drag coefficients of this shape were a result of the blunt (circular) leading edge, the region of boundary layer separation, and the existance of the blunt trailing edge. Although the JfS fairings also have circular leading edge profiles and blunt trailing edges, their separation free pressure recovery sections helped to reduce their total drag.

Clearly the Liebeck and the NACA sections best meet the criteria of low drag at the higher Reynolds numbers. However, the other sections have significantly lower drag coefficients than an unfaired circular cylinder. At a Reynolds number of 0.6×10^6 the drag coefficient of a circular cylinder is 0.312 and the coefficients based on frontal area for the Liebeck, NACA, Fathom, JfS 62M, and JfS 61M were 0.075,0.08, 0.136, 0.0875, 0.1325 respectively.

8.3. Hydrodynamic Center

The most important criterion for a successful fairing for line structures is its streamlining or "weathervane" behavior. In order to prevent tow-off or "kiting" of the structure due to hydrodynamic lift forces, the fairing must align itself with the direction of the fluid flow. This criterion requires the hydrodynamic center to be aft of the mechanical center of rotation. To overcome the friction forces between the fairing and the line structure the restoring moments about the rotational center must be high. Figure 8.5 depicts these properties for the five sections.

This criterion immediately eliminates the NACA 0040 section from consideration as an acceptable freely rotating fairing. The location of the hydrodynamic center was found to be forward of the leading edge. Thus, for all possible locations of the rotational center the fairing will misalign with the flow. The resultant lift forces will cause severe tow-off problems. The existance of a region of separated flow near the trailing edge at all Reynolds numbers will also contribute to the vibration and instability of this fairing.

The Liebeck section will have similiar problems. The hydrodynamic center for this fairing was found to be located just forward of the 1/4 chord. The maximum diameter circular cylinder that

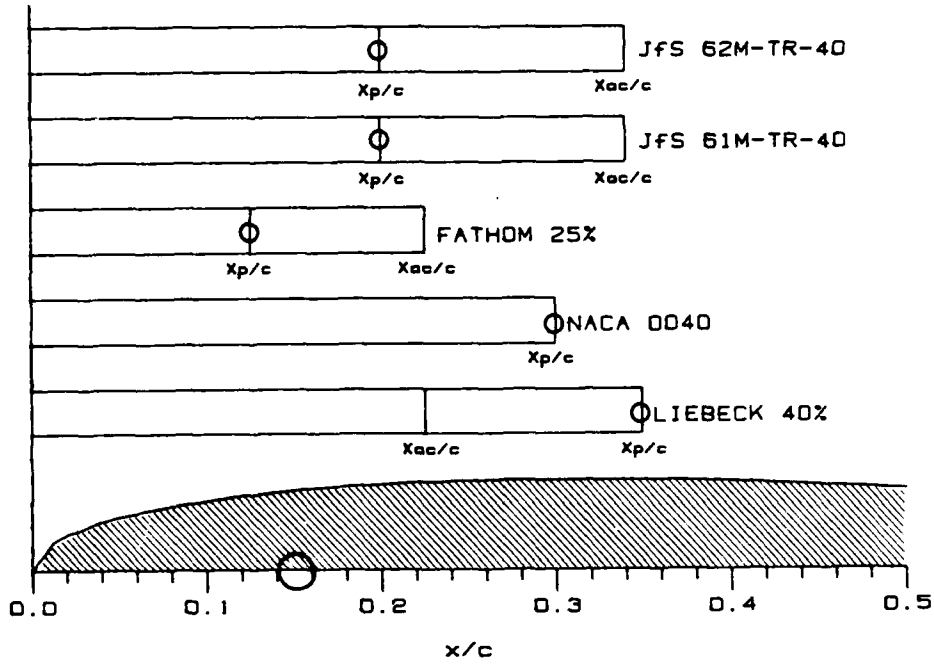

Fig. 8.5. Relative positions of the hydrodynamic center and mechanical center for the five tested sections.

the Liebeck section can fair would be centered at the 35 percent chord position. For this configuration the hydrodynamic center would be forward of the mechanical center resulting in flow misalignment and kiting.

There are two possible configurations of the Liebeck fairing that could be used to overcome this problem. First, the section could be used to fair line structures of smaller diameter. For acceptable streamlining behavior the maximum diameter must be less then 34 percent of the chord length with its center located forward of the 20 percent chord position. This is an inefficient use of the fairing shape.

The second configuration requires the addition of the trailing edge wedge. The hydrodynamic center was now found to be located at the 35 percent chord position, coincident with the center of the maximum incribed diameter. Line structures with smaller diameters, 35 to 39 percent of the chord length could be successfully faired. The improved streamlining performance is compromised by the higher drag that results from the presence of the wedge.

Problems with kiting of the prototype Fathom Flexnose 25 percent fairing were described by Henderson [2]. The location of the hydrodynamic center was the cause the problem. This investigation confirmed the location of the hydrodynamic center as being between .15c and .25c depending on Reynolds number. The rotational center of the Fathom fairing is the 12.5 percent chord position. The measured restoring moment gradient about the 10 and 15 percent positions were -0.428 and -0.215 respectively. Henderson measured dC_m/dC_L about the 12.5 percent chord position and found it to be -0.115. The low restoring moment about the mechanical center was unable to overcome

the frictional moments encountered between the fairing and cable. Thus the fairing would not maintain alignment with the flow and lift forces would result.

For both of JfS sections, the hydrodynamic centers were located significantly aft of the best rotational center. Both sections with circular leading edges had their best mechancical center located at the $x_p/c = 0.2$. The hydrodynamic center for both fairings was between the 30 and 35 percent chord position. The restoring moment slopes about this mechanical center were relatively high. The gradient was -1.09 about $x_p/c = 0.2$ for the thin trailing edge JfS 62M section and -.583 for the JfS 61M section.

With regard to the streamlining behavior of the five fairings, it was clear that the two JfS sections are superior. The hydrodynamic center was well aft of the rotational center and their restoring moment gradients are high.

8.4. Summary

In summarizing the hydrodynmaic characteristics of the five fairings it is evident that the JfS 62M-TR-40 section best meets the stated criteria. The boundary layer for this section was well behaved. Separation was a problem only at Reynolds numbers less than $.25 \times 10^5$. Its hydrodynamic center was well aft of the ideal rotational center. The restoring moment gradient was high. Tow-off should not be a problem. The drag coefficients, although higher than those of the NACA and Liebeck section, were within the range predicted by Hoerner [10] for other sections of comparable thickness. The JfS 62M section with its thin trailing edge has lower drag coefficients then the JfS 61M section. The JfS 61M section was in every other way comparable to the JfS 62M.

9.0. RECOMMENDATIONS

The first phase of the fairing study determined that the JfS 62M-TR-40 modified section is worthy of further study. The section utilizes a semi-circular forebody to move the mechanical rotation center as far forward as possible, a concave aft section for boundary layer separation control and a thick trailing edge for increased restoring moment.

It is recommended that the second phase of tests continue the two-dimensional characterization of the JfS modified section in the Venturi tunnel by measuring the lift, drag and pitching moments of a two-dimensional model mounted horizontally between two vertical plates to assure two-dimensional flow. The three-component wind tunnel balance would be used to determine the two-dimensional lift and pitching moment characteristics, which were not determined in the phase one tests, and to determine the drag coefficient as measured by the balance which would be used to check the wake measurement technique.

The purpose of the third phase of tests, which would be conducted in the University of Washington Kirsten Wind Tunnel, would be to examine the three-dimensional characteristics of the JfS section. The Kirsten Wind Tunnel is of a closed circuit, double return type, with a 2.44 by 3.66 m test section vented to the atmosphere. Wind velocities up to 111/75 m/sec can be generated in the test section, corresponding to dynamic pressures of 1 to 160 psf. A 30.5 cm model chord would allow tests in the Kirsten wind tunnel to a maximum Reynolds number of 2.5×10^6. A vertically mounted model comprising several discrete segments of the fairing section elements, Fig. 9.1, would be mounted in the tunnel. The 30.5 cm model would allow approximately eight

segments of the fairing to be simulated, assuming an aspect ratio of one for each fairing segment. It should be noted that aspect ratios of two would also be investigated. An instrumented floating fairing element, located at approximately midspan of the model, would be used to measure the following:

(1) The element section would be built with a distribution of chordwise pressure taps to measure the chordwise pressure distribution.

(2) The upper and lower ends of the section would be mounted with block gauges, Fig. 9.1, two of which would measure the normal force component and a third mounted at the top which would measure the tangential forces.

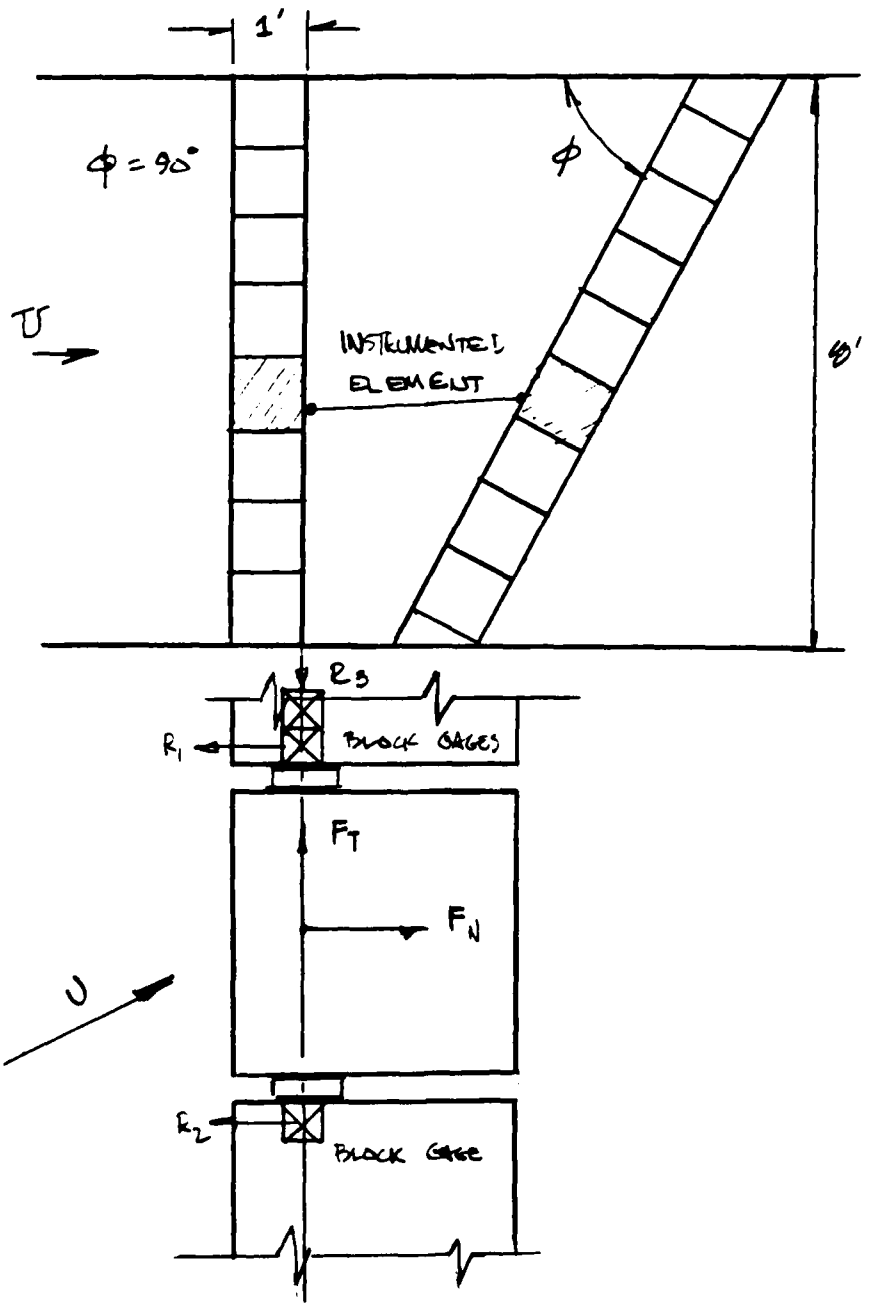

Fig. 9.1. Proposed three-dimensional wind tunnel model.

REFERENCES

(1) "Plastic Clam Shells," Popular Science, November 1978.

(2) Henderson, J. F., "Some Towing Problems With Faired Cables," Ocean Engineering, Vol. 5, pp. 105-125, 1978.

(3) Grant, Robert and Patterson, Dan, "Riser Fairing for Reduced Drag and Vortex Suppression," Offshore Technology Conference 1977, Paper 2921.

(4) Smith, A.M.O., "High-Lift Aerodynamics," AIAA 6th Aircraft Design, Flight Test and Operations Meeting, Paper No. 74-939, 1974.

(5) Thieme, H., "Design of Ship Rudders," (Zur Formgebung von Shiffsrudern"), translated by E. N. Labouvie, Department of the Navy, Trans. 321, November 1965.

(6) Wingham, P. J., "Comparative Steady State Deep Towing Performance of Base and Faired Cable Systems," Ocean Engineering, Vol. 10, No. 1, pp. 1-32, 1983.

(7) Goett, H. J. and Bullivant, W. K., "Tests of the N.A.C.A. 0009, 0012, and 0018 Airfoils in the Full-Scale Wind Tunnel," Report No. 647, NACA, 1938.

(8) Bullivant, W. K., "Tests of the NACA 0025 and 0035 Airfoils in the Full-Scale Wind Tunnel," Report No. 708, NACA, 1940.

(9) Eastman, N., Jacobs, E. N., and Abbot, I. H., "Airfoil Section Data Obtained in the N.A.C.A. Variable Density Tunnel as Affected by Support Interference and Other Corrections," Report No. 669, NACA, 1939.

(10) Abbott, I. H., and vonEDoenhoff, A. E., Theory of Wind Sections, Dover Publications, Inc., New York, 1959.

(11) Hoerner, S. F., Fluid Dynamic Drag, published by author, Midland

Park, New Jersey, 1958.

(12) Carmichael, B. H. and Meggitt, D., "Two Dimensional Aircraft Literature Survey," Autonetics (?), 1966.

(13) Althaus, D., Profilpolaren Fur Den Modellflug, Nekkar-Verlag, 1980.

(14) Liebeck, R. H., "A Class of Airfoils Designed for High Lift in Incompressible Flow," Journal of Aircraft, Vol. 10, No. 10, October 1973.

(15) Pope, A., and Harper, J. J. Low-Speed Wind Tunnel Testing, Wiley, New York, 1966.

(16) Hinze, J. O., Turbulence, McGraw-Hill, New York, 1975.

(17) Oakey, N. S., "Dissipation Within the Surface Mixing Layer," Journal of Physical Oceanography, Vol. 12, No. 2, February 1982.

(18) Osborn, T. R., "Measurements of Energy Dissipation Adjacent to an Island, Journal of Geophysical Research, Vol. 38, No. C6, June 1978.

(19) Raghunathan, S., and McAdam, R.J.W., "Free Stream Turbulence and Attached Subsonic Turbulent Boundary Layer," Department of Aeronautical Engineering, The Queens University of Belfast, December 1981.

(20) Pearcey, H. H., "Shock-Induced Separation and Its Prevention," Boundary Layer and Flow Control. Its Principles and Application. Vol. 2, Lachmann, G. V.,ed. Pergamon Press, 1961.

(21) Crowder, J. P., "Add Fluorescent Mini-tufts to the Aerodynamicist's Bag of Tricks," Astronautics and Aeronautics, November 1980, pp. 54-56.

(22) Crowder, J. P., Hill, E. G., and Pond, C. R., "Selected Wind Tunnel Testing Developments at the Boeing Aerodynamics

APPENDIX A

DRAG DATA ACQUISITION AND REDUCTION PROGRAM

DOCUMENTATION AND LISTING

Laboratory," AIAA 11th Aerodynamic Testing Conference, March 18-20, 1980, AIAA-80-0458-CP.

(23) Fritsch, F. N. and Carlson, R. E., "Piecewise Cubic Interpolation Methods," Lawrence Livermore Laboratory Report, UCRL-82230, November 1978.

(24) Hornbeck, R. W., Numerical Methods, Prentice-Hall, Inc., 1975.

(25) Shaw, R. J., Sotos, R. G., and Solano, F. R., "An Experimental Study of Airfoil Icing Characteristics," AIAA Paper No. 82-283, 1982.

(26) Fage, A., Falkner, V. M., and Walker, W. S., "Experiments on a Series of Symmetrical Joukowski Sections, British R&M No. 1241, April 1929.

```
      PROGRAM DRAG
C
C     DATA REDUCTION PROGRAM
C     FOR THE CALCULATION OF THE
C     DRAG COEFFICIENT
C     FROM WIND TUNNEL DATA
C
C     WRITTEN BY:
C     DAVID GRAY
C     DECEMBER 1982
C
      REAL M,INTEQ(25)
      DIMENSION Y(25),Q(25),QRATIO(25)
      BYTE PARAM(11),INFIL(11),DATFIL(11)
      BYTE XCONF(40),XNAME(6),XDATE(20),NRUN(2)
5000  FORMAT(2X,'TO RUN PROGRAM USING OLD DATA TYPE - "O"',/,
     1        2X,'TO COLLECT NEW DATA TYPE - "N"',/,
     2        2X,'(O/N)? -')
5005  FORMAT(2X,'TYPE FILENAME CONTAINING PARAMETER DATA -')
5010  FORMAT(A2)
5019  FORMAT(2X,'INPUT RUN NUMBER - ')
5020  FORMAT(2X,'INPUT QI, HIGH OR LOW SCALE',/,
     1        2X,'FORMAT(F6.0,H/L)-')
5025  FORMAT(2X,'INPUT ROOM TEMPERATURE (C) -')
5030  FORMAT(F6.0,A2)
5033  FORMAT(F6.0)
5035  FORMAT(2X,'OPEN VALVE NUMBER: ',I3,/,2X,'TYPE Y TO CONFIRM - ')
5040  FORMAT(2X,'TAP NO.',5X,'Y(IN.)',12X,'Q(PSF)',/)
5050  FORMAT(4X,I3,8X,F5.2,8X,F10.4)
5055  FORMAT(2X,'TYPE THE TWO TAP NUMBERS THAT DEFINE THE EDGE ',/,
     1  2X,'OF THE WAKE.  NEGATIVE TAP # FIRST: ')
5060  FORMAT(//,2X,'DO YOU WISH TO CONTINUE DATA REDUCTION [Y/N]? -')
5065  FORMAT(2I3)
5070  FORMAT(2X,'TYPE FILENAME OF OLD DATA -')
5071  FORMAT(2X,'TYPE FILENAME FOR DATA STORAGE -')
5072  FORMAT(2X,'WOULD YOU LIKE A PRINTED COPY OF THE RESULTS [Y/N]?
     1  - ')
5074  FORMAT(2A1)
5075  FORMAT(11A1)
5080  FORMAT(2X,'Q(I)=',F10.5,' (PSF)',/)
5090  FORMAT(2X,'OPEN VALVE FOR T.E. STATIC PRESSURE TAP',/,
     1  2X,'TYPE Y TO CONFIRM',/,
     2  2X,'TYPE N IF NO TE PRESSURE TAP [Y/N] - ')
5091  FORMAT(2X,'Q STATIC AT T.E.=',F10.5,' (PSF)',/)
5095  FORMAT(2X,'DO YOU WANT TO INPUT THE SEPARATION LOCATION [Y/N]? '
     1  )
5096  FORMAT(2X,'INPUT:  XSEP/C = ')
5098  FORMAT(F5.3)
5100  FORMAT(2X,'DO YOU WISH TO CHANGE TRANSDUCER CALIBRATION [Y/N] ')
5110  FORMAT(2X,'INPUT "Q=M*VBAR+B"; M,B= ')
```

```
6000    FORMAT(6A1,20A1)
6001    FORMAT(6A1,20A1,3F15.8)
6101    FORMAT(11A1,20A1,3F15.8)
6005    FORMAT(40A1)
6010    FORMAT(3F10.4)
6011    FORMAT(3F7.4)
6019    FORMAT(2F10.4,I2)
6020    FORMAT(2F10.4,I2,F5.3)
6030    FORMAT(I3)
6040    FORMAT(F10.5)
6050    FORMAT(3F15.10)
7000    FORMAT(I3)
7010    FORMAT(2F10.5)
9000    FORMAT(2X,'END OF PROGRAM',/)
9001    FORMAT(2X,'DO YOU WISH TO RUN THE PROGRAM AGAIN [Y/N]? -')
C
C
C       PART 1
C       DETERMINE IF OLD DATA IS TO BE RECALCULATED
C       OR IF NEW DATA IS TO BE TAKEN
C
        M=0.0
        B=0.0
1       CALL HOME
        WRITE(5,5000)
        READ(5,5010) IC
        IF(IC.NE.'N') GO TO 500
C
C       READ FILE CONTAINING OPERATING PARAMETERS
C
        WRITE(5,5005)
        READ(5,5075)PARAM
        CALL OPEN(6,PARAM,2)
        READ(6,6000) XNAME,XDATE
        READ(6,6005) XCONF
        READ(6,6010) B,C,T
        READ(6,6011)XTW,TWT,TWW
        READ(6,6019) THETA,XRAKE,NTAPS
        READ(6,6030) NPTS
        DO 10 I=1,NTAPS
        INTEQ(I)=0.0
10      READ(6,6040) Y(I)
        ENDFILE 6
C
C       GET PARAMETERS FROM TERMINAL
C
        WRITE(5,5019)
        READ(5,5074)NRUN
        WRITE(5,5020)
        READ(5,5030) QI,IS
```

```
      WRITE(5,5025)
      READ(5,5033) TC
      RHO=.002522/(1.0+.00367*TC)
      RMU=.14248E-8*TC+.35242E-6
      QTE=0.0
C
C     CALCULATE QU - UPSTREAM DYNAMIC PRESSURE
C
      IF(IS.EQ.'H') GO TO 30
      QU=.96*QI
      GO TO 40
30    QU=.983*QI-.24
40    CONTINUE
C
C     DATA COLLECTION
C
48    WRITE(5,5100)
      READ(5,5074)IB
      IF(IB.NE.'Y') GO TO 49
      WRITE(5,5110)
      READ(5,7010)M,BS
49    IF(M.EQ.0.0)GO TO 48
      NN=1+(NTAPS-1)/2
      DO 59 I=1,NTAPS
      J=I-NN
50    WRITE(5,5035) J
      READ(5,5010) IT
      IF(IT.NE.'Y') GO TO 50
      DO 54 KK=1,500
      DUM=SQRT((BS*M)*(BS*M))/2.
54    CONTINUE
55    CALL ADCONV(NPTS,VBAR)
      Q(I)=M*VBAR+BS
      WRITE(5,5080) Q(I)
      CALL BEEP(50,200)
      IF(Q(I).LT.0.0) GO TO 50
59    CONTINUE
60    WRITE(5,5090)
      READ(5,5010)IT
      IF(IT.EQ.'Y')GO TO 65
      IF(IT.EQ.'N')GO TO 70
      GO TO 60
65    CALL ADCONV(NPTS,TEV)
      QTE=M*TEV+BS
      WRITE(5,5091)QTE
70    WRITE(5,5095)
      READ(5,5010)IX
      XSEP=0.0
      IF(IX.NE.'Y') GO TO 100
      WRITE(5,5096)
```

```
      READ(5,5098)XSEP
100   CONTINUE
C
C     PLOT AND LIST DATA ON TERMINAL
C
      CALL SUBPLT(NTAPS,Y,Q)
      WRITE(5,5040)
      DO 110 I=1,NTAPS
      J=I-NN
110   WRITE(5,5050) J,Y(I),Q(I)
      WRITE(5,5060)
      READ(5,5010) I1
      IF(I1.EQ.'N') GO TO 9990
      WRITE(5,5055)
      READ(5,5065) K1,K2
      K1=K1+NN
      K2=K2+NN
      QO=(Q(K1)+Q(K2))/2.0
C
C     SAVE DATA ON FILE
C
      IF(IC.NE.'N') GO TO 600
      DO 115 I=1,6
115   DATFIL(I)=XNAME(I)
      DATFIL(7)=NRUN(1)
      DATFIL(8)=NRUN(2)
      DATFIL(9)='D'
      DATFIL(10)='A'
      DATFIL(11)='T'
      CALL OPEN(8,DATFIL,2)
      WRITE(8,6101)DATFIL,XDATE,QU,QI,QTE
      WRITE(8,6005)XCONF
      WRITE(8,6010)B,C,T
      WRITE(8,6011)XTW,TWT,TWW
      WRITE(8,6020)THETA,XRAKE,NTAPS,XSEP
      WRITE(8,6030)NPTS
      WRITE(8,6050)TC,RHO,RMU
      WRITE(8,7000) NTAPS
      DO 120 I=1,NTAPS
120   WRITE(8,7010) Y(I),Q(I)
      ENDFILE 8
      GO TO 600
C
C     GET OLD DATA FROM FILE IF REQUESTED
C
500   WRITE(5,5070)
      READ(5,5075) INFIL
      CALL OPEN(7,INFIL,2)
      READ(7,6101)DATFIL,XDATE,QU,QI,QTE
      READ(7,6005)XCONF
```

```
      READ(7,6010)B,C,T
      READ(7,6011)XTW,TWT,TWW
      READ(7,6020)THETA,XRAKE,NTAPS,XSEP
      READ(7,6030)NPTS
      READ(7,6050)TC,RHO,RMU
      READ(7,7000) NTAPS
      DO 510 I=1,NTAPS
      INTEQ(I)=0.0
510   READ(7,7010) Y(I),Q(I)
      ENDFILE 7
      NN=1+(NTAPS-1)/2
      GO TO 100
C
C     CALCULATION OF FLOW PARAMETERS
C
600   VU=SQRT(2.0*QU/RHO)
      VO=SQRT(2.0*QO/RHO)
      E=(VO-VU)/VU
      REN=C*RHO*VO/(RMU*12.)
      RENU=C*RHO*VU/(RMU*12.)
C
C     CALCULATION OF INTEGRAND FOR DRAG INTEGRATION
C
      DO 650 I=K1,K2
      QRATIO(I)=Q(I)/QO
650   INTEQ(I)=SQRT(QRATIO(I))-QRATIO(I)
      CALL INTGRL (Y,INTEQ,NTAPS,AREA)
C
C     CALCULATE DRAG COEFFICIENTS
C
      CDBC=(2./C)*AREA
      CDBT=CDBC*C/T
C
C     WRITE DATA AND RESULTS
C
      L=5
      CALL HOME
      IP='N'
675   WRITE(L,1790)
      WRITE(L,1800)XCONF,XDATE
      WRITE(L,1801)DATFIL
      WRITE(L,1805)QU,QI,RENU,TC,VU,T,RHO,C,RMU,B,E,XRAKE,QTE
      IF(XTW.EQ.0.0) GO TO 699
      WRITE(L,1806)XTW
      WRITE(L,1807)TWT,TWW
699   IF(L.EQ.5)PAUSE
      WRITE(L,1810)
      DO 700 I=1,NTAPS
      J=I-NN
700   WRITE(L,1820) J,Y(I),Q(I),INTEQ(I)
```

```
      WRITE(L,1835)REN
      WRITE(L,1830) CDBC,CDBT
      WRITE(L,1840)
      IF(XSEP.EQ.0.0)GO TO 720
      WRITE(L,1842)XSEP
      GO TO 730
720   WRITE(L,1843)
730   IF(L.EQ.2) WRITE(2,1831)
      WRITE(5,5072)
      READ(5,5010)IP
      IF(IP.NE.'Y') GO TO 9990
      L=2
      GO TO 675
C
1790  FORMAT(5X,'SYMMETRICAL FAIRING SECTIONS',/,5X,
     1  '2-DIMENSIONAL DRAG COEFFICIENT TESTING')
1800  FORMAT(/,5X,'MODEL CONFIGURATION - ',40A1,/,5X,'DATE - ',20A1)
1801  FORMAT(/,5X,'TEST DATA FILENAME -',11A1)
1806  FORMAT(5X,'LOCATION OF BOUNDARY LAYER TRIP WIRE, (XTW/C)= ',F4.2
     1  )
1807  FORMAT(5X,'TRIP WIRE DIMENSIONS:  THICKNESS= ',F7.4,' WIDTH= ',
     1  F7.4,'  INCHES',/)
1810  FORMAT(/,9X,'TAP NO.',7X,'Y (IN.)',7X,'Q (PSF)',7X,'DRAG
     1INTEGRATION',/,
     1  54X,'INTEGRAND',/,
     29X,'-------------------------------------------------------')
1820  FORMAT(10X,I3,2X,3(5X,F10.5))
1830  FORMAT(/,5X,'CD(BC)=',F10.4,/,5X,'CD(BT)=',F10.4)
1831  FORMAT(1H1)
1835  FORMAT(//,5X,'DOWNSTREAM REYNOLDS NUMBER; REN=  ',E8.3)
1840  FORMAT(//,5X,'SEPARATION LOCATION AS INDICATED BY MICROTUFT
     1BEHAVIOR:')
1842  FORMAT(5X,'XSEP/CHORD = ',F5.3,//)
1843  FORMAT(5X,'SEPARATION LOCATION WAS NOT RECORDED FOR THIS RUN')
1805  FORMAT(//,5X,'QU=',F8.4,1X,'(PSF)',14X,'QI=',F8.4,1X,'(PSF)',/,
     1  5X,'UPSTREAM REN= ',E8.3,9X,'TEMPERATURE=',F6.2,1X,'(CENTIGRADE)
     1  ',/,
     2  5X,'VEL=',F10.3,1X,'(FT/SEC)',8X,'THICKNESS=',F6.2,1X,'(IN.)',/,
     3  5X,'RHO=',F10.8,1X,'(TE UNITS)',6X,'CHORD=',F6.2,1X,'(IN.)',/,
     4  5X,'MU=',F12.10,1X,'(TE UNITS)',5X,'SPAN=',F6.2,1X,'(IN.)',/,
     5  5X,'BLOCKAGE=',F8.5,14X,'DISTANCE TO WAKE RAKE=',F6.2,1X,'(IN.)'
     6  ,/,36X,'T.E. STATIC PRESSURE=',F8.4,' (PSF)',/)
C
9990  WRITE(5,9001)
      READ(5,5010)IA
      IF(IA.NE.'N') GO TO 1
9999  WRITE(5,9000)
      STOP
      END
```

```
C  SUBROUTINE FOR A/D CONVERSION
C  OF 10 VOLT SIGNAL ON CHANNEL 0
C  OF A/D BOARD
C
        SUBROUTINE ADCONV(NPTS,VBAR)
        INTEGER A,A1,A2,A3
C
        A=57536
        A1=A+1
        A2=A+2
        A3=A+3
        CALL POKE(A,252)
        SUM=0.
C  CONVERSIONS ON CHANNEL 0
        CALL POKE(A1,0)
C  START CONVERSIONS
        DO 500 I=1,NPTS
        CALL POKE(A2,0)
C  TEST FOR END OF CONVERSION
10      IF(IPEEK(A1).LT.128) GO TO 10
C  READ REGISTERS
        L=IPEEK(A2)
        M=IPEEK(A3)
        D=256.*M+L
        IF(D.GT.2047.) GO TO 50
        PSUM=D/NPTS
        GO TO 500
50      PSUM=(D-4095)/NPTS
500     SUM=SUM+PSUM
        VBAR=(SUM*10.)/2047.
        WRITE(5,5001) VBAR
C
5001    FORMAT(2X,'VBAR=',F10.5)
        RETURN
        END
C
        SUBROUTINE SUBPLT(NTAPS,X,Q)
        REAL X(NTAPS),Q(NTAPS)
        INTEGER XPT,YPT
C
        WRITE(5,1000)
1000    FORMAT(2X,'WELCOME TO SUBPLOT, TYPE <CR> TO CONTINUE',/)
        PAUSE
        NT1=NTAPS-1
        QMAX=Q(1)
        DO 100 I=1,NT1
        IF(Q(I).LE.Q(I+1)) QMAX=Q(I+1)
100     CONTINUE
        YSCL=ABS(QMAX/40.)
        IF(QMAX.EQ.0.0) YSCL=1.
```

```
C
      CALL GR(1,0)
      CALL COLOR(15)
      CALL VLIN(0,47,0)
      CALL HLIN(0,39,47)
      CALL COLOR(7)
C
      DO 300 I=1,NTAPS
      XPT=19+INT(X(I)/.25)
      IF(XPT.LE.0.OR.XPT.GE.40) GO TO 300
      YPT=48-INT(Q(I)/YSCL)
      CALL VLIN(YPT,46,XPT)
300   CONTINUE
      PAUSE
      CALL HOME
      CALL TEXT
      RETURN
      END
```

```
      SUBROUTINE INTGRL(X,Y,N,AREA)
C
      DIMENSION Z(5),XP(10),F(5),XI(5)
      DIMENSION DY(110)
      REAL X(N),Y(N)
      NINT=10
      II=1
      AREA=0.0
      Z(1)=0.0
      Z(2)=0.53846931
      Z(3)=-Z(2)
      Z(4)=0.90617985
      Z(5)=-Z(4)
      W1=0.56888889
      W2=0.47862867
      W4=0.23692689
      W3=W2
      W5=W4
      CALL MONDER(X,Y,N,DY)
      DX=(X(N)-X(1))/NINT
      DO 10 I=1,NINT
10    XP(I)=X(1)+FLOAT(I-1)*DX
      DO 20 I=1,NINT
      XC=XP(I)+DX/2.
      DO 15 J=1,5
      XI(J)=XC+Z(J)*DX/2.
      CALL PWCFEV(II,N,X,Y,DY,II,XI(J),F(J))
      XINT=(W1*F(1)+W2*F(2)+W3*F(3)+W4*F(4)+W5*F(5))*DX/2.
20    AREA=AREA+XINT
      RETURN
      END
C
      SUBROUTINE MONDER(X,Y,N,DY)
C  IN THIS VERSION, ONLY 25 POINTS CAN BE FIT
C
      DIMENSION X(25),Y(25),DY(25),OCH(25)
C
C  CHECK THAT THERE ARE MORE THAN 3 POINTS
C
      IF(N.GT.3) GO TO 20
      TYPE 1100,N
 1100 FORMAT(//1X'ERROR--MONDER REQUIRES AT LEAST 4 DATA'
     1' POINTS--N= 'I4/ )
      STOP
   20 CONTINUE
C
C  EVALUATE THE CHORD LENGTHS
C
      IERR=0
      OCH(1)=0.0
      DO 10 I=2,N
```

```
      DC=X(I)-X(I-1)
      IF(DC.LE.0.0) IERR=1
      OCH(I)=OCH(I-1)+DC
   10 CONTINUE
      IF(IERR.EQ.0) GO TO 30
      TYPE 1110
 1110 FORMAT(//1X'ERROR--MONDER REQUIRES THAT THE X VALUES '
     1'STRICTLY INCREASE'/)
      STOP
   30 CONTINUE
C
C  NOW CALL MOND1 TO GENERATE THE DERRIVATIVES AT THE DATA POINTS
C
      CALL  MOND1 (N, OCH, Y, DY)
      RETURN
      END
      SUBROUTINE  MOND1 (N, X, F, D)
      INTEGER  N
      REAL  X(25), F(25), D(25), SLOPE(25), H(25)
C
C-----------------------------------------------------------------------
C
C     MOND1 USES THE FRITSCH-CARLSON FORUMLAS TO SET DERIVATIVE
C     VALUES FOR A PIECEWISE CUBIC INTERPOLANT TO THE DATA (X, F)
C     SO THAT THE INTERPOLANT IS MONOTONE ON ANY SUBINTERVAL ON
C     WHICH THE DATA ARE MONOTONE.
C
C     THIS VERSION USES..
C       1. THREE-POINT DIFFERENCE FORMULAS TO INITIALIZE DERIVATIVES
C          (INCLUDING ENDPOINTS).
C       2. REGION S(3).
C       3. ALGORITHM A FOR MOVING A POINT INTO REGION.
C       4. ANY NEGATIVE ALPHA OR BETA (INDICATING A CHANGE IN MONO-
C          TONICITY OF THE DATA) IS SET TO ZERO TO INSURE THE STRICT
C          PIECEWISE MONOTONICITY OF THE INTERPOLANT.
C
C     SUBROUTINE PWCFEV MAY BE USED TO EVALUATE THE RESULTING
C     PIECEWISE CUBIC FUNCTION.
C
C     REFERENCE.. F. N. FRITSCH AND R. E. CARLSON, PIECEWISE CUBIC
C       INTERPOLATION METHODS, LAWRENCE LIVERMORE LABORATORY REPORT
C       UCRL-81230 (NOVEMBER 1978).
C
C-----------------------------------------------------------------------
C
C     ON INPUT..
C        N      IS THE NUMBER OF DATA POINTS.
C               RESTRICTION.. N.GE.4  (NOT CHECKED).
C        X      IS THE ARRAY OF INDEPENDENT VARIABLE VALUES.
C               RESTRICTION.. X MUST BE STRICTLY INCREASING, THAT IS
C                  X(I) .LT. X(I+1), I=1(1)N-1  (NOT CHECKED).
```

```
C         F       IS THE ARRAY OF DEPENDENT VARIABLE VALUES.
C
C     ON OUTPUT..
C         D       WILL BE SET TO THE DESIRED DERIVATIVE VALUES.
C         H       WILL BE THE ARRAY OF INTERVAL LENGTHS,
C                    H(I) = X(I+1) - X(I), I=1(1)N-1.
C         SLOPE   WILL BE THE ARRAY OF SLOPES OF CHORDS,
C                    SLOPE(I) = (F(I+1) - F(I))/H(I), I=1(1)N-1.
C
C     NOTE.. ARRAYS H AND SLOPE ARE NO LONGER NEEDED AFTER THE CALL TO
C            MOND1.
C
C     FORTRAN INTRINSICS USED.. ABS.
C
C-----------------------------------------------------------------------
C
C     ALGORITHM BY.. F. N. FRITSCH, LAWRENCE LIVERMORE LABORATORY, AND
C                    R. E. CARLSON, GROVE CITY COLLEGE, PA.
C     PROGRAMMED BY..F. N. FRITSCH.
C     DATE LAST CHANGED.. 11 JANYARY 1979  (FNF)
C
C     CHANGE RECORD..
C         78-12-07    MINOR COSMETIC CHANGES TO GET READY FOR LIBRARY.
C         78-12-20    1. REMOVED ARGUMENT ICOUNT.
C                     2. CHANGED ARGUMENT Y TO F (TO BE CONSISTENT WITH
C                        PWCFEV).
C         79-01-11    1. CHANGED TREATMENT OF INTERVAL ADJACENT TO CHANGE
C                        IN MONOTONICITY OF DATA (SEE ITEM 4, ABOVE).
C                     2. MINOR ADDITIONS TO COMMENT SECTION.
C
C-----------------------------------------------------------------------
C
C         LOCAL DECLARATIONS.
C
      INTEGER  I, NLESS1
      REAL  ALPHA, BETA, DELTA, FUZZ, TAU
      DATA  FUZZ /1.0E-14/
C
C         INITIALIZE.
C
      NLESS1 = N - 1
C
C         COMPUTE INTERVAL LENGTHS AND SLOPES.
C
      DO 10  I = 1, NLESS1
         H(I) = X(I+1) - X(I)
         SLOPE(I) = (F(I+1) - F(I))/H(I)
   10 CONTINUE
C
C         INITIALIZE D(1) VIA NON-CENTERED THREE-POINT FORMULA.
C
```

```
      D(1) = ((H(1)+H(1)+H(2))*SLOPE(1) - H(1)*SLOPE(2))/(H(1)+H(2))
      IF (D(1)*SLOPE(1) .LT. 0.)  D(1) = 0.
C
C        CYCLE THROUGH ALL INTERVALS.
C
      DO 50  I = 1, NLESS1
         IF (I .LT. NLESS1)  GO TO 20
C
C        SPECIAL CASE OF RIGHT ENDPOINT.
            D(N) = ((H(N-1)+H(N-1)+H(N-2))*SLOPE(N-1)
     *                              - H(N-1) *SLOPE(N-2))/(H(N-2)+H(N-1))
            IF (D(N)*SLOPE(N-1) .LT. 0.)  D(N) = 0.
            GO TO 25
   20    CONTINUE
C
C        USE THREE-POINT FORMULA TO INITIALIZE RIGHT-HAND
C        DERIVATIVE FOR INTERVAL (X(I), X(I+1)) .
C
         D(I+1) = (H(I+1)*SLOPE(I) + H(I)*SLOPE(I+1))/(H(I)+H(I+1))
C
   25    CONTINUE
C
C        ADJUST D(I) AND/OR D(I+1), IF NECESSARY TO INSURE MONOTONICITY
C        ON INTERVAL (X(I), X(I+1)) .
C
C           TAKE CARE OF FLAT DATA.
C
         IF (ABS(SLOPE(I)) .GT. FUZZ)  GO TO 30
            ALPHA = 0.
            BETA = 0.
            GO TO 45
   30    CONTINUE
C
C           COMPUTE SCALED DERIVATIVES.
C
         ALPHA = D(I) / SLOPE(I)
         BETA = D(I+1) / SLOPE(I)
C
C           TAKE CARE OF NONMONOTONE DATA.
C
C        ASSERTION.. IF EITHER OF THE FOLLOWING TESTS IS SATISFIED,
C                    (ALPHA,BETA) IS NOT IN FIRST QUADRANT, WHICH
C                    MEANS THAT SLOPE CHANGES SIGN AT ONE OR BOTH ENDS
C                    OF INTERVAL.
         IF (ALPHA .LT. 0.)  ALPHA = 0.
         IF ( BETA .LT. 0.)   BETA = 0.
C
C        ASSERTION.. ALPHA AND BETA ARE NOW BOTH NONNEGATIVE.
C
C           MAKE    ALPHA + BETA .LE. 3 .
C
```

```
            DELTA = ALPHA + BETA
            IF (DELTA .LE. 3.)  GO TO 45
C           ASSERTION.. POINT IS OUTSIDE THE TRIANGLE.  NEED TO ADJUST.
               TAU = 3./DELTA
               ALPHA = TAU*ALPHA
               BETA  = TAU*BETA
C
C              RECOMPUTE DERIVATIVE VALUES.
C
   45       CONTINUE
            D(I) = ALPHA*SLOPE(I)
            D(I+1) = BETA*SLOPE(I)
C
   50    CONTINUE
C
C           END OF DERIVATIVE ASSIGNMENT.
C
         RETURN
         END
         SUBROUTINE  PWCFEV (IDERIV, N, X, F, D, NE, XE, FE)
         INTEGER  IDERIV, N, NE
         REAL  X(N), F(N), D(N), XE(NE), FE(NE)
C
C-----------------------------------------------------------------------
C
C           EVALUATE THE FIRST (IDERIV-1) DERIVATIVES OF THE PIECEWISE
C           CUBIC FUNCTION DEFINED BY  N, X, F, D  AT THE POINTS  XE(I),
C           I = 1(1)NE.
C
C-----------------------------------------------------------------------
C
C        ON INPUT..
C           IDERIV  INDICATES HOW MANY DERIVATIVES ARE DESIRED.
C                   RESTRICTION.. 1 .LE. IDERIV .LE. 3 (NOT CHECKED).
C                   NOTE.. IDERIV=1 IMPLIES ONLY FUNCTION VALUES REQUESTED.
C           N       IS THE NUMBER OF DATA POINTS.
C                   RESTRICTION.. N .GE. 2  (NOT CHECKED).
C           X       IS THE ARRAY OF INDEPENDENT VARIABLE VALUES.
C                   THE SEARCH PROCEDURE ASSUMES THAT X IS STRICTLY
C                   INCREASING.  (NOT CHECKED)
C           F       IS THE CORRESPONDING ARRAY OF FUNCTION VALUES.
C           D       IS THE CORRESPONDING ARRAY OF DERIVATIVE VALUES.
C           NE      IS THE NUMBER OF POINTS AT WHICH EVALUATION IS DESIRED.
C           XE      IS THE ARRAY OF EVALUATION POINTS.
C                   THE SEARCH PROCEDURE ASSUMES THAT XE +S MONOTONE
C                   INCREASING.  (NOT CHECKED)
C
C        ON RETURN.
C           FE      CONTAINS THE FUNCTION VALUES, AS FOLLOWS.
C                     FE(I,J)  IS THE VALUE OF THE (J-1)-ST DERIVATIVE OF
C                              THE PIECEWISE CUBIC AT XE(I), I=1(1)NE,
```

```
C                          J=1(1)IDERIV.
C
C     OTHER ROUTINES USED.. HBASEV, SEARCH.
C
C-----------------------------------------------------------------------
C
C        LOCAL DECLARATIONS.
C
      INTEGER  I, IER, IL
      REAL  DX, H(4), RDX, T
C
C        MAIN EVALUATION LOOP.
C
      IL = 0
      DO 50  I = 1, NE
C
C           LOCATE INTERVAL CONTAINING XE(I).
C
         CALL SEARCH (N, X, XE(I), IL, IER)
C
C           EVALUATE HERMITE BASIS FUNCTIONS AND NEEDED DERIVATIVES.
C
         CALL HBASEV (IDERIV, X(IL), X(IL+1), XE(I), H)
C
C           EVALUATE CUBIC AND APPROPRIATE DERIVATIVES.
C
         DO 40  ID = 1, IDERIV
            FE(I) =   F(IL)*H(1) + F(IL+1)*H(2)
     *                 + D(IL)*H(3) + D(IL+1)*H(4)
   40    CONTINUE
C
   50 CONTINUE
C
      RETURN
      END
      SUBROUTINE  SEARCH (N, X, XVAL, IL, IER)
      INTEGER  N, IL, IER
      REAL  X(N), XVAL
C
C-----------------------------------------------------------------------
C
C        SEARCH FOR XVAL IN ARRAY X.
C
C     PERFORMS A LINEAR SEARCH, FROM LEFT TO RIGHT.   FOR IMPROVED
C     EFFICIENCY WHEN LOCATING AN INCREASING SEQUENCE OF XVAL"S,
C     THE STARTING INDEX FOR THE SEARCH MAY BE SPECIFIED BY THE USER.
C
C-----------------------------------------------------------------------
C
C     ON INPUT..
C        N       IS THE NUMBER OF POINTS IN ARRAY X.
```

APPENDIX B

MOMENT DATA ACQUISITION AND REDUCTION PROGRAM LISTING

```
      PROGRAM TORQUE
C
C     DATA REDUCTION PROGRAM
C     FOR THE CALCULATION OF THE
C     TORQUE COEFFICIENT
C     FROM WIND TUNNEL DATA
C
C     WRITTEN BY:
C     DAVID GRAY
C     FEBURARY 1982
C
      DIMENSION Y(25),TM(25),CM(25)
      REAL M
      BYTE XCONF(40),XNAME(6),XDATE(20)
      BYTE PARAM(11)
5000  FORMAT(2X,'RESTORING MOMENT DATA COLLECTION PROGRAM',/,
     1 2X,'BE CERTAIN THAT THE ANALOG SIGNAL TO A/D IS INPUT TO
     2 CHANNEL 6',/,2X,'TYPE <CR> TO CONTINUE - ')
5005  FORMAT(/,2X,'TYPE FILENAME OF PARAMETER DATA - ')
5010  FORMAT(A2)
5019  FORMAT(2X,'INPUT RUN NUMBER - ')
5021  FORMAT(I3)
5020  FORMAT(2X,'INPUT QI, HIGH OR LOW SCALE',/,
     1        2X,'FORMAT(F6.0,H/L)-')
5025  FORMAT(2X,'INPUT ROOM TEMPERATURE (C): ')
5030  FORMAT(F6.0,A2)
5033  FORMAT(F6.0)
5072  FORMAT(2X,'WOULD YOU LIKE A PRINTED COPY OF THE RESULTS [Y/N]?
     1 - ')
5075  FORMAT(11A1)
5100  FORMAT(2X,'DO YOU WISH TO CHANGE TRANSDUCER CALIBRATION [Y/N] ')
5110  FORMAT(2X,'INPUT FORCE=M*VBAR+B; M,B= ')
5120  FORMAT(2F10.5)
6000  FORMAT(6A1,20A1)
6005  FORMAT(40A1)
6010  FORMAT(3F10.4)
6011  FORMAT(3F7.4)
6020  FORMAT(2F10.4,I2)
6030  FORMAT(I3)
6040  FORMAT(F10.5)
6050  FORMAT(3F15.10)
7000  FORMAT(2X,'INPUT PIVOT LOCATION: XP/C= ')
7005  FORMAT(F6.4)
7006  FORMAT(2X,'IS THERE A TRAILING EDGE FLAP [Y/N]? - ')
7007  FORMAT(2X,'INPUT POSITIVE EQUILIBRIUM YAW ANGLE IN DEGREES: ')
7008  FORMAT(2X,'INPUT NEGATIVE EQUILIBRIUM YAW ANGLE IN DEGREES: ')
7010  FORMAT(/,2X,'SET ANGLE OF ATTACK TO ',I3,1X,'DEGREES')
7018  FORMAT(/,2X,'PIVOT LOCATION =',F6.4)
7020  FORMAT(2X,'YAW ANGLE= ',I3,2X,'FORCE=',F8.4,2X,'TORQUE=',F8.4,
     1 2X,'CM=',F8.4)
```

```
7012    FORMAT(2X,'INPUT TORQUE DIRECTION:',/,
     1  2X,'POSITIVE=RESTORING, NEGATIVE=DESTABILIZING [P/N]? - ')
7004    FORMAT(2X,'TYPE Y TO CONTINUE - ')
9000    FORMAT(2X,'END OF PROGRAM',/)
9001    FORMAT(2X,'DO YOU WISH TO RUN THE PROGRAM AGAIN [Y/N]? -')
C
C       READ FILE CONTAINING OPERATING PARAMETERS
C
        M=0.0
        B=0.0
1       CALL HOME
        WRITE(5,5000)
        PAUSE
        WRITE(5,5005)
        READ(5,5075)PARAM
        CALL OPEN(6,PARAM,2)
        READ(6,6000) XNAME,XDATE
        READ(6,6005) XCONF
        READ(6,6010) B,C,T
        READ(6,6011)XTW,TWT,TWW
        READ(6,6020) THETA,XRAKE,NTAPS
        READ(6,6030) NPTS
        DO 10 I=1,NTAPS
10      READ(6,6040)Y(I)
        ENDFILE 6
C
C       GET PARAMETERS FROM TERMINAL
C
        WRITE(5,5019)
        READ(5,5021)NRUN
        WRITE(5,5020)
        READ(5,5030) QI,IS
        WRITE(5,5025)
        READ(5,5033) TC
        RHO=.002522/(1.0+.00367*TC)
        RMU=.14248E-8*TC+.35242E-6
C
C       CALCULATE QU - UPSTREAM DYNAMIC PRESSURE
C
        IF(IS.EQ.'H') GO TO 30
        QU=1.0898*QI-.11934
        GO TO 40
30      QU=1.1491*QI-.73495
40      CONTINUE
        VU=SQRT(2.0*QU/RHO)
        RENU=C*RHO*VU/(RMU*12.)
        CF=C/12.
        BF=B/12.
        TF=T/12.
        ARM=.4277
```

```
C
C       DATA COLLECTION
C
48      WRITE(5,5100)
        READ(5,5010)IB
        IF(IB.NE.'Y') GO TO 49
        WRITE(5,5110)
        READ(5,5120)M,BS
49      IF(M.EQ.0.0) GO TO 48
50      WRITE(5,7000)
        READ(5,7005)PIVT
        WRITE(5,7006)
        READ(5,5010)NT
        WRITE(5,7007)
        READ(5,6040)YAP
        WRITE(5,7008)
        READ(5,6040)YAN
        DO 75 I=2,22,2
        J=I-2
52      WRITE(5,7010)J
        WRITE(5,7004)
        READ(5,5010)IC
        IF(IC.NE.'Y') GO TO 52
        WRITE(5,7012)
        READ(5,5010)IN
        CALL ADCONV(NPTS,VBAR)
        F=M*VBAR+BS
        IF(IN.EQ.'N') F=-F
        TM(I)=F*ARM
        CM(I)=TM(I)/(QU*BF*CF*CF)
        WRITE(5,7018)PIVT
        WRITE(5,7020)J,F,TM(I),CM(I)
75      CONTINUE
C
C       WRITE DATA AND RESULTS
C
90      L=5
        CALL HOME
        IP='N'
91      WRITE(L,1790)
        WRITE(L,1800)XCONF,XDATE
        WRITE(L,1801)XNAME,NRUN
        WRITE(L,1805)QU,QI,RENU,TC,VU,T,RHO,C,RMU,B
        IF(NT.NE.'Y')GO TO  95
        WRITE(L,1806)
        GO TO 96
95      WRITE(L,1807)
96      CONTINUE
        IF(L.EQ.5) PAUSE
        WRITE(L,1840)
```

```
      WRITE(L,1850)PIVT
      DO 100 I=2,22,2
      J=I-2
100   WRITE(L,1860)J,TM(I),CM(I)
      WRITE(L,1870)YAP,YAN
      IF(L.EQ.2) WRITE(2,1831)
      WRITE(5,5072)
      READ(5,5010)IP
      IF(IP.NE.'Y') GO TO 9990
      L=2
      GO TO 91
C
1790  FORMAT(5X,'SYMMETRICAL FAIRING SECTIONS',//,5X,
     1'2-DIMENSIONAL TORQUE COEFFICIENT TESTING'
     2,/,5X,'AND DETERMINATION OF HYDRODYNAMIC CENTER')
1800  FORMAT(//,5X,'MODEL CONFIGURATION - ',40A1,/,5X,'DATE - '
     1,20A1)
1801  FORMAT(//,5X,'TEST RUN NAME -',6A1,/,
     1 5X,'TEST RUN NUMBER: ',I3)
1806  FORMAT(36X,'TRAILING EDGE FLAP:  YES')
1807  FORMAT(36X,'TRAILING EDGE FLAP:  NONE')
1870  FORMAT(///,5X,'POSITIVE EQUILIBRIUM YAW ANGLE = ',F7.2,
     1' (DEGREES)',/,
     2 5X.'NEGATIVE EQUILIBRIUM YAW ANGLE = ',F7.2,' (DEGREES)')
1831  FORMAT(1H1)
1840  FORMAT(//,5X,'PIVOT',5X,'YAW',7X,'TORQUE',4X,'TORQUE',/,
    " 1 5X,'POINT',5X,'ANGLE',15X,'COEFFICIENT',/,
     2 5X,'(XP/C)',4X,'(DEG)',5X,'(FT-LBS)',/,
     3 5X,41('-'))
1850  FORMAT(4X,F6.4)
1860  FORMAT(16X,I3,5X,F8.4,4X,F8.4)
1805  FORMAT(///,5X,'QU=',F8.4,1X,'(PSF)',14X,'QI=',F8.4,1X,'(PSF)',/,
     1 5X,'UPSTREAM REN= ',E8.3,9X,'TEMPERATURE=',F6.2,1X,'(CENTIGRADE)
     1 ',/,
     2 5X,'VEL=',F10.3,1X,'(FT/SEC)',8X,'THICKNESS=',F6.2,1X,'(IN.)',/,
     3 5X,'RHO=',F10.8,1X,'(TE UNITS)',6X,'CHORD=',F6.2,1X,'(IN.)',/,
     4 5X,'MU=',F12.10,1X,'(TE UNITS)',5X,'SPAN=',F6.2,1X,'(IN.)')
C
9990  WRITE(5,9001)
      READ(5,5010)IA
      IF(IA.EQ.'Y') GO TO 1
9999  WRITE(5,9000)
      STOP
      END
```